

The Surface Charge of Soft and Hard Sphere Colloidal Particles

-

Experimental Investigation and Comparison to Theory

DISSERTATION

ZUR ERLANGUNG DES AKADEMISCHEN GRADES EINES
DOKTORS DER NATURWISSENSCHAFTEN (DR. RER. NAT.)
IM FACH CHEMIE DER FAKULTÄT FÜR BIOLOGIE, CHEMIE UND
GEOWISSENSCHAFTEN DER

UNIVERSITÄT BAYREUTH

VORGELEGT VON

Christian Schneider

GEBOREN IN COBURG / DEUTSCHLAND

BAYREUTH, 2010

Die vorliegende Arbeit wurde in der Zeit von Mai 2007 bis November 2010 in Bayreuth am Lehrstuhl Physikalische Chemie I und am Helmholtz-Zentrum Berlin unter Betreuung von Herrn Prof. Dr. Matthias Ballauff angefertigt.

Vollständiger Abdruck der von der Fakultät für Biologie, Chemie und Geowissenschaften der Universität Bayreuth genehmigten Dissertation zur Erlangung des akademischen Grades eines Doktors der Naturwissenschaften (Dr. rer. nat.).

Dissertation eingereicht am: 17. November 2010

Zulassung durch die Prüfungskommission: 13. Januar 2011

Wissenschaftliches Kolloquium: 27. Mai 2011

Amtierender Dekan:

Prof. Dr. Stephan Clemens

Prüfungsausschuss:

Prof. Dr. Matthias Ballauff (Erstgutachter)

Prof. Dr. Andreas Fery

Prof. Dr. Mukundan Thelakkat (Vorsitz)

Prof. Dr. Josef Breu

Alles wissenschaftliche Arbeiten ist nichtl anderes,
all immer neuen Stoff in allgemeine Gesetze zu bringen.

Wilhelm von Humboldt

*Meinen Großeltern
Lidy, Hans, Gela und Horst.*

Table of Contents

1. Introduction	1
1.1. The DLVO Theory and Particle Stability	2
1.1.1. Electric Double Layer Interaction	2
1.1.2. Van der Waals Interaction	3
1.1.3. The DLVO Interaction Potential	3
1.1.4. Stability of Colloid Dispersions	5
1.2. Counterion Correlations	7
1.3. Spherical Polyelectrolyte Brushes	8
1.4. Stability Measurements of SPB Particles	11
1.5. Electrophoretic Mobility Measurements and ζ Potential	13
1.6. Force Measurements - a Comparison	14
1.7. Objective of this Thesis	15
1.8. References	15
2. Overview	23
2.1. Interaction of Colloidal Particles: the DLVO Potential and Charge Inversion	24
2.2. Microsurface Potential Measurements: Repulsive Forces between Polyelectrolyte Brushes in the Presence of Multivalent Counterions	26
2.3. Investigation of the Stability Behavior of Anionic Spherical Polyelectrolyte Brushes in the Presence of La(III) Counterions	28
2.4. Individual Contributions to Joint Publications	30
2.5. References	31
3. Interaction of Colloidal Particles: the DLVO Potential and Charge Inversion	33
3.1. Abstract	35
3.2. Introduction	35
3.3. Theory	36
3.3.1. Coagulation rate and surface potential	36
3.3.2. Charge densities and potentials	38
3.4. Materials and methods	39
3.4.1. Materials	39
3.4.2. Electrophoretic mobility and ζ potential.	40
3.4.3. Coagulation rate	40
3.5. Results and discussion	41
3.5.1. Electrophoretic mobility measurements	41
3.5.2. Microsurface potential measurements	42

3.6. Conclusion	45
3.7. Acknowledgements	45
3.8. References	45
4. Microsurface Potential Measurements: Repulsive Forces between Polyelectrolyte Brushes in the Presence of Multivalent Counterions	49
4.1. Abstract	51
4.2. Introduction	52
4.3. Experimental Section	53
4.4. Results and Discussion	55
4.4.1. Stability Ratio	55
4.4.2. Repulsive Force and Effective Surface Charge	57
4.5. Conclusion	58
4.6. Acknowledgements	58
4.7. References	58
5. Investigation of the Stability Behavior of Anionic Spherical Polyelectrolyte Brushes in the Presence of La(III) Counterions	61
5.1. Abstract	63
5.2. Introduction	64
5.3. Experimental Section	66
5.3.1. Materials and Methods	66
5.3.2. Simultaneous Static and Dynamic Light Scattering	69
5.4. Theory	70
5.4.1. Coagulation Kinetics of SPBs	70
5.4.2. Mean-field Model	74
5.5. Results and Discussion	75
5.5.1. Relative Form Factors	75
5.5.2. Stability Ratio	77
5.5.3. Force Balance: Repulsive Energy and Effective Surface Charge	79
5.6. Conclusion	80
5.7. Acknowledgements	80
5.8. References	81
6. Summary / Zusammenfassung	85
A. List of Publications	89
A.1. Publication of this Thesis	89
A.2. Publication as a co-Author	89
B. Presentations at International Conferences and Meetings	90
C. Abbreviations	91
D. Danksagung	93

E. Schlusserklärung

95

1. Introduction

Since the days of Faraday's gold sol [1, 2], colloidal particles have been the object of intense scientific investigation. The reasons for this interest are directly related to the size of colloidal particles. Typically, the colloidal size is defined to range from a few nanometers up to the micrometer scale. [3, 4] Therefore colloidal particles are small enough to be dispersed in liquid but large enough to scatter light waves. [5, 6] This makes them ideal components for cosmetics, paints, coatings, food products, and waste water treatment. [7–11] Colloidal particles are also used as delivery agents in medical applications and as components in sensor devices. [12, 13]

Colloid and interface science divides the stabilizing forces acting between nanoparticles into three major classes, shown in Figure 1.0.1. In the case of polyelectrolyte chains densely grafted to the surface of a spherical colloid, a spherical polyelectrolyte brush (SPB) results (Figure 1.0.1c). [14] In the dispersed state the colloidal dimensions of SPBs generate a large surface area, which makes SPBs ideal carriers for smaller inorganic particles and immobilized proteins. [15, 16] Due to the polyelectrolyte brush shell, dispersed SPBs display a nearly unimpeded stability in the presence of monovalent salt. [17] However, not much is known about the stability of SPBs in the presence of multivalent counterions. Therefore this thesis focuses on the investigation of the stability of SPB particles in aqueous medium. The introduction includes an overview of the established DLVO theory, which describes the stability of surface charged colloids, and the most important characteristics of SPB particles. Furthermore, some limitations of the mean-field DLVO theory and a comparison of common force measurement techniques are included.

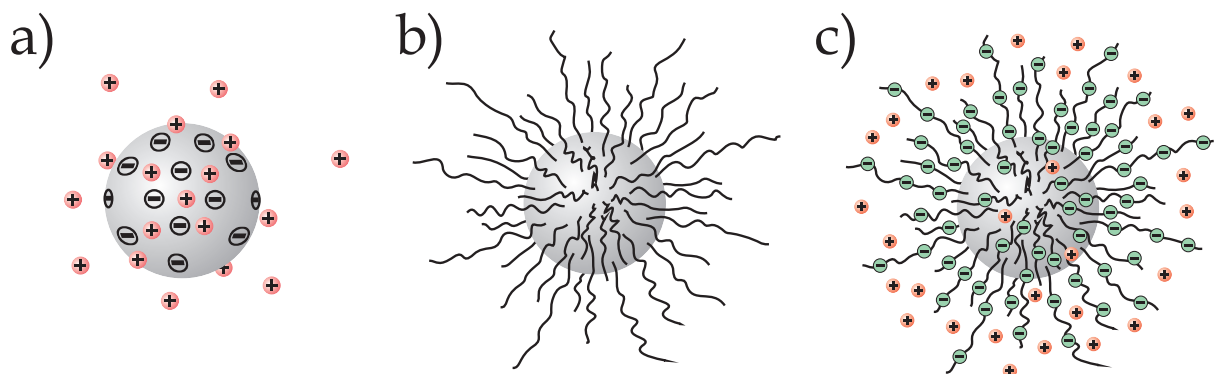


Figure 1.0.1.: Classification of colloidal particles according to the method of stabilization: electrostatic repulsion generated by surface localized charges (a), steric repulsion arising from surface grafted soluble oligomeric or polymeric chains (b), and densely surface grafted polyelectrolytes giving rise to electrosteric repulsive interactions (c).

1.1. The DLVO Theory and Particle Stability

B. V. Derjaguin and L. D. Landau, E. J. W. Verwey and J. Th. G. Overbeek (DLVO) published their theory for describing the stability of lyophobic colloids in 1943 and 1948. [18–20] In the frame of the DLVO theory the term *lyophobic colloids* refers to hydrophobic particles, which are dispersed in aqueous solution. Particle coalescence and a subsequent separation of the aqueous and particle phases are kinetically impeded by repulsive forces between the particles. Therefore lyophobic colloids are metastable. The DLVO theory treats the interactions between lyophobic colloids in terms of two independent interactions: a repulsive electrostatic force, which arises due to charges on the particle surface, and an attractive van der Waals force due to the solid particle cores. Superpositioning of the two independent interaction components results in the DLVO potential.

The necessary assumptions made for deriving the DLVO potential were summarized and discussed by Ninham. [21] Since this thesis involves a detailed discussion about the validity of the DLVO theory, the assumptions are listed briefly not accounting for curved surfaces:

- molecularly smooth and solid interfaces, which are chemically inert except as a source for counterions
- the intervening solvent has bulk properties up to the particle surface
- the electric double layer and the van der Waals forces are independent and additive
- the double layer interaction is described by the non-linear Poisson-Boltzmann equation
- the boundary condition of the double layer is constant charge or constant potential
- the van der Waals force is obtained by pair wise summation of London dispersion forces and calculated assuming a uniform structure and orientation of the intervening solvent

1.1.1. Electric Double Layer Interaction

If a surface with ionizable groups is placed in a polar medium, dissociation takes place and an electric double layer is formed. The electric double layer consists of the charged surface and the corresponding oppositely charged ions, the counterions. The distribution of the counterions inside the electric double layer can be calculated by the Poisson-Boltzmann equation. In the Poisson-Boltzmann theory the ions are treated as point charges, that are bound to the surface via the Coulomb attraction but balanced by their configurational entropy due to their thermal energy. The solution of the Poisson-Boltzmann equation gives a maximum concentration of the counterions at the surface, which then decreases exponentially with distance until reaching the bulk electrolyte concentration. The thickness of the electric double layer is determined by a decay length, called the Debye length

$1/\kappa$. The Debye length scales with the absolute concentrations $c_{i,0}^*$ of the ions in solution and their valency z_i and is given by [22]

$$\frac{1}{\kappa} = \left(\frac{\epsilon\epsilon_0 k_B T}{\sum_i (z_i e)^2 c_{i,0}^*} \right), \quad (1.1.1)$$

where ϵ and ϵ_0 are the permittivities of the medium and the vacuum, respectively, e is the charge of an electron, and $k_B T$ is the thermal energy. For a solution with 0.01 and 0.1 mol/l of monovalent salt the respective Debye lengths result to 3.04 and 0.96 nm. The same concentrations for a 3:3 electrolyte give 1.24 and 0.39 nm, respectively, indicating a much thinner electric double layer.

Upon the approach of two charged surfaces the concentration of counterions at the field-free plane, where the two overlapping electric fields cancel each other out, increases with decreasing surface separation. This results in an increase of the osmotic pressure at the field-free midplane. Therefore a repulsive force counteracts the approach of two like-charged particles. This electrostatic repulsion stabilizes the dispersed particles against coagulation. Electrostatically stabilized particles are stable at low concentrations of monovalent counterions. At high concentrations of monovalent salt or in the presence of multivalent counterions, however, the electric double layer is much thinner. Here, the osmotic pressure at the field-free plane is not sufficient to induce stabilization against the thermal energy of the colloidal particles. Thus, the colloids adhere due to the attractive van der Waals force. [23]

1.1.2. Van der Waals Interaction

In the frame of the DLVO theory the London, dispersion or induced-dipole forces are merged into the van der Waals interaction force. The van der Waals force arises from the interaction of induced dipoles in the molecules of two opposing bodies. [22] The total force acting between the bodies reaches several nanometer across the intervening medium. Therefore the van der Waals force is a long range force which is present in every condensed phase. The van der Waals force can be either attractive or repulsive. In the DLVO case of two interacting similar bodies the van der Waals force is always attractive. In contrast to the electric double layer repulsion the van der Waals force is independent of the electrolyte concentration in solution. [22]

1.1.3. The DLVO Interaction Potential

The DLVO interaction potential is obtained by simple superposition of the electric double layer repulsion with the van der Waals attraction. For two homogeneously charged spherical colloids dispersed in solution containing a symmetric electrolyte, the DLVO potential $V_{2s}^{z:z}(h)$ results to [22]

$$V_{2s}^{z:z}(h) = \frac{64\pi k_B T R c_0^* \gamma^2}{\kappa^2} \exp[-\kappa h] - \frac{H R}{12h}, \quad (1.1.2)$$

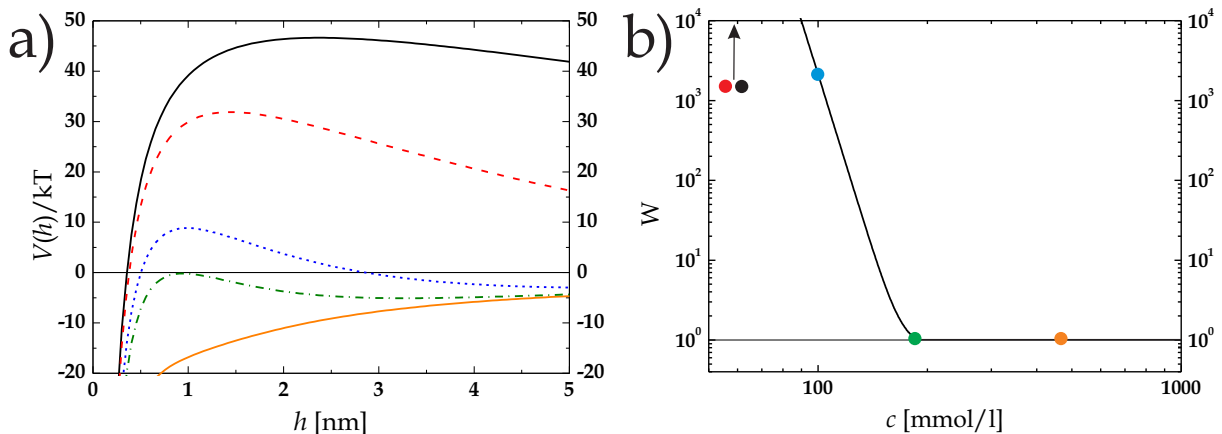


Figure 1.1.1.: (a) Normalized DLVO interaction potential $V_{2s}^{z:z}(h)$ as a function of the particle separation h for five concentrations c of a 3:3 salt in water: 100 mmol/l (solid orange line), 21 mmol/l (dash-dotted green line), 10 mmol/l (dotted blue line), 1 mmol/l (dashed red line), and 0.1 mmol/l (solid black line). At the concentration of 21 mmol/l the maximum of $V(h)$ is exactly zero, indicating the critical coagulation concentration ccc of the system. (b) Stability ratio W as a function of the salt concentration c according to eq. (1.1.6). The colored dots correspond to the interaction curves shown in plot (a). The green dot indicates the ccc of the system. In the case of the red and black dots $W \gg 10^6$, indicating a very stable system. In all plots the parameters are: $\sigma_d = 0.1 \text{ C/m}^2$, $R_h = 128 \text{ nm}$, $T = 298 \text{ K}$, $z = 3$, and $H = 0.9 \times 10^{-20} \text{ J}$.

where $\gamma = \tanh [ze\Psi_0/4k_B T]$, R is the particle radius, c_0^* is the absolute salt concentration, and z the valency of the ions, Ψ_0 is the potential at the surface, H is the Hamaker constant [24], and h is the surface-surface distance. The repulsive contribution exceeds the van der Waals attractive force at low electrolyte concentrations where κ is small. At high salt concentrations κ becomes large and the attractive term dominates the DLVO interaction potential (Figure 1.1.1a).

The relation between the surface charge density σ_0 and the surface potential Ψ_0 becomes accessible by solving the Poisson-Boltzmann equation. According to Grahame the solution for potentials below 25 mV and planar surfaces is [25]

$$\sigma_0 = \epsilon\epsilon_0\kappa\Psi_0. \quad (1.1.3)$$

The DLVO theory assumes a surface charge density σ_0 that is constant in regard to the electrolyte concentration and the counterion valency. [23] The electrolyte affects the DLVO interaction only through the Debye length κ as described by eqs. (1.1.2) and (1.1.3).

The Poisson-Boltzmann model neglects a number of effects which become prominent in real systems. These include specific surface-ion interactions, the solvent structure near the charged surface, the excluded volume of the counterions, and ion-ion correlations (see Chapter 1.2). Thus, at close proximity to the charged surface the real electric double layer deviates measurable from the prediction of the Poisson-Boltzmann model. Consequently, Stern divided the electric double layer into an inner part which does not follow the Poisson-Boltzmann theory and an outer diffuse part correctly described by the Poisson-

Boltzmann model as shown in Figure 1.1.2. [26] The borderline between this Stern layer and the diffuse part of the electric double layer is called the outer Helmholtz plane (oHp). As a consequence, Lyklema defined the surface potential Ψ_0 as the potential at $x = 0$ (Figure 1.1.2) and the potential which determines the electric double layer as the diffuse potential Ψ_d located at the oHp. [27] The Stern model thus replaces Ψ_0 and σ_0 in eqs. (1.1.2) and (1.1.3) with Ψ_d and σ_d , respectively, as shown in Figure 1.1.2. Therefore Ψ_d is accessible in experiments via measurements of the stability or the ζ potential of dispersed colloids, whereas Ψ_0 is the potential measured by titration of the charged groups or the counterions.

The DLVO interaction potential has been extensively investigated by direct force measurements. Measurements with the surface forces apparatus (SFA) showed, that eq. (1.1.2) describes the interaction of charged surfaces across aqueous media well at long distances for low molecular weight mono-, di-, and trivalent counterions. [22, 28, 29] Direct force measurements with colloidal particles using the colloidal probe atomic force microscopy (AFM) [30–34], optical tweezers (OT) [35], and total internal reflection microscopy (TIRM) [36, 37] also confirmed that the electrostatic interactions at long distances are well described by the DLVO potential in eq. (1.1.2). At separations below 1 nm the DLVO theory breaks down in many cases due to effects such as hydration, chemical adsorption, surface roughness, inhomogeneous charge distribution, and counterion correlations. [22, 23, 38, 39]

Furthermore, the studies of Pashley [28] and Kremer and co-workers [35] revealed, that multivalent counterions adsorb to the charged surface. This causes a decrease of the surface charge density σ_d which is not accounted for by the mean-field DLVO theory. The adsorption of multivalent counterions leads to very low values of σ_d and Ψ_d , and induces particle coagulation in dispersions. Under these conditions it is difficult to measure repulsive forces with the established force measurement techniques (see Chapter 1.6). Therefore we utilize the flocculation properties of multivalent counterions on dispersed colloids to propose a new technique for the determination of very weak repulsive forces. This new method now makes a detailed experimental investigation of counterion adsorption possible.

1.1.4. Stability of Colloid Dispersions

A prediction of the stability of the dispersed particles can be made by combining eq. (1.1.2) with the theory for particle motion. [23] The rate constant for coagulation k is defined by the decrease of the singlet particle concentration $[P]$ with the time t according to $d[P]/dt = k[P]^2$. [40] Von Smoluchowski derived the theoretical first order rate constant for binary particle coagulation $k_{11,\text{Sm}}$ by taking Fick's law of diffusion as the basis and assuming monodisperse particles undergoing only thermal motion without acting repulsive forces as [41, 42]

$$k_{11,\text{Sm}} = \frac{4k_{\text{B}}T}{3\eta}. \quad (1.1.4)$$

Here the coagulation of particles is only limited by diffusion, expressed through the viscosity of the medium η . If stabilizing repulsive forces act between the particles, not every

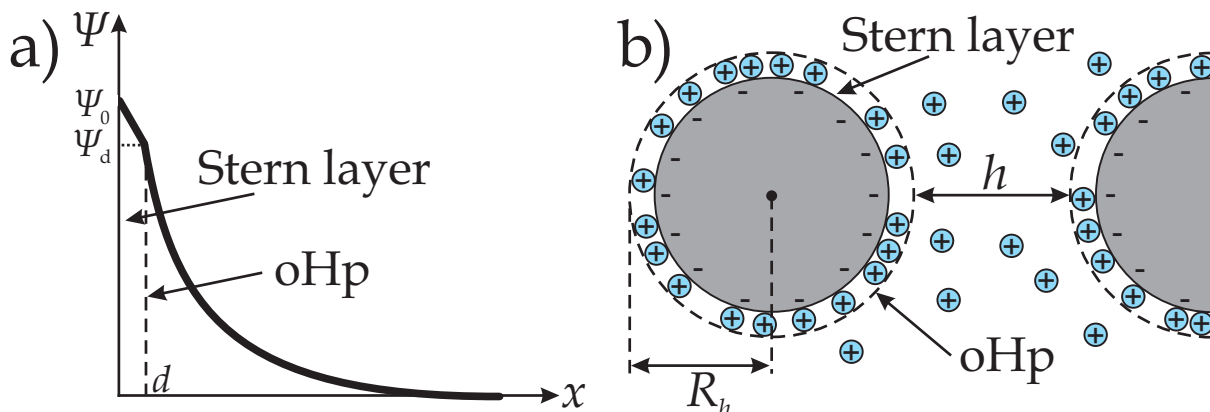


Figure 1.1.2.: (a) Potential of the electric double layer Ψ as a function of the distance from the surface x as proposed by Stern. Many of the counterions adsorb to the surface and form a layer of thickness d in which the ion distribution is not described by the Poisson-Boltzmann theory. The boundary of this layer is the outer Helmholtz plane (oHp) at $x = d$. The diffuse part where the electric double layer is described by the Poisson-Boltzmann theory is located beyond the oHp at $x > d$. The surface potential Ψ_0 at $x = 0$ is screened by the adsorbed counterions in the Stern layer to give the diffuse potential Ψ_d at the oHp. Ψ_d thus determines the properties of the electric double layer in the Stern model. The charge densities corresponding to Ψ_0 and Ψ_d are σ_0 and σ_d , respectively. (b) Measurement of the hydrodynamic radius R_h yields the particle radius including the Stern layer thickness d . The separation distance h is the distance between the oHps of two particles.

approach of two particles results in the formation of a new aggregate. Thus the rate constant $k_{11,\text{Sm}}$ of the fast or diffusion limited colloidal aggregation (DLCA) regime is reduced by a factor W to give the rate constant [23]

$$k_{11,\text{slow}} = \frac{k_{11,\text{Sm}}}{W}. \quad (1.1.5)$$

Hereby, $k_{11,\text{slow}}$ is the rate constant in the reaction limited colloidal aggregation (RLCA) regime and W is the stability ratio. For aggregate formation the thermal energy of the particles must overcome the repulsive forces. Hence, aggregation is an activated process and W becomes accessible via [3]

$$W = 2R \int_0^\infty \exp\left[-\frac{V(h)}{k_B T}\right] (2R + h)^{-2} dh. \quad (1.1.6)$$

The stability of dispersed particles is expressed through W and determined by $V(h)$, which for dispersed charged particles in symmetric electrolytes is the interaction potential of eq. (1.1.2). [19, 20] For low electrolyte concentrations $V(h)$ is repulsive so that $W > 1$, whereas W becomes unity in the DLCA regime, where the van der Waals attraction prevails $V(h)$. This is usually the case at high salt concentrations (Figure 1.1.1b).

Light scattering studies on the stability of model latex particles showed that the aggregation in moderate concentrations of low molecular monovalent salt ions is well described by the DLVO theory. However, at high ionic strength the location of the repulsive peak

becomes less than 1 nm. Then, discrepancies between the DLVO prediction and the experimental results are observed. [43–47] This is mainly attributed to surface heterogeneities, which cause a lower experimental particle stability as compared to the DLVO prediction. [48] However, excluded volume effects and the breakdown of the continuum approach are also held responsible for these discrepancies. [21, 27, 47]

Chapter 3 includes an experimental study and a detailed discussion about the validity of the DLVO theory. Especially the mean-field approach of the DLVO model will be discussed in light of counterion correlations, which can become dominant in the case of multivalent counterions.

1.2. Counterion Correlations

The Poisson-Boltzmann theory regards ions as dimensionless point charges with only Coulomb interactions between the ions in solution and the charged wall. [22, 23] Therefore ions of the same valency are treated equally in the frame of the Poisson-Boltzmann model without regard to their exact chemical nature. However, since the early days of the Poisson-Boltzmann theory experimental studies showed the significant impact of the chemical nature of the counterions on many properties of the charged surface. [21, 49–53] For example, in the case of ions with big organic ligands strong hydrophobic forces cause adsorption onto the charged surface. [50, 54] Excluded volume effects and ion hydration give rise to ion specific effects, which are experimentally classified in terms of the Hofmeister series. [21, 27, 49] Therefore the reasons for deviations from the Poisson-Boltzmann behavior were sought to be chemical in nature for a long time. [50] Since the DLVO theory is based on the Poisson-Boltzmann theory, the same arguments were put forward to explain discrepancies between the predicted DLVO behavior and experimental results.

Newer theoretical models also include ion-ion correlations besides coulombic ion-surface interactions. [55–59] In the case of high surface charge densities and high counterion valency, the solutions of the Poisson-Boltzmann equation predicts an accumulation of the multivalent counterions in the first molecular layer from the charged surface. Here, the high valency leads to lateral interactions between the counterions. These interactions are neglected in the Poisson-Boltzmann approach. [60] Computer simulations showed that ion correlations can cause an overcompensation of the surface charge by multivalent counterions located in the Stern layer. [61, 62] This means that the charge at the oHp σ_d (Figure 1.1.2) reverses its sign relative to the sign of the surface charge σ_0 . This effect is termed inversion of charge or charge reversal. Analytical approaches describe the layer in which correlations arise as a one-component plasma or a Wigner crystal with a charged background, as depicted in Figure 1.2.1. [55, 56] Due to the high order of the counterions inside this strongly correlated liquid, an additional attractive energy results which can induce charge reversal. Charge reversal is observed experimentally for a number of systems. Dispersed charged colloids reverse their direction of motion in an electric field, if the concentration of multivalent counterions is high enough. [63, 64] The force between a charged wall and a colloid can turn from attractive to repulsive in the presence of multivalent counterions. [65, 66] Charge reversal occurs for organic and inorganic

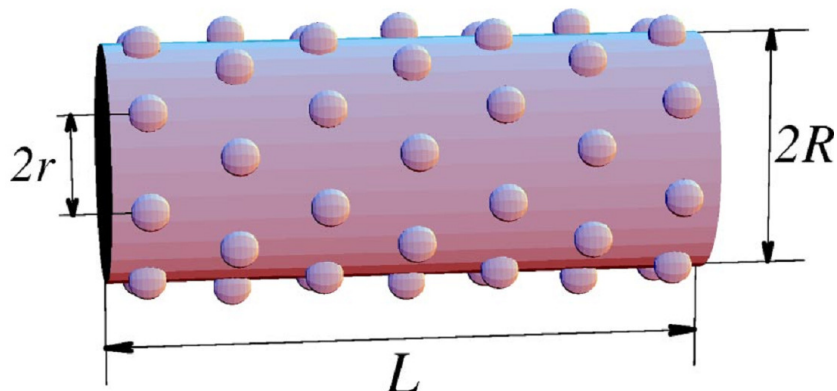


Figure 1.2.1.: Schematic representation of a negatively charged macroion of the length L and the radius R with positively charged counterions. The counterions form a two-dimensional Wigner crystal-like liquid. The highly correlated structure gives rise to an attractive force, which causes overcompensation of the charge of the macroion by its counterions. Therefore the charge at the oHp inverses its sign if the counterion concentration is high enough. This effect is called charge reversal. [74]

colloids [65, 66], planar and curved surfaces [67, 68], and also plays an important role in biological systems. [60, 69–71] However, charge reversal is not limited to multivalent counterions and correlations are not the only driving force. Low molecular weight monovalent counterions with bulky organic ligands induce charge reversal by adsorbing onto the charged surface. [54] Surfaces sensitive to the pH value of the solution can reverse the sign via protonation or deprotonation. [72, 73] Charged polymers adsorb to surfaces beyond the isoelectric point of the system due to binding energies per segment of about $0.7 k_B T$ caused by hydrophobic interactions. Thus correlations are not the driving force for charge reversal in the case of polymeric multivalent counterions. [50] Small ions show the Hofmeister series and can adsorb onto surfaces by covalent bonding and complexation. [50, 51] Therefore it is experimentally challenging to determine counterion correlations as a dominant driving force for charge reversal. Nevertheless, Lyklema and co-workers proved that correlations are responsible for charge reversal at the $MgSO_4$ /mercury interface. [75]

Adsorption of multivalent counterions with low molecular weight occurs in real systems and is not described by the Poisson-Boltzmann and the DLVO theories. The determination of the dominant driving force for adsorption in each system and its impact on the stability of dispersed surface charged particles remains to be addressed in an experimental study. Therefore we investigate counterion adsorption on dispersed colloids in stability (see Chapter 1.4) and electrophoretic mobility (see Chapter 1.5) experiments in this study.

1.3. Spherical Polyelectrolyte Brushes

Polymer brushes are characterized by polymer chains densely tethered to a surface. [77, 78] Hereby, the distance between the grafted chain ends on the surface must be much less

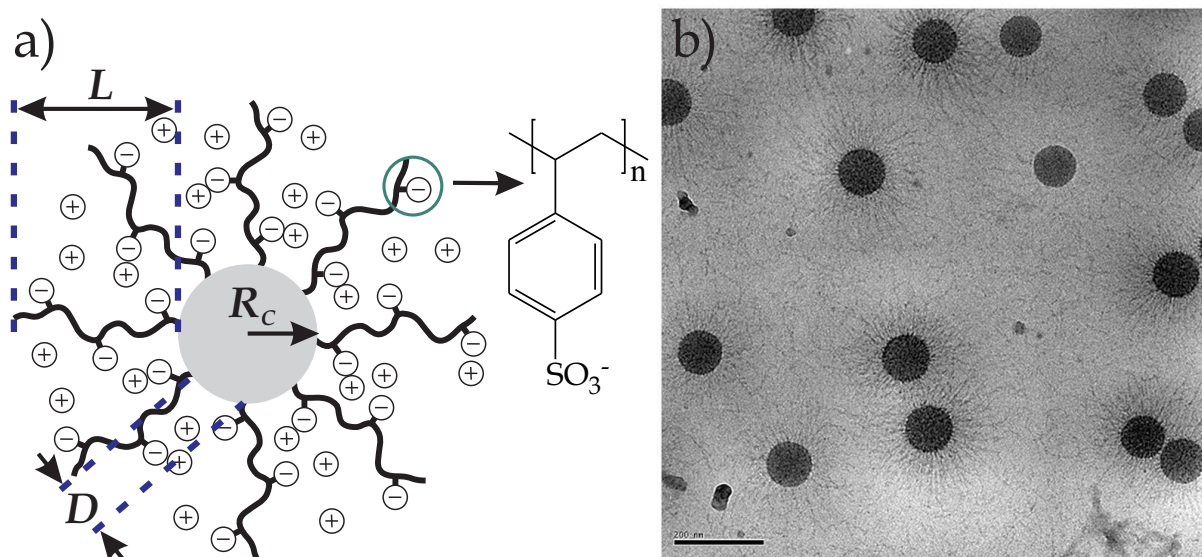


Figure 1.3.1.: (a) Schematic depiction of an anionic spherical polyelectrolyte brush (SPB) including the most important parameters: the radius of the core particle R_c , the hydrodynamic thickness of the shell layer L , and the distance between the grafted chain ends D . (b) Cryo-TEM of SPB particles at low ionic strength. The polyelectrolyte chains are strongly stretched due to the high osmotic pressure inside the shell layers. [76]

than the chains radius of gyration in a good solvent. [79, 80] The properties of such end-constrained polymer chains strongly differ from those of free chains, since the overlapping chains stretch perpendicular away from the surface. [81] The height of the brush layer is determined by the balance between the conformational entropy of the chains and excluded volume effects. [79, 80] In the case of densely grafted charged polymer chains a polyelectrolyte brush results. The polyelectrolyte chains can be grafted onto a planar surface or onto spherical colloidal particles. [82–84] In the latter case a spherical polyelectrolyte brush (SPB) with a curved surface results, which is shown in Figure 1.3.1. [14, 84] In the case of weak electrolytes as building blocks for the polyelectrolytes chains an annealed brush is generated, which is sensitive to the pH value of the aqueous phase. [17] On the contrary, a quenched brush is insensitive to the pH value as the chains consist of strong electrolyte units. [17]

In the scope of this work quenched SPBs with styrenesulfonate as the monomeric chain units are used for the anionic model systems. The synthesis follows the three step synthesis established by Guo and co-workers. [84–86] First, monodisperse core particles are synthesized via an emulsion polymerization of styrene. In a follow-up step, the particles are coated with a thin layer of photoinitiator. In the final reaction step, the particles are immersed in aqueous solution containing the monomers for building the shell layer. By irradiating the dispersion with strong UV light the polyelectrolyte chains are grown from the particle surface via free radical polymerization yielding SPB particles.

A prominent effect of polyelectrolyte brushes is the confinement of the counterions inside the brush layer. This was first predicted by Pincus [87, 88] and later confirmed in experiments [85, 89–91] and computer simulations. [92, 93] Only 2-6 % of the counter-

ons contribute to the osmotic pressure of the bulk solution, while the remaining ions are confined to the brush layers. [94] Computer simulations showed, that the confined counterions are either highly correlated to the polyelectrolyte chains or free inside the brush layer. [92, 93, 95, 96] Depending on the bulk salt concentration, a polyelectrolyte brush exhibits two regimes. In the case of a low bulk ionic strength $I = 1/2 \sum_i z_i^2 c_i$, the high osmotic pressure of the confined counterions inside the brush compared to the bulk leads to a strong stretching of the polyelectrolyte chains. [87] This is called the osmotic regime, where the height of the brush layer L is close to the contour length L_c of the chains and independent of I . However, if I is high enough the osmotic pressure inside the brush layer decreases. As shown in Figure 1.3.2a, in this osmotic regime L scales with the concentration of monovalent counterions outside the brush layer c_s according to $L \propto c_s^{-1/3}$. This relationship was first predicted in theory and later confirmed in experiments for planar brushes and SPBs. [85, 87–89, 91]

A direct consequence of the high osmotic pressure inside the brush layer is the pronounced stability against coagulation of dispersed SPBs. This is due to the fact that a strong osmotic repulsion acts between two SPB particles. [92, 97] In addition, the stretched chains provide steric repulsion. [89, 98] However, this is only the case for monovalent counterions where the SPBs are stable up to salt concentrations of 2 mol/l, shown in Figure 1.3.2a. [85] In multivalent counterion environment the stability of SPBs is dramatically reduced, as depicted in Figure 1.3.2b. [97] The reason for this is an ion exchange of the monovalent with multivalent counterions in the brush layer according to the Donnan equilibrium. [97]

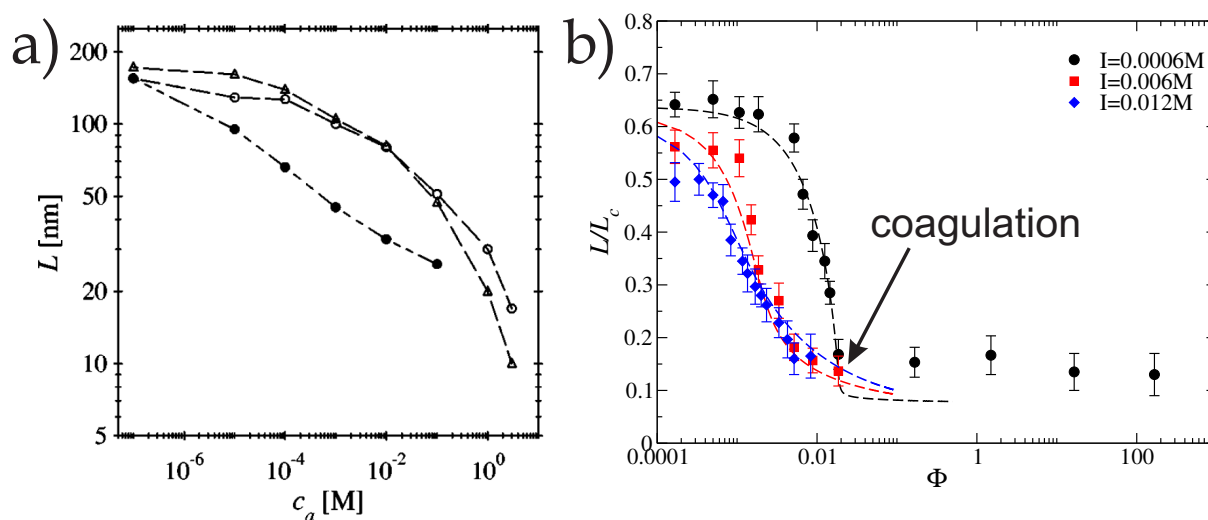


Figure 1.3.2.: (a) Dependence of the hydrodynamic shell thickness L on the concentration of added salt for quenched brushes: KCl (triangles and open circles) and $MgCl_2$ (filled circles). No coagulation occurs in the investigated salt concentration range. [17] (b) Collapse of the normalized shell layer thickness L/L_c (L_c : contour length) with increasing La^{3+} concentration. In each curve the ionic strength I of the dispersions is kept constant. Φ is the concentration ratio between the La^{3+} and Na^+ counterions, $\Phi = c(La^{3+})/c(Na^+)$. After the full shell collapse occurred at high ionic strengths coagulation is observed. [97] The dashed lines are predictions from a mean-field model. [93]

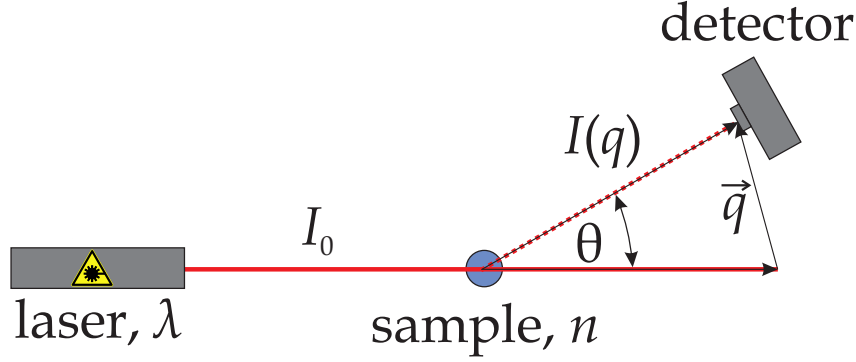


Figure 1.4.1.: Schematic representation of a light scattering device. A laser emits coherent and monochromatic light of the wavelength λ . The sample with the refractive index n of the medium scatters the incoming laser beam of the intensity I_0 . The intensity of the scattered light $I(q)$ is detected and analyzed as a function of the scattering angle θ from which the absolute value of scattering vector \vec{q} follows as $q = 4\pi n/\lambda \sin(\theta/2)$.

The driving force of the ion exchange is a gain in entropy as more monovalent ions are released than multivalent ions are confined. Hereby the electroneutrality of the polyelectrolyte brush layer is maintained. [97] The exchange reduces the total osmotic pressure inside the brush dramatically mainly due to two effects. Firstly, the number of counterions inside the brush decreases according to the ratio of the counterion valency. Secondly, computer simulations showed that the multivalent counterions are strongly correlated to the chains. Therefore the number of osmotically active multivalent counterions in the brush is drastically reduced as compared to the case of monovalent counterions. [92, 93, 97, 99] The polyelectrolyte shell thus collapses at minute concentrations of multivalent counterions, as shown in Figure 1.3.2b. [97, 100]

This makes multivalent counterions effective coagulation agents of dispersed SPBs. After the shell collapse the stability ratio W of the SPBs is only determined by electrostatic repulsions arising from the number of residual charges Q^* inside the polyelectrolyte shell layer. The electrostatic repulsion is predicted by the mean-field model that was used to describe the shell layer collapse in Figure 1.3.2b as well. A comparison between theory and experimental data is still lacking, however, due to the absence of a technique to measure Q^* . To overcome this problem we first established a method to determine W of the SPBs, which is described in the next chapter. The results allowed us to experimentally deduce the repulsive energy of the SPBs within an accuracy of $k_B T$, as presented in Chapter 4. In Chapter 5 we show, that this resolution is high enough to experimentally determine Q^* of the SPBs.

1.4. Stability Measurements of SPB Particles

From the temporal intensity fluctuations of the scattered light $\delta I(t)$ the size of dispersed diluted particles can be determined by photon correlation spectroscopy (PCS), commonly referred to as dynamic light scattering (DLS), in terms of the hydrodynamic radius

R_h . [101] Using static light scattering (SLS) the radius of gyration R_g of the diluted particles is measured from the angle dependent absolute intensity of the scattered light $I(q)$. [102]

Figure 1.4.1 shows a schematic representation of a typical light scattering setup. The mean radius of the particles increases in the case of coagulation, due to the formation of aggregates. Therefore both methods yield information about the stability ratio W of the dispersions in terms of the time dependent growth in size of the scattering centers. However, one cannot determine absolute coagulation rate constants by one of the methods alone, if the particle form factor is unknown. [103] By combining time-resolved static and dynamic light scattering in a simultaneous experiment at an arbitrary scattering vector q , the particle form factor is resolved and one obtains the binary absolute coagulation rate constant k_{11} according to [103]

$$k_{11}[P]_0 = \frac{R_{h,2}}{R_{h,2} - R_{h,1}} \left(\frac{dR_h(t)/dt}{R_h(0)} \right) - \left(\frac{dI(q,t)/dt}{I(q,0)} \right), \quad (1.4.1)$$

where $[P]_0$ is the initial particle concentration, $R_{h,1}$ and $R_{h,2}$ are the hydrodynamic radii of single spheres and doublets, respectively, $R_h(t)$ is the hydrodynamic radius of the particles at a specific time t , and $I(q,t)$ is the angle dependent scattering intensity of the suspension at time t . The doublet hydrodynamic radius is calculated using the equation $R_{h,2} = 1.38R_{h,1}$, as introduced by Borkovec and co-workers. [103] The particle stability in terms of W is then obtained from measurements of k_{11} at electrolyte concentrations in the fast and slow coagulation regime via $W = k_{11,\text{fast}}/k_{11,\text{slow}}$. [23] Simultaneous static and dynamic light scattering is applicable to determine k_{11} in the very beginning of the coagulation process (see Figure 1.4.2) at $[P]_0$ up to $10^{16}/\text{m}^3$. The particle stability can be precisely measured in the range of $1 < W < 10000$, without the knowledge of the particle doublet form factor, e.g. as is the case for SPB doublets.

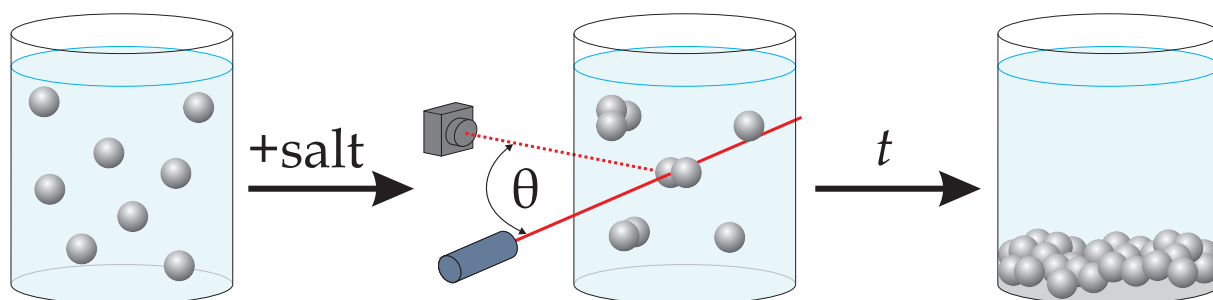


Figure 1.4.2.: In a metastable dispersion instability is induced by the addition of salt. The coagulation process starts with the formation of stable doublets out of the singlet particles. In the early stage of the coagulation process mostly doublets are formed. Here, the coagulation rate constant k_{11} is measured with simultaneous static and dynamic light scattering. After some time t , the formerly dispersed particles eventually form a stable particle phase separated from the aqueous medium, thus concluding the phase transition.

1.5. Electrophoretic Mobility Measurements and ζ Potential

Electrokinetic phenomena appear when a fluid is moving tangential and adjacent to a charged surface. [27] Due to the structure of the electric double layer, the counterions are then partially sheared off and the surface becomes macroscopically charged. [104] The charge at the shear plane is called the electrokinetic charge σ_{ek} and the corresponding potential is the ζ potential, shown in Figure 1.5.1. [104] ζ and σ_{ek} are electrical properties of charged interfaces in steady-state and isothermal conditions. Therefore measurement of ζ and σ_{ek} is one of the classical experiments in colloidal science, since they are closely related to the theories about the electric double layer and electrostatic surface forces. [27] For example, the diffuse potential Ψ_d at the oHp, which describes the double layer repulsion in the DLVO model, is easily accessible through the ζ potential as $\zeta \simeq \Psi_d$ in many cases. [50, 105, 106] Thus the shear plane is located in close proximity to the oHp.

A common method to determine the ζ potential of dispersed colloids is through electrophoresis. [27] During an electrophoresis experiment an applied electric field leads to the motion of the charged dispersed particles and their counterions. [107] The measured quantity is the electrophoretic mobility μ_e . It is defined as the velocity of the moving particles divided by the magnitude of the applied external field (Figure 1.5.1a). Since the magnitude of the applied electric field is known, the velocity and the direction of motion of the particles remains to be determined to give μ_e . Both parameters can be precisely measured by laser Doppler velocimetry. [108]

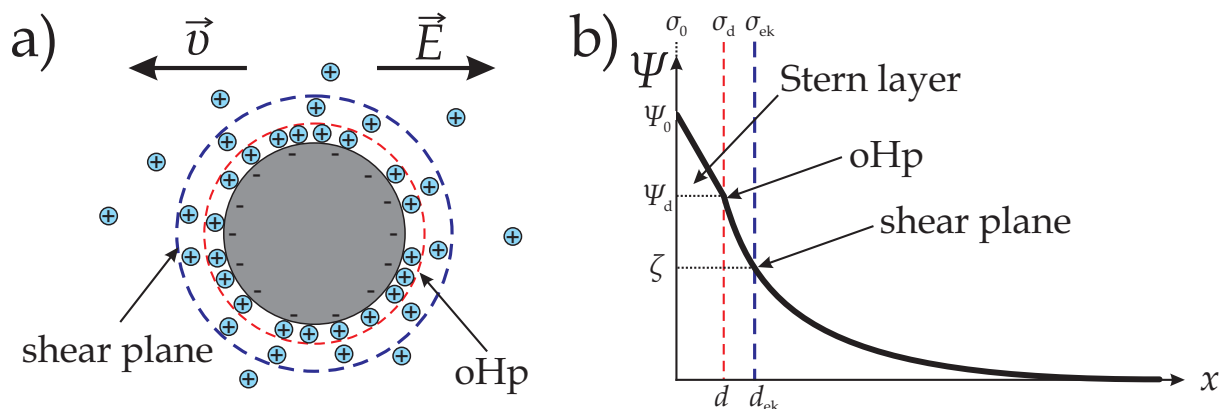


Figure 1.5.1.: (a) Schematic representation of a negatively charged model colloid with its counterions immersed in aqueous solution and the corresponding potential curve. The applied electric field \vec{E} causes the charged colloid with the surface potential Ψ_0 to move along the velocity vector \vec{v} . All counterions beyond the shear plane at the distance $x = d_{ek}$ move in the opposite direction relative to the center particle. Therefore these counterions are sheared off from the electric double layer of the colloid, generating a potential at the plane of shear. (b) This potential is called the electrokinetic or ζ potential. The shear plane is located further away but close to the outer Helmholtz plane (oHp) at $x = d$, which marks the extend of the Stern layer and the beginning of the diffuse part of the electric double layer. Thus the ζ potential is smaller than the diffuse potential Ψ_d . [104]

The conversion of μ_e into ζ potentials can be performed with various models as discussed in an IUPAC report. [104] In this work we always use the O'Brien and White model, which accounts for conduction in the diffuse layer and polarization effects of the ion cloud, for converting the measured μ_e values into ζ potentials. [107, 109]

1.6. Force Measurements - a Comparison

The measurement of forces between surfaces and colloidal particles is crucial for investigating dispersed systems and the adhesion of films. Several techniques are available for determining these surface forces. [110] Here, a brief overview of today's most common methods and their limitations is given.

The surface forces apparatus (SFA) was designed by Israelachvili to measure forces across liquid media with a high accuracy. [111] Possible surface modifications include surfactant bilayers, protein layers and polymer brushes. [89, 112, 113] However, due to its setup the SFA is limited to planar surfaces. The distance between the surfaces is measured on a sub nanometer range by multiple-beam interference fringes. One surface is attached to a cantilever. In the case of surface interactions the amount and sign of the acting force between the surfaces can be determined via Hooke's law. Therefore experiments with the SFA yield force-distance curves with a separation accuracy in the sub nanometer range and a force resolution of about $0.5 \mu\text{N}/\text{m}$. [111]

Recently, colloidal probe atomic force microscopy (AFM) has become a common method to measure the forces between a colloid particle and another surface. [110] The other surface can either be a planar surface or a colloidal particle. The setup allows for a variety of surface modifications. However, the process of attaching the colloidal probe to the AFM tip involves the use of a light microscope. Thus the resolution of the microscope gives the lower size limit of the colloidal probe. Similar to the SFA, the colloidal probe is attached to a cantilever. The separation between the surfaces is calculated relative to a hard wall. [114] From the distance measured within 1 nm accuracy one can calculate the interaction force within 20 pN/m as a function of the surface separation using Hooke's law. [115]

Total internal reflection microscopy (TIRM) uses the scattering intensity from an evanescent wave to determine the distance between dispersed colloidal particles and a surface. The potential energy, which contains mainly gravitational forces, can be determined if the particles and the surface repel each other. This is done by monitoring the separation between the particles and the flat surface over a sufficiently long time. The probability of finding a particle at any given separation is determined by the Boltzmann distribution, so that the potential can be calculated as a function of the distance. The measurements of the repulsive energy are accurate in the order of $k_B T$. However, the particles must be large and dense enough to exhibit a pronounced potential energy relative to the particle-wall repulsion. [116]

Optical tweezers (OT) can be used for direct force measurements between a colloid pair confined by two laser beams. Dispersed styrene based particles are held in the middle of a laser beam by a photonic potential. In the case of interactions the particles are

displaced out of the equilibrium positions in the photonic potential. Since the strength of the confining photonic potential is known, force vs. distance curves are obtained by quantitatively analyzing the displacement of the particles via microscopic video imaging techniques. Thus the lower limit of the particle dimensions is determined by the size resolution of the imaging technique. For large enough particles the resolution of the OT is about ± 6 nm in regard to the separation and ± 0.5 pN for the force measurements. [35, 115]

Israelachvili and co-workers showed that direct force measurements using the SFA quantitatively predict particle-particle interactions in stable colloid dispersions deduced from static light scattering experiments. [117] However, a technique to measure the interactions of small colloids undergoing coagulation has not been established yet.

1.7. Objective of this Thesis

The repulsive energies between colloidal particles determine the stability of the dispersion. For many industrial and scientific applications colloidal stability is the most important parameter in need of control. Therefore this thesis focuses on the development of a method suited to measure inter particle repulsions between dispersed colloids with various surface modifications. In particular, the main goal of this thesis is to measure the repulsive energies of dispersed SPB particles in the presence of multivalent counterions. For this we use simultaneous static and dynamic light scattering to investigate the aggregation kinetics of SPBs. By combining the light scattering data with SFA measurements we propose for the first time a method to determine repulsive interactions between colloids in the order of magnitude of $k_B T$. The experimental data is then compared to the predictions of a mean-field model. This line of reasoning yields insights in the driving force of the destabilization of the SPBs through the adsorption of multivalent counterions.

In addition the interactions of surface charged colloids are studied in terms of the repulsive energies of the electric double layer interactions and their electrokinetic potential. The experiments are performed in the presence of low molecular weight counterions of different valency. The comparison between these quantities then leads to new insights about the impact of counterion adsorption on the stability of electrostatically stabilized particles and the validity of the DLVO approach.

1.8. References

- [1] Faraday, M. *Philos. Trans. R. Soc. London* **1857**, 147, 145.
- [2] Turkevich, J.; Stevenson, P. C.; Hillier, J. *Discuss. Faraday. Soc.* **1951**, 11, 55.
- [3] Lyklema, J. *Fundamentals of Interface and Colloid Science*, 1st ed.; Elsevier: Amsterdam, 2005; Vol. 4.
- [4] Mokrushin, S. G. *Nature* **1962**, 195, 861.

- [5] Mie, G. *Ann. d. Phys.* **1908**, *25*, 377.
- [6] van de Hulst, H. C. *Light scattering by small particles*, 1st ed.; Dover Publications: Mineola, 1981.
- [7] Tadros, T. F. *Colloids and Interface Science Series*, 1st ed.; Wiley-VCH:Weinheim, 2008; Vol. 4.
- [8] Tadros, T. F. *Colloids and Interface Science Series*, 1st ed.; Wiley-VCH:Weinheim, 2010; Vol. 6.
- [9] Ghosh, S. K. *Functional Coatings*, 1st ed.; Wiley-VCH: Weinheim, 2006.
- [10] Dickinson, E. *Soft Matter* **2006**, *2*, 642.
- [11] Purchas, D. B. *Handbook of Water Purification*, 2nd ed.; Wiley-VCH: New York, 1987.
- [12] Bourgeat-Lami, E. *J. Nanosci. Nanotechnol.* **2002**, *2*, 1.
- [13] Shipway, A. N.; Katz, E.; Willner, I. *Chem. Phys. Chem.* **2000**, *1*, 18.
- [14] Ballauff, M. *Prog. Polym. Sci.* **2007**, *32*, 1135.
- [15] Schrunner, M.; Ballauff, M.; Talmon, Y.; Kauffmann, Y.; Thun, J.; Möller, M.; Breu, J. *Science* **2009**, *323*, 617.
- [16] Henzler, K.; Haupt, B.; Lauterbach, K.; Wittemann, A.; Borisov, O.; Ballauff, M. *J. Am. Chem. Soc.* **2010**, *132*, 3159.
- [17] Guo, X.; Ballauff, M. *Phys. Rev. E* **2001**, *64*, 051406.
- [18] Lyklema, J. *Fundamentals of Interface and Colloid Science*, 1st ed.; Elsevier: Amsterdam, 2005; Vol. 1-4.
- [19] Derjaguin, B. V.; Landau, L. D. *Acta Physicochim. USSR* **1941**, *14*, 633.
- [20] Verwey, E. J. W.; Overbeek, J. Th. G. *Theory of the stability of lyophobic colloids*, 1st ed.; Elsevier: Amsterdam, 1948.
- [21] Ninham, B. W. *Adv. Colloid Interface. Sci.* **1999**, *83*, 1.
- [22] Israelachvili, J. N. *Intermolecular and Surface Forces*, 2nd ed.; Academic Press: New York, 1998.
- [23] Evans, D. F.; Wennerström, H. *The Colloidal Domain*, 2nd ed.; Wiley-VCH: New York, 1999.
- [24] Hamaker, H. C. *Physica* **1937**, *4*, 1058.
- [25] Grahame, D. C. *Chem. Revs.* **1947**, *41*, 441.

-
- [26] Stern, O. *Z. Electrochem.* **1924**, *30*, 508.
- [27] Lyklema, J. *Fundamentals of Interface and Colloid Science*, 1st ed.; Elsevier: Amsterdam, 2005; Vol. 2.
- [28] Pashley, R. M. *J. Colloid Interface Sci.* **1984**, *102*, 23.
- [29] Meyer, E. E.; Rosenberg, K. J.; Israelachvili, J. N. *Proc. Natl. Acad. Sci. U.S.A.* **2006**, *103*, 15739.
- [30] Ducker, W. A.; Senden, T. J.; Pashley, R. M. *Nature* **1991**, *353*, 239.
- [31] Bosio, V.; Dubreuil, F.; Bogdanovic, G.; Fery, A. *Colloids Surf. A* **2004**, *243*, 147.
- [32] Butt, H. J.; Cappella, B.; Kappl, M. *Surf. Sci. Rep.* **2005**, *59*, 1.
- [33] Rentsch, S.; Pericet-Camara, R.; Papastavrou, G.; Borkovec, M. *Phys. Chem. Chem. Phys.* **2006**, *8*, 2531.
- [34] Pericet-Camara, R.; Papastavrou, G.; Borkovec, M. *Macromolecules* **2009**, *42*, 1749.
- [35] Gutsche, C.; Keyser, U. F.; Kegler, K.; Kremer, F.; Linse, P. *Phys. Rev. E* **2007**, *76*, 031403.
- [36] Prieve, D. C. *Adv. Colloid Interface Sci.* **1999**, *82*, 93.
- [37] Liebert, R. B.; Prieve, D. C. *Biophys. J.* **1995**, *69*, 66.
- [38] Israelachvili, J. N.; Pashley, R. M. *Nature* **1983**, *306*, 249.
- [39] Ducker, W. A.; Xu, Z.; Clarke, D. R.; Israelachvili, J. N. *J. Am. Ceram. Soc.* **1994**, *77*, 437.
- [40] Elimelech, M.; van Zanten, J. H. *J. Colloid Interface Sci.* **1992**, *154*, 1.
- [41] von Smoluchowski, M. *Phys. Z.* **1916**, *17*, 557.
- [42] von Smoluchowski, M. *Z. Phys. Chem.* **1917**, *92*, 129.
- [43] Behrens, S. H.; Borkovec, M.; Schurtenberger, P. *Langmuir* **1998**, *14*, 1951.
- [44] Behrens, S. H.; Borkovec, M. *J. Phys. Chem. B* **1999**, *103*, 2918.
- [45] Behrens, S. H.; Christl, D. I.; Emmerzael, R.; Schurtenberger, P.; Borkovec, M. *Langmuir* **2000**, *16*, 2566.
- [46] Fritz, G.; Schädler, V.; Willenbacher, N.; Wagner, N. J. *Langmuir* **2002**, *18*, 6381.
- [47] Hanus, L.; Hartzler, R.; Wagner, N. *Langmuir* **2001**, *17*, 3136.
- [48] Walz, J. Y. *Adv. Colloid Interface Sci.* **1998**, *74*, 119.

- [49] Lyklema, J. *Adv. Colloid Interface Sci.* **2003**, 100-102, 1.
- [50] Lyklema, J. *Colloids Surf. A* **2006**, 291, 3.
- [51] Lyklema, J. *Adv. Colloid Interface Sci.* **2009**, 147-148, 205.
- [52] Peula-García, J. M.; Ortega-Vinuesa, J. L.; Bastos-González, D. *J. Phys. Chem.* **2010**, 114, 11133.
- [53] Schwierz, N.; Horinek, D.; Netz, R. R. *Langmuir* **2010**, 26, 7370.
- [54] Martín-Molina, A.; Rodríguez-Beas, C.; Hidalgo-Álvarez, R.; Quesada-Pérez, M. *Soft Matter* **2009**, 5, 1350.
- [55] Shklovskii, B. I. *Phys. Rev. E* **1999**, 60, 5802.
- [56] Levin, Y. *Rep. Prog. Phys.* **2002**, 65, 1577.
- [57] Levin, Y.; Arenzon, J. J. *J. Phys. A: Math. Gen.* **2003**, 36, 5857.
- [58] Martín-Molina, A.; Maroto-Centeno, J. A.; Hidalgo-Álvarez, R.; Quesada-Pérez, M. *J. Chem. Phys.* **2006**, 125, 144906.
- [59] Diehl, A.; Levin, Y. *J. Chem. Phys.* **2006**, 125, 054902.
- [60] Nguyen, T. T.; Rouzina, I.; Shklovskii, B. I. *J. Chem. Phys.* **2000**, 112, 2562.
- [61] Martín-Molina, A.; Maroto-Centeno, J. A.; Hidalgo-Álvarez, R.; Quesada-Pérez, M. *Colloids Surf. A* **2008**, 319, 103.
- [62] Labbez, C.; Jönsson, B.; Skarba, M.; Borkovec, M. *Langmuir* **2009**, 25, 7209.
- [63] Martín-Molina, A.; Quesada-Pérez, M.; Galisteo-González, F.; Hidalgo-Álvarez, R. *J. Chem. Phys.* **2003**, 118, 4183.
- [64] Martín-Molina, A.; Quesada-Pérez, M.; Galisteo-González, F.; Hidalgo-Álvarez, R. *J. Phys.: Condens. Matter* **2003**, 15, 3475.
- [65] Besteman, K.; Zevenbergen, M. A. G.; Heering, H. A.; Lemay, S. G. *Phys. Rev. Lett.* **2004**, 93, 170802.
- [66] Besteman, K.; Zevenbergen, M. A. G.; Lemay, S. G. *Phys. Rev. E* **2005**, 72, 061501.
- [67] Pashley, R. M. *J. Colloid Interface Sci.* **1984**, 102, 23.
- [68] van der Heyden, F. H. J.; Stein, D.; Besteman, K.; Lemay, S. G. L.; Dekker, C. *Phys. Rev. Lett.* **2006**, 96, 224502.
- [69] Allahyarov, E.; Löwen, H.; Gompper, G. *Phys. Rev. E* **2003**, 68, 061903.
- [70] Besteman, K.; van Eijk, K.; Lemay, S. G. *Nature* **2007**, 3, 641.

-
- [71] García-Giménez, E.; Alcaraz, A.; Aguilera, V. M. *Phys. Rev. E* **2010**, *81*, 021912.
- [72] Allen, L. H.; Matijević, E. *J. Colloid Interface Sci.* **1969**, *31*, 287.
- [73] Elimelech, M.; O'Melia, C. R. *Colloids Surf.* **1990**, *44*, 165.
- [74] Zhang, R.; Shklovskii, B. I. *Phys. Rev. E* **2004**, *69*, 021909.
- [75] Wernersson, E.; Kjellander, R.; Lyklema, J. *J. Phys. Chem. C.* **2010**, *114*, 1849.
- [76] Wittemann, A.; Drechsler, M.; Talmon, Y.; Ballauff, M. *J. Am. Chem. Soc.* **2005**, *127*, 9688.
- [77] Milner, S. T. *Science* **1991**, *251*, 905.
- [78] Dukes, D.; Li, Y.; Lewis, S.; Benicewicz, B.; Schadler, L.; Kumar, S. K. *Macromolecules* **2010**, *43*, 1564.
- [79] Alexander, S. *J. Phys. (Paris)* **1977**, *38*, 983.
- [80] de Gennes, P. *Macromolecules* **1980**, *13*, 1069.
- [81] Halperin, A.; Tirrell, M.; Lodge, T. P. *Adv. Colloid Interface Sci.* **1992**, *100*, 31.
- [82] Konradi, R.; Rühle, J. *Macromolecules* **2005**, *38*, 4345.
- [83] Li, F.; Balastre, M.; Schorr, P.; Argillier, J.-F.; Yang, J.; Mays, J. W.; Tirrell, M. *Langmuir* **2006**, *22*, 4084.
- [84] Guo, X.; Weiss, A.; Ballauff, M. *Macromolecules* **1999**, *32*, 6043.
- [85] Guo, X.; Ballauff, M. *Langmuir* **2000**, *16*, 8719.
- [86] Schrunner, M.; Haupt, B.; Wittemann, A. *Chem. Eng. J.* **2008**, *144*, 138.
- [87] Pincus, P. *Macromolecules* **1991**, *24*, 2912.
- [88] Borisov, O. V.; Birshstein, T. M.; Zhulina, E. B. *J. Phys. II (Fr.)* **1991**, *1*, 521.
- [89] Balastre, M.; Li, F.; Schorr, P.; Yang, J.; Mays, J. W.; Tirrell, M. V. *Macromolecules* **2002**, *35*, 9480.
- [90] Dingenouts, N.; Patel, M.; Rosenfeldt, S.; Pontoni, D.; Narayanan, T.; Ballauff, M. *Macromolecules* **2004**, *37*, 8152.
- [91] Dunlop, I. E.; Briscoe, W. H.; Titmuss, S.; Jacobs, R. M. J.; Osborne, V. L.; Edmondson, S.; Huck, W. T. S.; Klein, J. *J. Phys. Chem. B* **2009**, *113*, 3947.
- [92] Jusufi, A.; Likos, C. N.; Ballauff, M. *Colloid Polym. Sci.* **2004**, *282*, 910.
- [93] Mei, Y.; Hoffmann, M.; Ballauff, M.; Jusufi, A. *Phys. Rev. E.* **2008**, *77*, 031805.

- [94] Das, B.; Guo, X.; Ballauff, M. *Prog. Colloid Polym. Sci.* **2002**, *121*, 34.
- [95] Jusufi, A.; Likos, C. N.; Löwen, H. *Phys. Rev. Lett.* **2002**, *88*, 018301.
- [96] Jusufi, A.; Likos, C. N.; Löwen, H. *J. Chem. Phys.* **2002**, *116*, 11011.
- [97] Mei, Y.; Lauterbach, K.; Hoffmann, M.; Borisov, O. V.; Ballauff, M.; Jusufi, A. *Phys. Rev. Lett.* **2006**, *97*, 158301.
- [98] Napper, D. H. *Polymeric Stabilization of Colloidal Dispersions*, 3rd ed.; Academic Press: London, 1989.
- [99] Jusufi, A. *J. Chem. Phys.* **2006**, *124*, 044908.
- [100] Ishikubo, A.; Mays, J. W.; Tirrell, M. *Polym. Prepr.* **2005**, *46*, 27.
- [101] Berne, B. J.; Pecora, R. *Dynamic Light Scattering*, 1st ed.; Dover Publications: Mineola, 2000.
- [102] Brown, W. *Light Scattering*, 1st ed.; Oxford University Press: New York, 1996.
- [103] Holthoff, H.; Egelhaaf, S. U.; Borkovec, M.; Schurtenberger, P.; Stricher, H. *Langmuir* **1996**, *12*, 5541.
- [104] Delgado, A. V.; González-Caballero, F.; Hunter, R. J.; Koopal, L. K.; Lyklema, J. *J. Colloid Interface Sci.* **2007**, *309*, 194.
- [105] Lyklema, J. *Curr. Opin. Colloid Interface Sci.* **2010**, *15*, 125.
- [106] Smith, A. I. *J. Colloid Interface Sci.* **1976**, *55*, 525.
- [107] O'Brien, R. W.; White, L. R. *J. Chem. Soc. Faraday Trans II* **1978**, *2*, 1607.
- [108] Kobayashi, M. *Colloid Polym. Sci.* **2008**, *286*, 935.
- [109] Hunter, R. J. *Adv. Colloid Interface Sci.* **2003**, *100-102*, 153.
- [110] Claesson, P. M.; Ederth, T.; Bergeron, V.; Rutland, M. W. *Adv. Colloid Interface Sci.* **1996**, *67*, 119.
- [111] Israelachvili, J. N.; Adams, G. E. *J. Chem. Soc., Faraday Trans. I* **1978**, *74*, 975.
- [112] Stiernstedt, J.; Froberg, J. C.; Tiberg, F.; Rutland, M. W. *Langmuir* **2005**, *21*, 1875.
- [113] Marra, J.; Israelachvili, J. *Biochemistry* **1985**, *24*, 4608.
- [114] Popa, I.; Papastavrou, G.; Borkovec, M. *Phys. Chem. Chem. Phys.* **2010**, *12*, 4863.
- [115] Elmahdy, M. M.; Drechsler, A.; Gutsche, C.; Synytska, A.; Uhlmann, P.; Kremer, F.; Stamm, M. *Langmuir* **2009**, *25*, 12894.

- [116] Prieve, D. C; Frej, N. A. *Langmuir* **1990**, *6*, 396.
- [117] Gee, M. L.; Tong, P.; Israelachvili, J. N.; Witten, T. A. *J. Chem. Phys.* **1990**, *93*, 6057.

2. Overview

The main objective of this thesis was to establish an experimental technique to measure the repulsion between dispersed colloidal particles. The technique was based on the measurement of particle stability with simultaneous static and dynamic light scattering and named microsurface potential measurements (MSPM). The publication presented in Chapter 3 outlines the MSPM on surface charged particles at salt concentrations close to the charge reversal concentration. A comparison of the MSPM data with the experimental results of electrophoretic mobility measurements gave new insights into the impact of counterion adsorption on colloidal stability.

The publication presented in Chapter 4 describes the MSPM on SPB particles in multivalent counterion environment. The interaction profile of planar polyelectrolyte brushes in the presence of multivalent counterions was experimentally determined using the surface forces apparatus (SFA). The resulting interaction profile could be described by a simple interaction model. Therefore we were able to apply MSPM on dispersed SPB particles. By these means the effective charge of the SPB particles as a function of the salt concentration was determined. Furthermore, the experimental results were compared to the prediction of a mean-field model.

The publication presented in Chapter 5 follows up on the results of the work outlined in Chapter 4. Here, the theoretical basis of the MSPM on SPB particles in multivalent counterion environment was refined and the experimental resolution was improved. Additionally, the form factor of SPB doublets was investigated and compared to the established Rayleigh-Debye model. For the first time, the mean-field model was used to successfully predict the stability of the SPB particles.

This doctoral thesis comprises three publications given in the Chapters 3, 4, and 5.

2.1. Interaction of Colloidal Particles: the DLVO Potential and Charge Inversion

We investigated the impact of counterion adsorption on the stability of colloidal polystyrene particles with sulfonate surface charges. Similar particles have been successfully used in stability and electrophoretic mobility experiments in other studies. [1, 2]

First, we performed measurements of the rate constant of coagulation as a function of the electrolyte concentration with KCl, MgCl₂, and LaCl₃ as electrolytes. The absolute coagulation rate constants were determined using static and dynamic light scattering in the slow and fast coagulation regime. [1] Therefore the stability ratio at every electrolyte concentration was accessible (Figure 2.1.1a and 2.1.1c). We then deduced the diffuse potential Ψ_d of the particles from the data with the di- and trivalent counterions via the

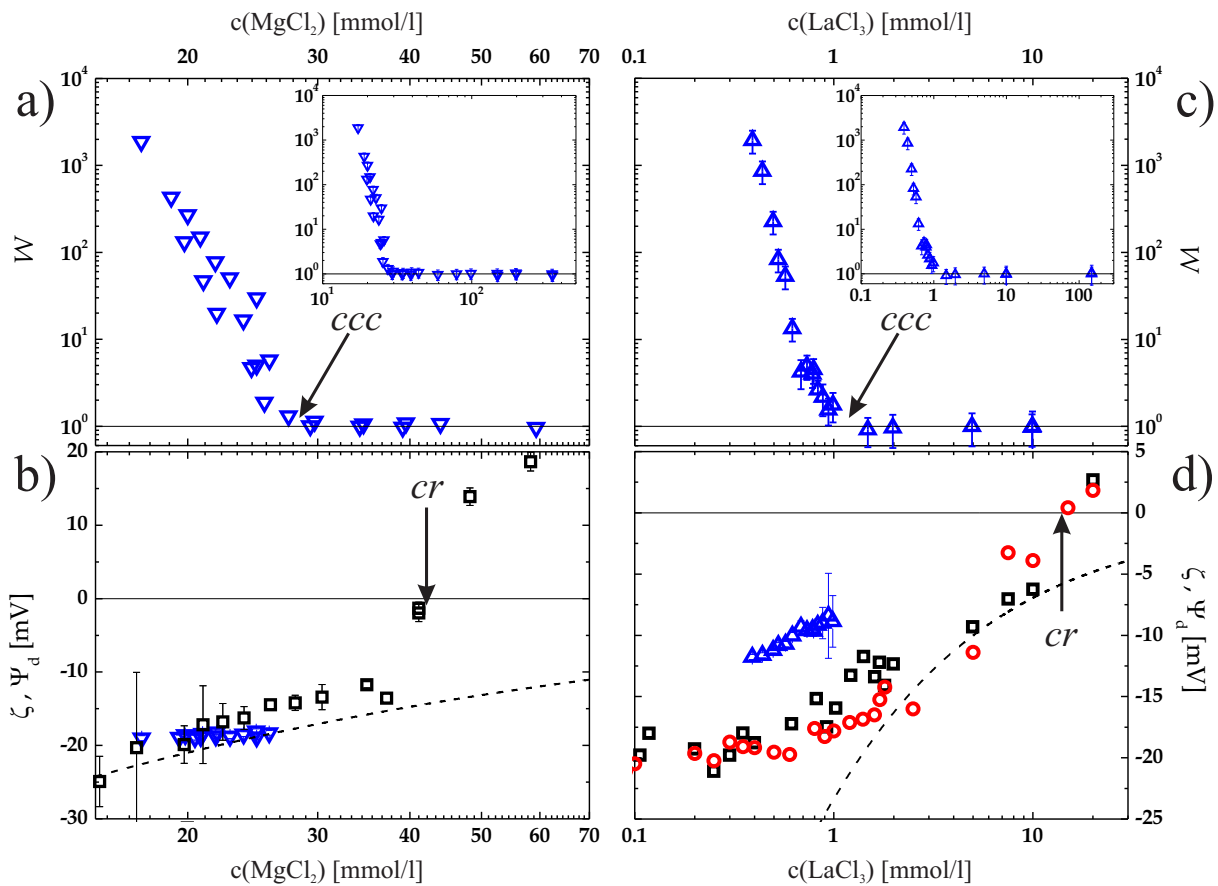


Figure 2.1.1.: Stability ratio W of the anionic particles as a function of the Mg²⁺ (a) and La³⁺ (c) concentration. Experimental data points are indicated by triangles. The insets show the complete data range of W . From the stability data in the slow coagulation regime we fit the respective values of $\Psi_d(c)$. In (b) and (d) the values of Ψ_d (triangles) are compared to the measured ζ potentials (squares and circles). The ζ potential data reveal that in both cases charge reversal cr of the anionic particles occur at concentrations higher than the critical coagulation concentration ccc . The dotted lines indicate the results calculated according to solutions of the Poisson-Boltzmann theory for a constant surface charge density.

microsurface potential measurements (MSPM) shown in Figure 2.1.1b and 2.1.1d. To complement the results of the MSPM and expand the electrolyte concentration range, electrophoretic mobility measurements were performed to determine the ζ potential. [3] The ζ potential data for the monovalent K^+ counterions indicated no charge reversal and were accurately described by the Poisson-Boltzmann theory. However, the ζ potential measurements with the Mg^{2+} and La^{3+} counterions showed charge reversal of the anionic colloids (Figure 2.1.1b and 2.1.1d). The charge density σ_d , which determines the electric double layer, was not constant in regard to the counterion concentration and thus was not described by the Poisson-Boltzmann theory. The comparison between the values of Ψ_d and ζ for the di- and trivalent counterions revealed, that ζ is of the same magnitude as Ψ_d in the Mg^{2+} experiments. However, in the La^{3+} experiments the absolute values of ζ exceeded the values of the diffuse potential Ψ_d . Thus ζ is not a proper indicator of the particle stability in the experiments with trivalent counterions. This finding contradicts the established relationship between ζ and the diffuse potential [4], and may be an experimental indication of counterion correlations. [5, 6] For the first time, we showed the strong impact of adsorption of low molecular weight counterions on the stability of surface charged particles.

The full publication can be found in Chapter 3.

2.2. Microsurface Potential Measurements: Repulsive Forces between Polyelectrolyte Brushes in the Presence of Multivalent Counterions

For the first time we applied microsurface potential measurements (MSPM) on dispersed SPB particles in the presence of La^{3+} counterions. As a SPB model system we used an anionic quenched poly(styrenesulfonate) brush.

The force between two planar poly(styrenesulfonate) brush layers was measured as a function of the distance in aqueous medium containing La^{3+} counterions using the surface forces apparatus (SFA) (Figure 2.2.1a). At large separations the interaction curve is dominated by a repulsion of purely electrostatic origin. However, upon contact of the shell layers an attractive force caused a jump-in of the surfaces. Due to the absence of steric repulsion at large separations we concluded that the polyelectrolyte brush layers are fully collapsed.

On the basis of the measured force curves, an interaction potential profile for dispersed SPB particles with fully collapsed shell layers was proposed (Figure 2.2.1b). The most important variable is the maximum of the repulsive interaction potential termed prefactor A .

The stability was determined via simultaneous static and dynamic light scattering in terms of the stability ratio W as a function of the La^{3+} concentration, plotted in Figure 2.2.2a. [1] From the stability data, we deduced the values of A in units of $k_B T$ using the interaction potential of SPB particles with collapsed shell layers shown in Figure 2.2.1b. The results of A are shown in Figure 2.2.2b. Due to a more pronounced saturation of the polyelectrolyte shell layers with trivalent counterions the prefactor A is decreasing with increasing lanthanum concentration. Furthermore, the experimental data was compared to the prediction of a mean-field model, that has been described in detail previously. [7]

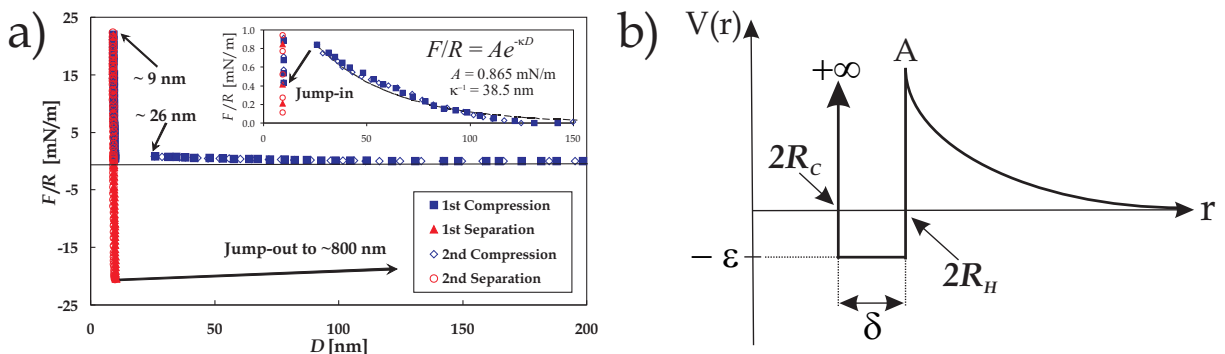


Figure 2.2.1.: (a) Measurement of forces between two planar polyelectrolyte brushes (PtBS₁₅-LaPSS₄₃₈) adsorbed onto hydrophobic cylindrical surfaces using the SFA. The counterions in the brushes are La^{3+} ions and the added salt is 0.06 mM $\text{La}(\text{NO}_3)_3$. The height of the two compressed planar brush layers is 9 nm, which corresponds to the parameter δ in the spherical brush system. (b) Interaction potential of the SPB particles in the aqueous lanthanum solutions used in our study.

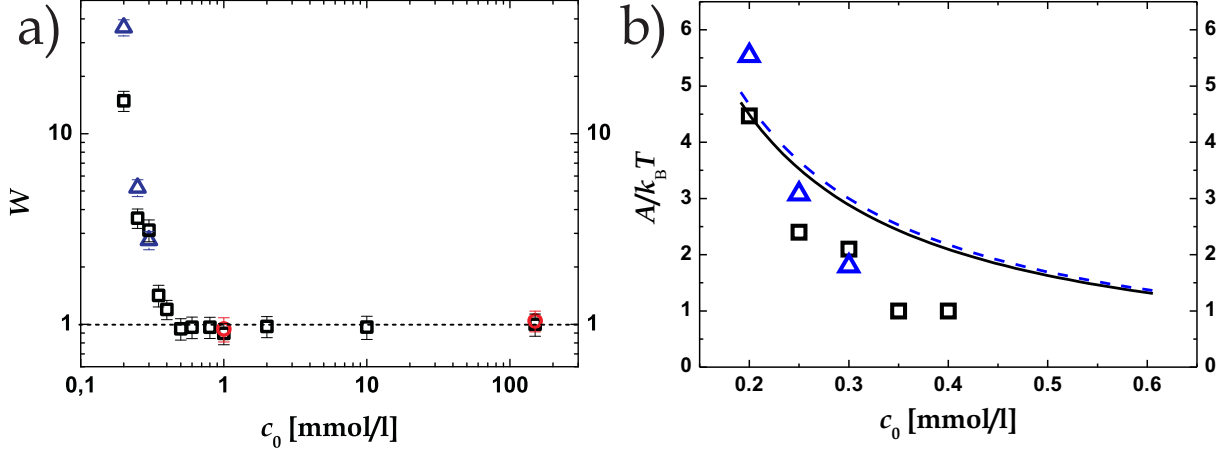


Figure 2.2.2.: (a) Stability ratio W of the SPB as a function of the lanthanum concentration c_0 for different SPB number concentrations $[P]_0$. (b) Prefactor A as a function of the salt concentration c_0 of LaCl_3 for different $[P]_0$. In both plots $[P]_0$ is: $1.23 \times 10^{15} \text{ m}^{-3}$ (triangles); $1.64 \times 10^{14} \text{ m}^{-3}$ (squares); $8.20 \times 10^{13} \text{ m}^{-3}$ (circles). The lines are the predictions from the mean-field theory for the same SPB concentrations $[P]_0$: $1.23 \times 10^{15} \text{ m}^{-3}$ (broken line); $1.64 \times 10^{14} \text{ m}^{-3}$ (solid line).

The good agreement between the mean-field model and the experimental data is shown in Figure 2.2.2b. Therefore we demonstrated for the first time that the repulsive energy between SPB particles can be measured within an accuracy of $k_B T$. Furthermore, the prefactor A of the SPB particles was well described by the prediction of the mean-field model.

The full publication can be found in Chapter 4.

2.3. Investigation of the Stability Behavior of Anionic Spherical Polyelectrolyte Brushes in the Presence of La(III) Counterions

After successfully establishing the microsurface potential measurements (MSPM) for SPB particles (see Chapter 4), we improved the procedure in regard to a refined theoretical basis and an enhanced experimental resolution. An anionic poly(styrenesulfonate) SPB in aqueous solution containing multivalent counterions was used as a model system.

The MSPM were performed as described in Chapter 4. However, the underlying theory of the MSPM was improved in three important points. Firstly, we used a more accurate expression to correct for the hydrodynamic drag between two approaching particles during the doublet formation process. Secondly, retardation effects in the van der Waals interaction of the SPB core particles were considered, and thirdly, we assigned very weak van der Waals interactions to the collapsed polyelectrolyte shell layers.

Using simultaneous static and dynamic light scattering we measured $dR_h(t)/dt$ and $dI(t)/dt$ for different scattering angles θ . This provided information about the form factor of the SPB particle doublets as a function of θ . [1] We compared the experimental data of the soft sphere SPB doublets to the prediction of the Rayleigh-Debye theory for hard spheres. Figure 2.3.1 reveals, that the Rayleigh-Debye approximation describes the experimental data well only at low values of θ .

The stability ratio W of the SPB particles was obtained via simultaneous static and dynamic light scattering at a scattering angle of 90° (Figure 2.3.2a). The maximum of the interaction potential termed V_{max} was deduced from the W data with an accuracy in the order of magnitude of $k_B T$. The resulting values of V_{max} are plotted in Figure 2.3.2b.

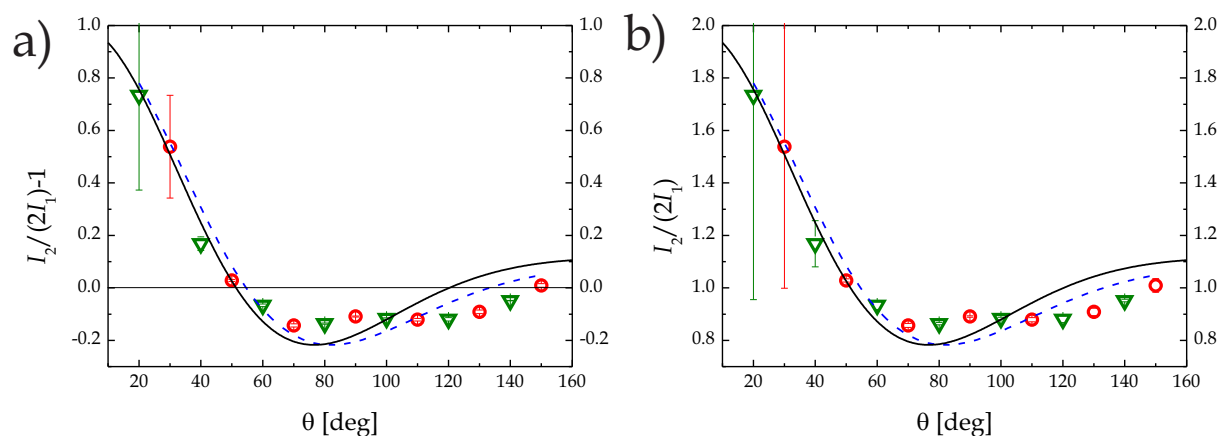


Figure 2.3.1.: Relative doublet form factor $I_2(q)/[2I_1(q)]$ measured by (a) static and (b) dynamic light scattering. The solid lines are calculated via the Rayleigh-Debye approximation with singlet particle diameters of 137 nm (solid line) and 129 nm (broken line). The data points were obtained from multi angle simultaneous static and dynamic light scattering measurements in 1 mmol/l (reversed triangles) and 5 mmol/l (circles) LaCl_3 solutions. In all cases the number concentration $[P]_0$ is $3.00 \times 10^{14} \text{ m}^{-3}$.

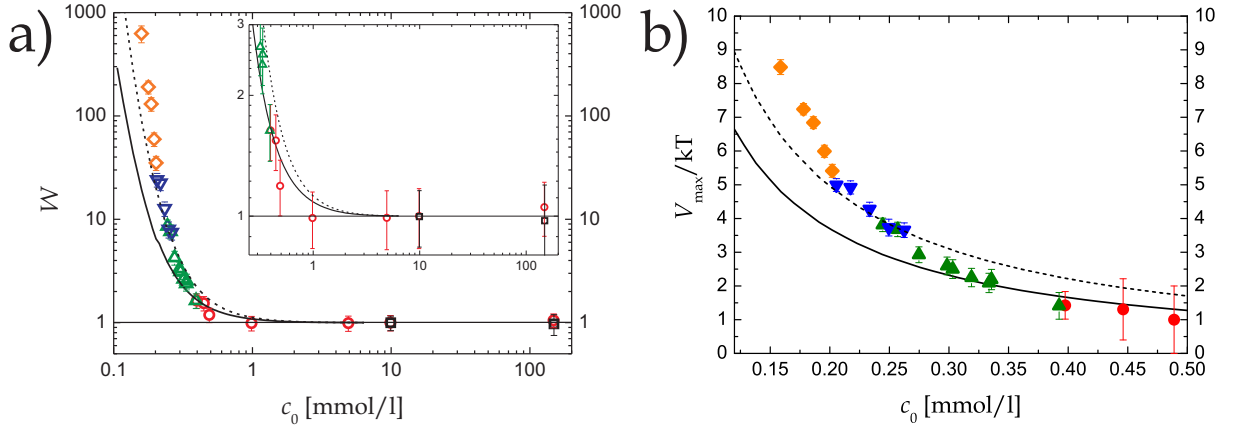


Figure 2.3.2.: (a) Stability ratio W of the SPB as a function of the lanthanum concentration c_0 for different SPB concentrations $[P]_0$. (b) Prefactor $V_{max}/k_B T$ as a function of the salt concentration c_0 of LaCl_3 . In both plots, the solid lines show the a priori predictions from the mean-field model. The broken lines are calculated by increasing the prediction of the effective charge of the SPB particles by 15%. In both plots the SPB concentrations $[P]_0$ are: $8.00 \times 10^{15} \text{ m}^{-3}$ (diamonds); $2.00 \times 10^{15} \text{ m}^{-3}$ (reversed triangles); $6.01 \times 10^{14} \text{ m}^{-3}$ (triangles); $3.00 \times 10^{14} \text{ m}^{-3}$ (circles); $1.40 \times 10^{13} \text{ m}^{-3}$ (squares).

Both the experimental data for W and V_{max} were compared to the predictions of the mean-field model. [7] For both variables the predictions were accurate within $\pm 20\%$. Therefore we predicted the stability of dispersed SPB particles in multivalent counterion environment for the first time.

The full publication can be found in Chapter 5.

2.4. Individual Contributions to Joint Publications

The results presented in this thesis were obtained in close collaboration with different co-workers and published or submitted as indicated below. The individual contribution of each co-author to the publications is specified. The asterisk denotes the corresponding author(s).

Chapter 3

This work was submitted to the *Journal of Colloid and Interface Science* under the title: **"Interaction of Colloidal Particles: the DLVO Potential and Charge Inversion"** by Christian Schneider, Mathias Hanisch, Bastian Wedel, Arben Jusufi and Matthias Ballauff*

- I performed and evaluated the light scattering experiments and the microsurface potential measurements. Also, I performed the mobility experiments in KCl and MgCl₂ and evaluated all of the mobility data. Furthermore, I wrote the publication.
- Mathias Hanisch and Bastian Wedel performed the mobility experiments in LaCl₃.
- Dr. Arben Jusufi and Prof. Matthias Ballauff contributed to the scientific discussion.

Chapter 4

This work was published in *Langmuir* under the title: **"Microsurface Potential Measurements: Repulsive Forces between Polyelectrolyte Brushes in the Presence of Multivalent Counterions"** by Christian Schneider, Arben Jusufi, Robert Farina, Feng Li, Philip Pincus, Matthew Tirrell* and Matthias Ballauff*

- I synthesized and characterized the SPB. Also, I performed and evaluated the light scattering experiments and the microsurface potential measurements. Furthermore, I wrote the publication.
- Dr. Arben Jusufi performed the theoretical description and contributed to the writing of the paper regarding the theoretical model.
- Robert Farina evaluated the SFA experiments and contributed to the writing of the paper regarding the SFA experiments and results.
- Dr. Feng Li performed the SFA experiments.
- Prof. Philip Pincus, Prof. Matthew Tirrell and Prof. Matthias Ballauff contributed to the scientific discussion.

Chapter 5

This work was published in *Physical Review E* under the title: **”Investigation of the Stability Behavior of Anionic Spherical Polyelectrolyte Brushes in the Presence of La(III) Counterions”** by Christian Schneider, Arben Jusufi, Robert Farina, Philip Pincus, Matthew Tirrell* and Matthias Ballauff*

- I synthesized and characterized the SPB. Also, I performed and evaluated the light scattering experiments and the microsurface potential measurements. Furthermore, I wrote the publication.
- Dr. Arben Jusufi performed the theoretical description and contributed to the writing of the paper regarding the theoretical model.
- Robert Farina, Prof. Philip Pincus, Prof. Matthew Tirrell and Prof. Matthias Ballauff contributed to the scientific discussion.

2.5. References

- [1] Holthoff, H.; Egelhaaf, S. U.; Borkovec, M.; Schurtenberger, P.; Stricher, H. *Langmuir* **1996**, *12*, 5541.
- [2] Martín-Molina, A.; Quesada-Pérez, M.; Galisteo-González, F.; Hidalgo-Álvarez, R. *J. Chem. Phys.* **2003**, *118*, 4183.
- [3] O’Brien, R. W.; White, L. R. *J. Chem. Soc. Faraday Trans II* **1978**, *2*, 1607.
- [4] Delgado, A. V.; González-Caballero, F.; Hunter, R. J.; Koopal, L. K.; Lyklema, J. *J. Colloid Interface Sci.* **2007**, *309*, 194.
- [5] Shklovskii, B. I. *Phys. Rev. E* **1999**, *60*, 5802.
- [6] Lyklema, J. *Colloids Surf. A* **2006**, *291*, 3.
- [7] Jusufi, A.; Likos, C. N.; Ballauff, M. *Colloid Polym. Sci.* **2004**, *282*, 910.

3. Interaction of Colloidal Particles: the DLVO Potential and Charge Inversion

Christian Schneider¹, Mathias Hanisch², Bastian Wedel², Arben Jusufi³,
Matthias Ballauff^{1,†}

¹F-I2 Soft Matter and Functional Materials, Helmholtz-Zentrum Berlin, Hahn-Meitner-Platz 1,
14109 Berlin, Germany, and
Department of Physics, Humboldt University Berlin, Newtonstr. 15, 12489 Berlin, Germany

²Physikalische Chemie I, University of Bayreuth, 95440 Bayreuth, Germany

³Institute for Computational Molecular Science, Temple University, Philadelphia, PA
19122-6081, USA

[†]Email: matthias.ballauff@helmholtz-berlin.de

Published in *Journal of Colloid and Interface Science*, 2011, 358, 62.

Reproduced with permission from
J. Colloid Interface Sci., 2011, 358, 62.
© 2011 Elsevier Inc.

DOI: 10.1016/j.jcis.2011.02.039

3.1. Abstract

We consider the interaction of colloidal spheres in the presence of mono-, di-, and trivalent ions. The colloids are stabilized by electrostatic repulsion due to surface charges. The repulsive part of the interaction potential Ψ_d is deduced from precise measurements of the rate of slow coagulation. These ‘microsurface potential measurements’ allow us to determine a weak repulsion in which Ψ_d is of the order of a few $k_B T$. These data are compared to ζ potential measured under similar conditions. At higher concentrations both di- and trivalent counterions accumulate at the very proximity of the particle surface leading to charge reversal. The salt concentration c_{cr} at which charge reversal occurs is found to be always above the critical coagulation concentration c_{ccc} . The analysis of Ψ_d and of the ζ potential demonstrates, however, that adsorption of multivalent counterions starts far below c_{cr} . Hence, colloid stability in the presence of di- and trivalent ions cannot be described in terms of a DLVO ansatz assuming a surface charge that is constant with regard to the ionic strength.

3.2. Introduction

The stability of colloidal dispersions in aqueous media is the central problem of colloid physics. Up to now, the classical DLVO (Derjaguin-Landau-Verwey-Overbeek) theory has been used extensively to describe the balance of attractive and repulsive forces for charged colloidal particles: [1] at low ionic strength the van der Waals attraction between the colloidal particles is checked by the electrostatic repulsion brought about by the surface charges. Screening this electrostatic interaction by adding salt then leads to destabilization and subsequent coagulation of the particles. Central to this approach is the Debye length $1/\kappa$ that scales inversely with the ionic strength $I = \sum z_i^2 c_i / 2$, where c_i is the absolute concentration of the ion species and z_i is their valency. [2] The height of the electric double layer is determined by the potential at the outer Helmholtz plane (see Figure 3.3.1) Ψ_d . [3] Within the frame of the DLVO theory the effective surface charge is treated as a constant with regard to the ionic strength and multivalent ions destabilize colloidal particles much stronger than monovalent ions only through a far more effective screening of the electrostatic repulsion. [4]

A direct consequence of the destabilization through added salt is the coagulation of the particles. In the dilute regime where binary interaction of the particles prevail, this process can be modeled in terms of the classical von Smoluchowski kinetics. [4] If the maximum of the particle interaction potential $V(h)$ (h : distance between the outer Helmholtz planes of the particles) is of the order of $k_B T$ and more, reaction-limited colloidal aggregation results. Diffusion-limited colloidal aggregation results for $V(h) \approx 0$. [4] The rate constants k_{slow} and k_{fast} of the reaction- and the diffusion-limited colloidal aggregation, respectively, can be measured precisely by light scattering. [5] The stability ratio $W = k_{fast}/k_{slow}$ gives direct insight into the relation of salt concentration and colloidal stability. [5] In particular,

the critical coagulation concentration c_{ccc} necessary for fast coagulation follows directly by extrapolation of W to unity. [4]

Recently, Shklovskii and co-workers pointed out that a basic assumption of the DLVO approach, namely the treatment of electrostatic repulsion in terms of a mean-field model, must be questioned. [6] These workers demonstrated that multivalent counterions will accumulate very close to the surface of the colloidal particles (in the first molecular layer) and form a strongly correlated liquid. If the concentration of the counterions is high enough, this process will lead to charge reversal (CR). Hence, there is a well-defined concentration c_{cr} where the surface charge of the particles is exactly balanced by the counterions in the strongly correlated liquid. For $c = c_{cr}$, the stability ratio W should be unity. [7]

Up to now, CR has been verified for a number of colloidal systems and compared quantitatively to the predictions of theory. [8–14] However, it remains difficult to unambiguously determine the driving force for CR in experiments. [15] The problem of CR for the stability of colloidal particles is thus at hand: di- and trivalent ions will exhibit a strong tendency to accumulate on the surface and compensate the surface charge at least partially. Hence, any DLVO model assuming a constant surface charge with respect to the ion concentration will lead to erroneous conclusions. Only a few experimental studies, however, have considered the relation between the colloidal stability and CR for low molecular weight counterions. [16] This is due to general difficulties to measure a weak repulsive potential in the vicinity of CR.

Here we consider the role of CR for electrostatic stabilization in a quantitative manner. The analysis presented here is based on the deduction of Ψ_d of colloidal particles by precise measurements of the stability ratio W as a function of the salt concentration. These 'microsurface potential measurements' (MSPM) allow us to determine Ψ_d down to the order of $k_B T$. [17, 18] Thus, even the weak repulsive potential of particles in the vicinity of CR can be deduced precisely. Moreover, the values of Ψ_d obtained by the MSPM will be compared to ζ potentials determined under similar conditions in order to discuss the role of CR for colloidal stability in an unambiguous fashion.

3.3. Theory

3.3.1. Coagulation rate and surface potential

The coagulation rate constant k for the formation of doublets from singlet particles undergoing Brownian motion is defined as [19]

$$\frac{d[P]}{dt} = k[P]^2, \quad (3.3.1)$$

where $[P]$ is the singlet particle concentration at a given time t . [4] In this study, we investigate the aggregation kinetics at an early stage where only doublets are formed. Therefore, we can safely assume that the rate of doublet dissociation does not play any role and eq. (3.3.1) holds.

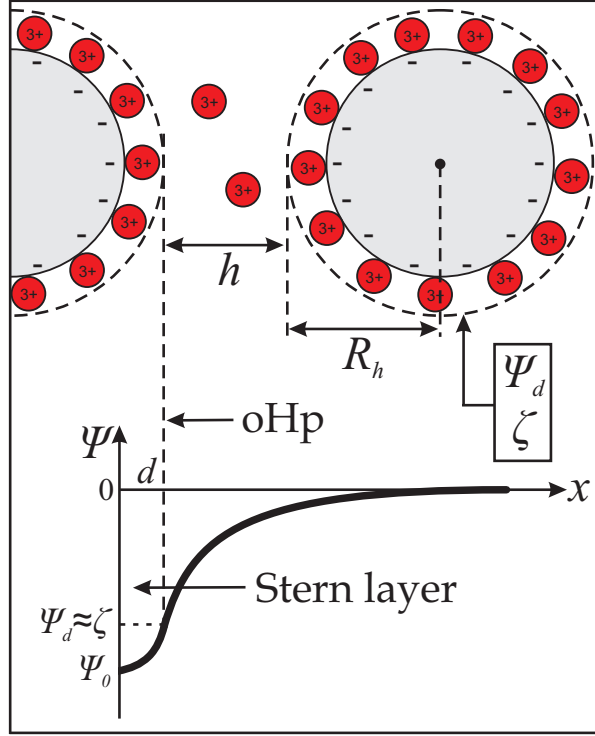


Figure 3.3.1.: Modeling of the interaction of charged colloidal particles in the presence of multivalent counterions. The interaction $V(h)$ between the particles is a function of the separation h between each outer Helmholtz plane. The slip plane determining R_h and the ζ potential corresponds in good approximation to the outer Helmholtz plane ($\Psi_d \simeq \zeta$). Therefore the charge density at the outer Helmholtz plane σ_d coincides with the electrokinetic charge density σ_{ek} . Di- and trivalent counterions are bound to the charged surface forming the Stern layer at $x < d$, where x is the distance between the counterions and the particle surface. Beyond $x > d$, the diffuse part of the electric double layer starts where $\Psi(x)$ exhibits an exponential decay.

For particles of the size used herein, coagulation in a secondary minimum of the interaction potential can be neglected. [20] Thus, the stability ratio W is related to the total interaction potential of the particles $V(h)$ through [4]

$$W = \frac{\int_0^\infty B(h) \exp\left(\frac{V(h)}{k_B T}\right) (2R_h + h)^{-2} dh}{\int_0^\infty B(h) \exp\left(\frac{V_A(h)}{k_B T}\right) (2R_h + h)^{-2} dh}, \quad (3.3.2)$$

where R_h is the hydrodynamic radius of the spheres, $V_A(h)$ is the interaction potential including only attractive forces, h is defined according to Figure 3.3.1, $k_B T$ is the thermal energy, and $B(h)$ is the correction for the hydrodynamic drag. [21] The total interaction potential $V(h)$ is the sum of the repulsive interactions arising from the electric double layers $V_{2s}(h)$, and the attractive van der Waals interactions of the solid particle cores $V_{vdW}(h)$, so that $V(h) = V_{2s}(h) + V_{vdW}(h)$.

For charged spheres in the presence of symmetric electrolytes, the repulsive electrostatic term of the interaction potential can be calculated according to the weak-overlap appro-

ximation via [22]

$$V_{2s}^{z:z}(h) = \frac{64\pi k_B T R_h c_0 \gamma^2}{\kappa^2} \exp[-\kappa h], \quad (3.3.3)$$

where $\gamma = \tanh[z e \Psi_d / 4 k_B T]$, c_0 is the absolute concentration of the electrolyte, z is the charge of the ions, and e is the charge of the electron. The inverse screening length is defined as $\kappa = \sqrt{2e^2 I / (\epsilon_0 \epsilon k_B T)}$ with ϵ_0 and ϵ being the dielectric permittivity of vacuum and the relative dielectric permittivity of water, respectively. The weak-overlap approximation holds true for $\kappa R_h \gg 1$ and $e \Psi_d / k_B T < 1$. [23] As will be shown further below the measured ζ potential is always smaller than 25 mV ($e|\zeta|/k_B T < 1$) within the relevant concentration range where coagulation takes place. Since $|\Psi_d| \simeq |\zeta|$ (see Section 3.5), the above conditions of the weak-overlap approximation are also fulfilled for the asymmetric di- and trivalent salts. [24] Therefore, one can simplify eq. (3.3.3) so that the repulsive term is then given by [22]

$$V_{2s}^{z_i:1}(h) = \frac{\alpha_{z_i:1} \pi R_h c_0 (e \Psi_d)^2}{\kappa^2 k_B T} \exp[-\kappa h], \quad (3.3.4)$$

where the factor $\alpha_{z_i:1}$ depends on the valency of the counterions z_i . It results to $\alpha_{2:1} = 12$ for a 2:1 electrolyte and to $\alpha_{3:1} = 24$ for a 3:1 salt.

The van der Waals term including retardation effects is given by [25]

$$V_{\text{vdW}}(h) = -\frac{H R_h}{12h} \left(1 - \frac{5.32h}{\lambda_{\text{vdW}}} \ln \left[1 + \frac{\lambda_{\text{vdW}}}{5.32h} \right] \right), \quad (3.3.5)$$

where H denotes the Hamaker constant of the particles and λ_{vdW} is the wave length of the van der Waals interactions. The parameter λ_{vdW} is set to 100 nm and H is set to 0.9×10^{-20} J for polystyrene. [18]

If W is known with high precision, Ψ_d can be determined through the use of eqs. (3.3.2)-(3.3.5). For a given concentration of added salt, Ψ_d is varied until the calculated stability ratio W matches the measured one.

3.3.2. Charge densities and potentials

Due to electroneutrality of the system, the charge on the surface and in the surrounding ion cloud must be equal. Therefore,

$$\sigma_0 + \sigma_i + \sigma_d = 0, \quad (3.3.6)$$

where σ_0 is the charge density at the particle surface and equals the titrated surface charge density σ_{ct} , σ_i is the charge density at the inner Helmholtz plane, and σ_d is the charge density at the outer Helmholtz plane. [15] We converted the electrokinetic charge densities σ_{ek} at the slip plane into ζ potentials using solutions of the Poisson-Boltzmann (PB) equation for 1:1, 1:2, and 1:3 electrolytes. For curved surfaces with $R_h \kappa > 1/2$ and any ζ [26], the solution for a symmetric monovalent salt can be written as

$$Q_{ek} = \frac{2R_h(1 + R_h \kappa)}{l_B} \sinh \left[\frac{ez\zeta}{2k_B T} \right], \quad (3.3.7)$$

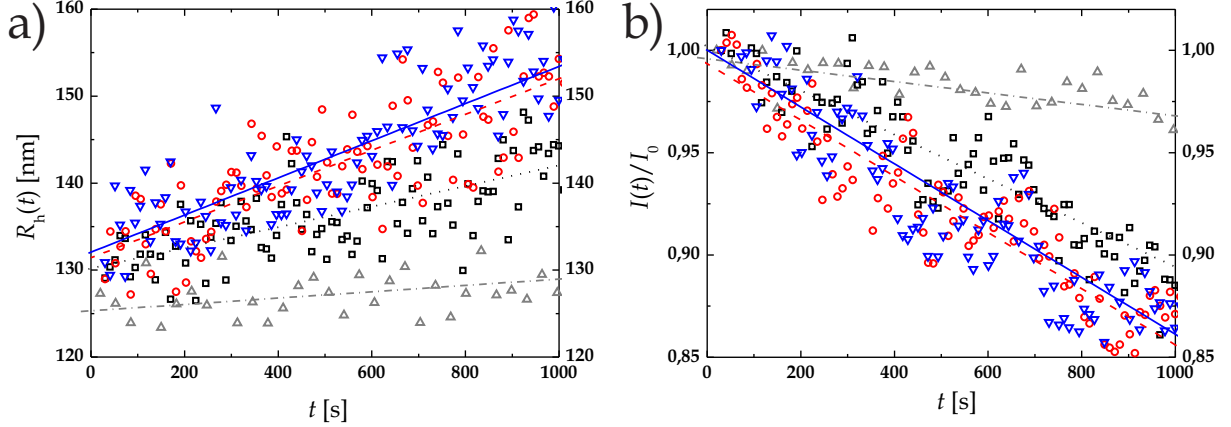


Figure 3.3.2.: The hydrodynamic radius $R_h(t)$ (a) and the normalized scattering intensity $I(q, t)/I_0(q)$ (b) as a function of the time t for different lanthanum concentrations c_0 with linear fits: 5 mmol/l (reversed triangles, broken line); 1.5 mmol/l (circles, solid line); 0.95 mmol/l (squares, dotted line); 0.8 mmol/l (triangles, broken dotted line). The number concentration $[P]_0$ is $2.60 \times 10^{14} \text{ m}^{-3}$ and the scattering angle θ is 90° .

where Q_{ek} is the number of charges per particle at the slip plane and l_B is the Bjerrum length. [27] Then σ_{ek} can be calculated via $\sigma_{ek} = eQ_{ek}/(4\pi R_h^2)$. For a 1:2 electrolyte Zhou derived the analytical expression

$$\Xi_{ek} = \pm \left\{ 2y^2 \left(\frac{1}{2(R_h\kappa)^2} + \frac{1}{R_h\kappa} \right) - \frac{1}{3} \left[3 - 2 \exp[y] - \exp[-2y] \right] \right\}^{1/2}, \quad (3.3.8)$$

where $y = e\zeta/k_B T$ and the scaled electrokinetic charge density $\Xi_{ek} = \sigma_{ek}e/\epsilon_0\epsilon k_B T\kappa$. [28] The expression for a 1:3 electrolyte is also given in the work of Zhou. [28] In the case of $R_h\kappa \geq 0.03$ and $|\zeta| < 330 \text{ mV}$ the error of the PB approximations are smaller than 5% compared to the exact PB solutions. [28, 29]

3.4. Materials and methods

3.4.1. Materials

The anionic, sulfonated latex system used in this study synthesized via emulsifier-free emulsion polymerization was supplied by Interfacial Dynamics Corporation, Portland, and used as received. The average particle size of the monodisperse particles was (115 ± 7) nm measured with transmission electron microscopy. The hydrodynamic radius R_h was (122 ± 5) nm, measured in 10 mmol/l NaCl solution with dynamic light scattering. The surface charge density σ_{ct} of the latex was 0.22 C/m^2 , which was provided by the company and measured via conductometric titration. The surface charge is mainly made up of sulfonate groups, where hydroxyl and carboxyl groups are also present in small amounts. However, due to the excess of sulfonate groups, the surface charge of the anionic particles is independent of the pH value of the suspension. It was shown in numerous studies that this kind of latex system is well suited for stability and mobility experiments. [5, 8, 9, 30, 31]

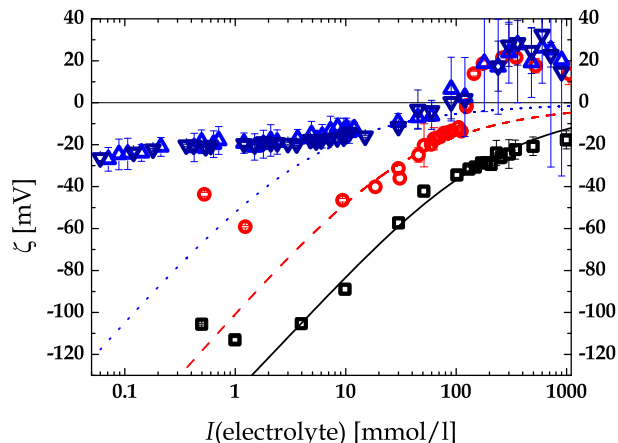


Figure 3.4.1.: Measured ζ potentials of the sulfonated latex particles in the presence of KCl (black squares), MgCl_2 (red circles), and LaCl_3 for two sets of measurements (light blue triangles and dark blue reversed triangles) as a function of the ionic strength I . The black solid line is the fit for the data taken in the presence of monovalent salt using eq. (3.3.7), whereas the red dashed line and the blue dotted line are the curves for a 1:2 electrolyte according to eq. (3.3.8) and a 1:3 salt, respectively, with a constant surface charge density. In the case of the di- and trivalent counterions we observe charge reversal (CR) at a concentration of 40 mmol/l MgCl_2 and 1 mmol/l of LaCl_3 .

The $p\text{H}$ value of the solutions in the electrophoretic mobility and stability experiments was not adjusted inasmuch small amounts of buffer molecules would adsorb at the latex particles and significantly alter the experimental results. However, the $p\text{H}$ values of the suspensions and salt solutions used for the measurements were found to be constant in the range of 6-7.5. According to Ottewill and Shaw, only 0.01-1% of the La^{3+} ions exist as LaOH^{2+} in the $p\text{H}$ range of 6-8 with no relevant amount of $\text{La}(\text{OH})_2^+$ and $\text{La}(\text{OH})_3$ being present. [32]

3.4.2. Electrophoretic mobility and ζ potential.

The electrophoretic mobility μ_e of the particles was measured using a Malvern Zetasizer NS. For the conversion of the mobilities into ζ potentials we used the method of O'Brien and White [33] with the software MPEK. [34] The concentration of latex particles $[P]$ in each mobility experiment was kept constant at $(1.5 \pm 0.3) \times 10^{14}$ particles per m^3 . The temperature equilibration time before each mobility experiment was kept short at 5 min to minimize particle coagulation. Five independent measurements were performed for one data point.

3.4.3. Coagulation rate

The stability data was obtained using simultaneous static and dynamic light scattering. This method was introduced by Borkovec and co-workers. [5] It allows the measurement of k in a highly precise manner at arbitrary scattering angles from the change of dR_h/dt

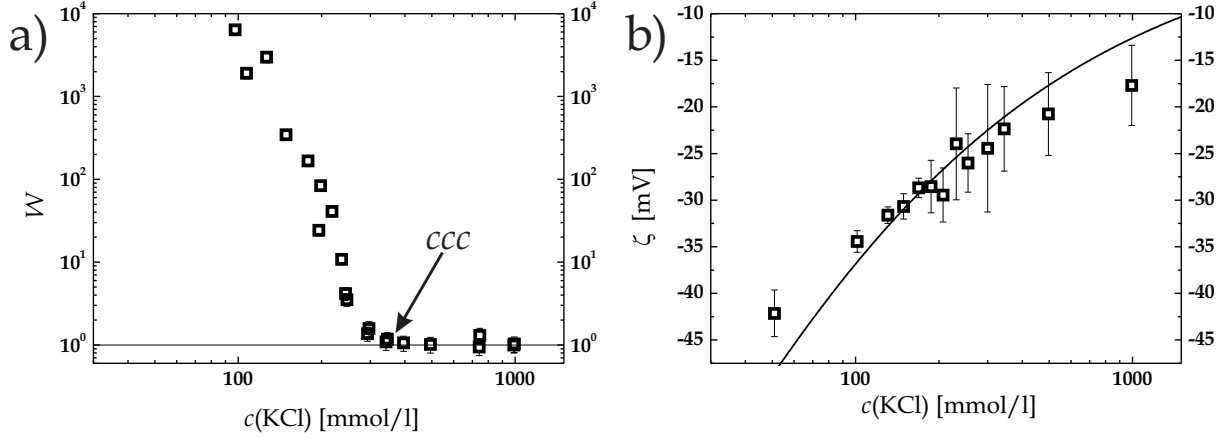


Figure 3.4.2.: (a) Stability ratio W of the anionic particles as a function of the K^+ concentration $c(\text{KCl})$. (b) Measured ζ potential as a function of $c(\text{KCl})$. The solid line displays the fit by eq. (3.3.7) assuming a constant surface charge density.

and the time dependent scattering intensity $dI(q, t)/dt$ according to

$$k[P]_0 = \frac{R_{h,2}}{R_{h,2} - R_{h,1}} \left(\frac{dR_h(t)/dt}{R_h(0)} \right) - \left(\frac{dI(q, t)/dt}{I(q, 0)} \right), \quad (3.4.1)$$

where $[P]_0$ is the initial particle concentration, $R_{h,1}$ and $R_{h,2}$ are the hydrodynamic radii of single spheres and doublets, respectively, $R_h(t)$ is the hydrodynamic radius of the particles at time t , and $I(q, t)$ is the angle dependent scattering intensity of the suspension at time t . The doublet hydrodynamic radius is given by $R_{h,2} = 1.38R_{h,1}$. [5] Details about the experimental procedure and instrumentation are outlined in an earlier study. [18] The scattering angle in the stability experiments was always 90° .

3.5. Results and discussion

3.5.1. Electrophoretic mobility measurements

The measured ζ potential of the latex particles as a function the ionic strength I in KCl is shown in Figure 3.4.1. These data have been fitted by eq. (3.3.7) assuming that the charge σ_{ek} at the outer Helmholtz plane is independent of the bulk salt concentration. For monovalent salt, a satisfactory fit can be achieved over almost three orders of magnitude in concentration. There is no indication of charge reversal as expected. The best fit gives a σ_{ek} of 0.11 C/m^2 , which corresponds to the charge σ_d , [35] and is 50% of the titrated bare charge density σ_0 of 0.22 C/m^2 . Thus, for KCl approximately half of all counterions are located inside the Stern layer.

In contrast to the KCl measurements the MgCl_2 data indicate CR at roughly 40 mmol/l . This value for CR compares well to observations made for similar systems. [31, 36] Beyond 40 mmol/l , ζ becomes positive and increases to a maximum value of roughly 20 mV . We also find CR in the LaCl_3 experiments at 15 mmol/l . This compares well with c_{cr} values found for lanthanum counterions and colloids of similar bare charge densities. [8, 9, 13]

Beyond CR, ζ increases to a maximum value of roughly 25 mV in the presence of the La^{3+} counterions.

The fits of the data obtained in the presence of MgCl_2 and LaCl_3 using approximate solutions of Zhou (see Section 3.4.2) are shown as dashed lines in Figure 3.4.1. Obviously, there is no meaningful description of the data anymore. At low counterion concentrations the deviations between the PB model and the experimental data can be explained by stagnant layer effects or conduction inside the shear plane. [3, 37] However, in both cases ζ is not described by the mean-field PB model assuming a constant charge density at high concentrations. Therefore, the data derived from these fits can be discussed only in a qualitative manner. In the case of MgCl_2 , the fit leads to a σ_{ek} of 0.01 C/m^2 which is only 5% of the bare surface charge density. For trivalent LaCl_3 counterions σ_{ek} results to 0.003 C/m^2 . These results point to the fact that the adsorption of the trivalent counterions is more pronounced as compared to the divalent ions. The lower value of c_{cr} for LaCl_3 confirms this finding. Since we do not determine the driving forces for CR in this study, we refer to all counterion accumulation in the Stern layer simply as 'adsorption'.

3.5.2. Microsurface potential measurements

As already shown in previous papers [17, 18] the MSPM lead to precise data on weak repulsive potentials. In order to assess the role of counterion valency on CR and colloidal stability, we performed MSPM for the same colloidal particles in the presence of KCl, MgCl_2 , and LaCl_3 . Some typical curves for $R_h(t)$ and $I(q, t)$ obtained in the stability experiments with simultaneous static and dynamic light scattering are depicted in Figure 3.3.2. The particle concentration was raised from $(1.3 \pm 0.2) \times 10^{14} \text{ 1/m}^3$ in the fast to $(1.2 \pm 0.3) \times 10^{16} \text{ 1/m}^3$ in the slow coagulation regime, in order to yield a good signal to noise ratio at all counterion concentrations. The experimental fast coagulation rate constant k_{fast} was calculated by averaging all experimental rate constants in the fast coagulation regime. The values of k_{fast} in the KCl, MgCl_2 , and LaCl_3 experiments were $(2.2 \pm 0.1) \times 10^{-18} \text{ m}^3/\text{s}$, $(3.0 \pm 0.2) \times 10^{-18} \text{ m}^3/\text{s}$ and $(2.7 \pm 0.2) \times 10^{-18} \text{ m}^3/\text{s}$, respectively. These data compare well to values found in the literature for similar systems. [5, 30, 38, 39] In each case we obtained the experimental values of the stability ratio W via $k(c)/k(c = c_{\text{fast}})$ where c_{fast} is 1000 mmol/l, 350 mmol/l, and 150 mmol/l for experiments in the presence of K^+ , Mg^{2+} , and La^{3+} , respectively. Since the MSPM can only measure the repulsive part of the interaction potential, no data are obtained in the DLCA regime where the interaction potential is attractive. At low values of W the repulsive energy between the particles approaches $k_B T$ and the determination of $\Psi_d(c)$ is less reliable at $W \leq 2$. Therefore we only obtained $\Psi_d(c)$ for $W > 2$. In the following the results for counterions of different valency will be discussed in detail.

Monovalent counterions

In Figure 3.4.2 we show the experimental data for the stability ratio W and the ζ potential of the sulfonated latex particles in KCl. The stability plot has the typical form for surface charged particles. At small salt concentrations the slow coagulation regime is found where

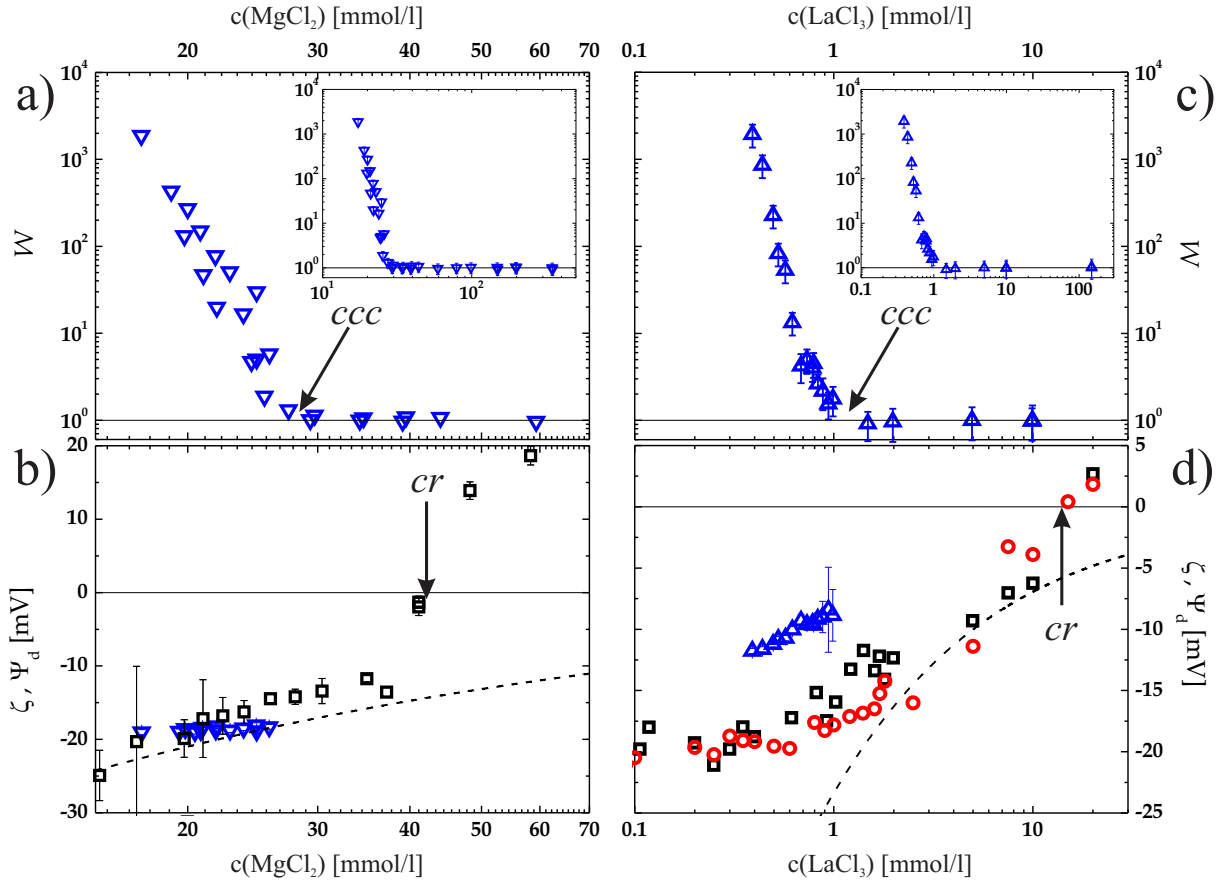


Figure 3.5.1.: Stability ratio W of the anionic particles as a function of the Mg^{2+} (a) and La^{3+} (c) concentration. Experimental data points are indicated by triangles. The insets show the complete data range of W . From the stability data in the slow coagulation regime we fit the respective values of $\Psi_d(c)$ using eq. (3.3.2). In (b) and (d) the values of Ψ_d (triangles) are compared to the measured ζ potentials (squares and circles). The dotted lines indicate the results calculated for a constant surface charge density.

$W > 1$. Only one out of W particle-particle hits results in the formation of an aggregate. [4] The stability ratio decreases with increasing salt concentration until W becomes unity at $c = c_{ccc}$. In the case of KCl we find the c_{ccc} at 350 mmol/l.

For monovalent ions it is not possible to calculate Ψ_d from the stability ratio W through eqs. (3.3.2)-(3.3.5). This is due to the fact that the maximum of the repulsive barrier is located less than 1 nm away from the particle surface. In this case the DLVO theory does not lead to a quantitative description of W due to specific ion effects, surface roughness, and hydration forces acting at separations less than 1 nm. [27, 30, 40–42]

However, the ζ potential as the function of the concentration of monovalent salt can be analyzed in the reaction-limited colloidal aggregation regime (see the discussion of Figure 3.4.1). For the sake of comparison we plot the ζ potential in the range of 150–350 mmol/l in Figure 3.4.2 as well. As already discussed above, these data are well described by an ansatz assuming a constant surface charge density. Hence, the stability of charged colloids in the presence of monovalent ions is well-described by the DLVO theory which assumes a constant surface charge with regard to the ionic strength of the solution.

Multivalent Counterions

In Figure 3.5.1 we show the experimental results of W together with the resulting Ψ_d for divalent magnesium and trivalent lanthanum counterions. We find the c_{ccc} at 30 and 1 mmol/l in the Mg^{2+} and the La^{3+} experiments, respectively. Consistent with the recent work of Bastos-González and co-workers [43] no restabilization of the dispersion at high salt concentrations is observed. This is due to the hydrophobic nature of the latex system. [43]

For divalent ions the maximum of $V(h)$ is located around 1 nm above the surface and more than 1.5 nm in the case of the trivalent counterions. Furthermore, direct force measurements with the surface forces apparatus and optical tweezers showed that the repulsive interactions between two charged surfaces in the presence of Mg^{2+} and La^{3+} ions are well described by an exponential decay. [45, 46] Thus, we could use the MSPM to obtain Ψ_d at every data point of W using eqs. (3.3.2)-(3.3.5) for the di- and trivalent counterions.

Close to the c_{ccc} the surface potential Ψ_d for Mg^{2+} depends only very weakly on c as shown in Figure 3.5.1b. For the trivalent lanthanum counterions, however, $\Psi_d(c)$ exhibits a marked dependence on c (Figure 3.5.1d). To analyze this point in further detail, we compare $\Psi_d(c)$ with the data of the ζ potential measured in the same range of salt concentration (see Figures 3.5.1b and 3.5.1d). For MgCl_2 the values of Ψ_d coincide with the ζ potential within the experimental error (see also the discussion of this point in Ref. [47]). However, ζ grows markedly beyond $c = c_{ccc}$ and CR occurs at ca. 40 mmol/l MgCl_2 . The good agreement of both quantities may therefore be rather accidental. Furthermore, c_{cr} is definitely above c_{ccc} for the divalent ions. The data of Ψ_d and ζ in the presence of LaCl_3 reveal similar results. The ζ potential increases with the electrolyte concentration continuously from -20 mV at 0.1 mmol/l LaCl_3 to zero around 15 mmol/l LaCl_3 . Thus, for the La^{3+} counterions the c_{cr} exceeds c_{ccc} by a factor of ca. 10.

Figure 3.5.1d shows that the absolute values for Ψ_d are smaller than the ζ potentials. This finding is in direct contradiction to the fact that the electrokinetic slip plane is located further away from the particle surface than the outer Helmholtz plane. [35] The ζ potential is expected to be always smaller than the corresponding Ψ_d . [48] The discrepancies between Ψ_d and ζ for the trivalent ions may be explained by counterion correlations occurring very close to the surface of the particles. Correlations can lead to lateral inhomogeneities in the counterion distribution, which are followed by surface dipoles that lead to an attractive contribution to the interaction potential. [4] This mechanism is similar to the patch-charge attraction proposed by Borkovec and co-workers to explain an attractive component in the interaction between particles with adsorbed dendrimers which is not accounted for in the DLVO model. [44]

The CR by adsorption of trivalent lanthanum ions has been observed on mica surfaces by Pashley. [45] Our finding is also in accord with the results of Besteman and co-workers. [10, 11] More recently, Kremer and co-workers found a marked reduction of the effective surface charge for polymer particles in lanthanum solutions. [46] Hence, these data cannot be explained by the usual DLVO theory assuming a surface charge which is independent of the ionic strength of the solution. The present data show unambiguously that adsorption

of multivalent counterions plays an important role and is dependent on the counterion concentration.

3.6. Conclusion

The stability of charged colloidal particles in the presence of mono-, di-, and trivalent counterions has been considered. Microsurface potential measurements have been used to obtain the effective surface potential Ψ_d . This method relies on precise measurements of the stability ratio W that leads to an exact determination of the critical coagulation concentration c_{ccc} . A comparison with the ζ potential measured under similar conditions leads to the conclusion that adsorption of di- and trivalent ions on the surface of the particles is a major reason for destabilization. Charge reversal is always observed at concentrations higher than the c_{ccc} . However, the present data show that in the case of di- and trivalent counterions the stability cannot be calculated assuming a surface charge that is constant with regard to the electrolyte concentration. A further finding that commands interest is the marked difference between $|\zeta|$ and $|\Psi_d|$ for colloidal dispersions under consideration here in the presence of LaCl_3 . Additional attractive contributions, possibly caused by correlations of condensed La^{3+} ions, lower the effective potential barrier $|\Psi_d|$. These attractive contributions have not been observed for spherical polyelectrolyte brushes under similar conditions. [17, 18] This suggests that the observed effect will occur only for colloidal particles with well-defined, solid surfaces.

3.7. Acknowledgements

The authors thank J. Dzubiella for helpful discussions. M.B. gratefully acknowledges support by the Deutsche Forschungsgemeinschaft in the frame of a NSF/DFG-project. C.S. thanks the Elite Study Program Macromolecular Science in the Elite Network Bavaria and the Bavarian Graduate Support Program for financial support during this work. We very much thank R. Hill for the extensive support provided for using the MPEK software.

3.8. References

- [1] Verweij, E. J. W.; Overbeek, J. Th. G. *Theory of the stability of lyophobic colloids*, 1st ed.; Elsevier: Amsterdam, 1948.
- [2] Ninham, B. W. *Adv. Colloid Interface Sci.* **1999**, *83*, 1.
- [3] Lyklema, J. *Fundamentals of Interface and Colloid Science*, 1st ed.; Academic Press: London, 2001; Vol.2.
- [4] Evans, D. F.; Wennerström, H. *The Colloidal Domain*, 1st ed.; Wiley-VCH: New York, 1999.

- [5] Holthoff, H.; Egelhaaf, S. U.; Borkovec, M.; Schurtenberger, P.; Stricher, H. *Langmuir* **1996**, *12*, 5541.
- [6] Shklovskii, B. I. *Phys. Rev. E* **1999**, *60*, 5802.
- [7] Nguyen, T. T.; Rouzina, I.; Shklovskii, B. I. *J. Chem. Phys.* **2000**, *112*, 2562.
- [8] Martín-Molina, A.; Quesada-Pérez, M.; Galisteo-González, F.; Hidalgo-Álvarez, R. *J. Chem. Phys.* **2003**, *118*, 4183.
- [9] Martín-Molina, A.; Quesada-Pérez, M.; Galisteo-González, F.; Hidalgo-Álvarez, R. *J. Phys.: Condens. Matter* **2003**, *15*, 3475.
- [10] Besteman, K.; Zevenbergen, M. A. G.; Heering, H. A.; Lemay, S. G. *Phys. Rev. Lett.* **2004**, *93*, 170802.
- [11] Besteman, K.; Zevenbergen, M. A. G.; Lemay, S. G. *Phys. Rev. E* **2005**, *72*, 061501.
- [12] Labbez, C.; Jönsson, B.; Skarba, M.; Borkovec, M. *Langmuir* **2009**, *25*, 7209.
- [13] Martín-Molina, A.; Rodríguez-Beas, C.; Hidalgo-Álvarez, R.; Quesada-Pérez, M. *J. Phys. Chem. B* **2009**, *113*, 6834.
- [14] Wernersson, E.; Kjellander, R.; Lyklema, J. *J. Phys. Chem. C* **2010**, *114*, 1849.
- [15] Lyklema, J. *Colloids Surf. A* **2006**, *291*, 3.
- [16] Lyklema, J. *Adv. Colloid Interface Sci.* **2009**, *147-148*, 205.
- [17] Schneider, C.; Jusufi, A.; Farina, R.; Li, F.; Pincus, P.; Tirrell, M.; Ballauff, M. *Langmuir* **2008**, *24*, 10612.
- [18] Schneider, C.; Jusufi, A.; Farina, R.; Pincus, P.; Tirrell, M.; Ballauff, M. *Phys. Rev. E* **2010**, *82*, 011401.
- [19] Hunter, R. J. *Foundations of Colloid Science*, 2nd ed.; Oxford University Press: New York, 2004.
- [20] Behrens, S. H.; Borkovec, M. *J. Colloid Interface Sci.* **2000**, *225*, 460.
- [21] Honig, E. P.; Roeberson, G. J.; Wiersema, P. H. *J. Colloid Interface Sci.* **1971**, *36*, 97.
- [22] Israelachvili, J. N. *Intermolecular and Surface Forces*; Academic Press: New York, 1998.
- [23] P.M. Biesheuvel, *J. Colloid Interface Sci.* 238 (2001) 362.
- [24] Regarding the MSPM for the divalent and trivalent counterions, the smallest $R_h\kappa = 3 \gg 1$ and the highest $e\Psi_d/k_B T = 0.73 < 1$, so that the conditions of the weak-overlap approximation are fulfilled.

-
- [25] Gregory, J. J. *Colloid Interface Sci.* **1981**, *83*, 138.
- [26] In the KCl mobility experiments the smallest $R_h\kappa = 10.5 > 1/2$, so that the conditions are met.
- [27] Hanus, L. H.; Hartzler, R. U.; Wagner, N. J. *Langmuir* **2001**, *17*, 3136.
- [28] Zhou, S. *J. Colloid Interface Sci.* **1998**, *208*, 347.
- [29] In the mobility experiments in the presence of MgCl_2 , the highest measured absolute value of the ζ potential is $39 \text{ mV} < 330 \text{ mV}$ and the smallest $R_h\kappa = 6.8 \geq 0.03$, so that both conditions are fulfilled. In the case of the experiments in the presence of LaCl_3 , the highest measured absolute value of the ζ potential is $33 \text{ mV} < 330 \text{ mV}$ and the smallest $R_h\kappa = 3.0 \geq 0.03$, so that both conditions are fulfilled.
- [30] Behrens, S. H.; Christl, D. I.; Emmerzael, R.; Schurtenberger, P.; Borkovec, M. *Langmuir* **2000**, *16*, 2566.
- [31] Quesada-Pérez, M.; González-Tovar, E.; Martín-Molina, A.; Lozada-Cassou, M.; Hidalgo-Álvarez, R. *Colloids Surf. A* **2005**, *267*, 24.
- [32] Ottewill, R. H.; Shaw, J. N. *J. Colloid Interface Sci.* **1968**, *26*, 110.
- [33] O'Brien, R. W.; White, L. R. *J. Chem. Soc. Faraday Trans II* **1978**, *2*, 1607.
- [34] The manual for the MPEK-software package can be download from Reghan J. Hill from: <http://people.mcgill.ca/files/reghan.hill/MPEK-0.02.pdf>
- [35] Delgado, A. V.; González-Caballero, F.; Hunter, R. J.; Koopal, L. K.; Lyklema, J. *J. Colloid Interface Sci.* **2007**, *309*, 194.
- [36] Martín-Molina, A.; Maroto-Centeno, J. A.; Hidalgo-Álvarez, R.; Quesada-Pérez, M. *Colloids Surf. A* **2008**, *319*, 103.
- [37] Midmore, B. R.; Hunter, R. J. *J. Colloid Interface Sci.* **1988**, *122*, 1.
- [38] Sonntag, H.; Strenge, K. *Coagulation and Structure Formation*; VEB Deutscher Verlag der Wissenschaften: Berlin, 1987.
- [39] van Zanten; J. H.; Elimelech, M. *J. Colloid Interface Sci.* **1992**, *154*, 1.
- [40] Behrens, S. H.; Borkovec, M.; Schurtenberger, P. *Langmuir* **1998**, *14*, 1951.
- [41] Ducker, W. A.; Xu, Z.; Clarke, D. R.; Israelachvili, J. N. *J. Am. Ceram. Soc.* **1994**, *77*, 437.
- [42] Pericet-Camara, R.; Papastavrou, G.; Borkovec, M. *Macromolecules* **2009**, *42*, 1749.
- [43] Peula-García, J. M.; Ortega-Vinuesa, J. L.; Bastos-González, D. J. *Phys. Chem.* **2010**, *114*, 11133.

- [44] Popa, I.; Papastavrouz, G.; Borkovec, M. *Phys. Chem. Chem. Phys.* **2010**, *12*, 4863.
- [45] Pashley, R. M. *J. Colloid Interface Sci.* **1984**, *102*, 23.
- [46] Gutsche, C.; Keyser, U. F.; Kegler, K.; Kremer, F. *Phys. Rev. E* **2007**, *76*, 031403.
- [47] Lyklema, J. *Curr. Opin. Colloid Interface Sci.* **2010**, *15*, 125.
- [48] The observed discrepancy may be attributed to a wrong Hamaker constant of poly(styrene) in eq. (3.3.5). In order to shift the data points of Ψ_d to the ζ potentials, a value for H_c of at least 5×10^{-20} J would be necessary. This is more than five times higher than the established value of 0.9×10^{-20} J for poly(styrene) used here. Therefore, it is safe to assume that the observed effect is not caused by an incorrect value for H_c .

4. Microsurface Potential Measurements: Repulsive Forces between Polyelectrolyte Brushes in the Presence of Multivalent Counterions

Christian Schneider¹, Arben Jusufi², Robert Farina³, Feng Li³, Philip Pincus³, Matthew Tirrell^{3,†}, Matthias Ballauff^{1,‡}

¹Physikalische Chemie I, University of Bayreuth, 95440 Bayreuth, Germany

²Department of Chemical Engineering, Princeton University, Princeton, New Jersey 08544

³Departments of Chemical Engineering and Materials, Materials Research Laboratory, University of California-Santa Barbara, Santa Barbara, California 93106, 2050

[†]Email: tirrell@engineering.ucsb.edu

[‡]Email: matthias.ballauff@uni-bayreuth.de

Published in *Langmuir*, 2008, 24, 10612.

Reproduced with permission from
Langmuir, 2008, 24, 10612.
© 2008 American Chemical Society.

DOI: 10.1021/la802303z

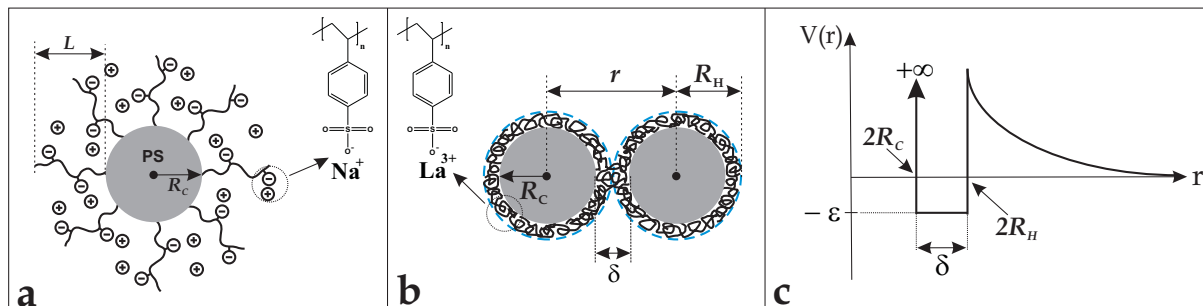


Figure 4.1.1.: Schematic representation of the spherical polyelectrolyte brush investigated in this study. Anionic polyelectrolyte chains are grafted from colloidal particles (radius $R_c = 121$ nm) made from solid poly(styrene). The particles are immersed in aqueous salt solutions with defined ionic strength. The thickness L of the brush layer is measured for different ionic strengths by dynamic light scattering. The ionic strength in the system is adjusted through the concentration of added salt (a). Schematic of two aggregated SPB particles upon contact of the polyelectrolyte shells with fully collapsed brush layer. Hereby, the particle-particle center distance r equals $2R_H = 2R_c + \delta$ with δ being twice the brush thickness L . In all concentrations of lanthanum ions used, here the hydrodynamic radius R_H of the particles is practically constant at 128 nm (b). Interaction potential of the SPB particles in the aqueous lanthanum solutions used in our study (c).

4.1. Abstract

We propose a new way to determine weak repulsive forces operative between colloidal particles by measuring the rate of slow coagulation. The rate of slow coagulation is directly related to the competition of the repulsion with thermal motion. Since the thermal forces are weak, measurements of the coagulation rate can lead to precise information on repulsive potentials having a magnitude of just a few $k_B T$. We demonstrate this novel way by studying colloidal spherical polyelectrolyte brush (SPB) particles in aqueous solution containing trivalent La^{3+} counterions. The particles consist of a monodisperse polystyrene core of 121 nm radius from which linear sodium poly(styrenesulfonate) (PSS) chains are densely grafted (contour length 48 nm). We determine the rate of coagulation by time-resolved simultaneous static and dynamic light scattering in the presence of LaCl_3 (0.2 to 150 mM). Direct measurements of the repulsive force between macroscopic brush layers demonstrate that the potential is decaying exponentially with distance. This is in good agreement with a simple theoretical treatment that furthermore leads to the effective surface potential Ψ_0 . The good agreement of data obtained by the novel microscopic method with direct macroscopic measurements underscores the general validity of our approach.

4.2. Introduction

The stability and dynamics of colloidal systems are determined by the forces with which the colloidal particles interact. Forces between colloidal objects hence have been the objective of a great number of theoretical and experimental studies for the last 70 years. A central point in this field is the measurement of forces between two surfaces or directly between two colloidal particles. Here, the surface force apparatus (SFA) has led to tremendous progress in the field since it leads to force-distance curves down to the sub nanometer range. [1–3] More recently, forces operative between colloidal particles have been measured using optical tweezers, [4–6] the TIRM, [7–9] and the colloidal probe AFM. [10–12] A problem of all force measurements is the sensitivity which sets the lower bound for the strength of the force under consideration. For all methods used so far, the force is imposed externally by a mechanical or optical device or by gravity. Moreover, measuring forces by the above methods requires the preparation of macroscopic surfaces or the use of particles large enough to be resolved by optical microscopy. The ultimate goal, however, is often the modeling of the interaction of nanometric particles with different structure and curvature. Here we demonstrate for the first time that the lower bound of conventional techniques may be overcome by using thermal forces. For particles with radius R , thermal motion imposes forces of the order of $k_B T/R$ where k is the Boltzmann constant and T denotes the temperature. In order to explore a repulsive force of this magnitude, we use particles that stick on direct contact but exhibit a small but finite repulsion at finite distances. Thermal motion will lead to the reaction-limited colloidal aggregation (RLCA) which in its earliest stage results in the formation of doublets of spheres. Measuring the kinetics of the formation of doublets by a combination of static and dynamic light scattering [13] then leads to quantitative comparison of the repulsive interaction of colloidal particles with predictions from theoretical models.

As an example for demonstrating our method, we chose spherical polyelectrolyte brushes

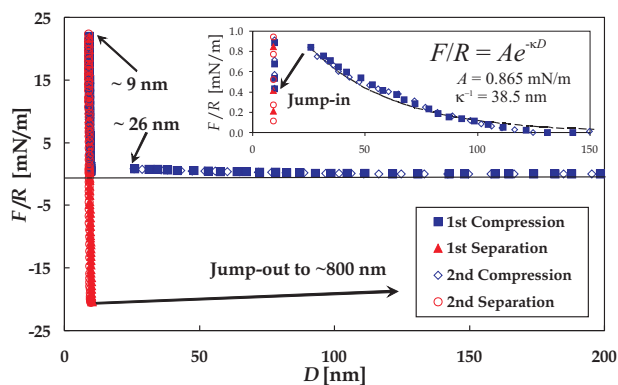


Figure 4.2.1.: Measurement of forces between two planar polyelectrolyte brushes (PtBS₁₅-LaPSS₄₃₈) adsorbed onto hydrophobic cylindrical surfaces using the SFA. The counterions in the brushes are La³⁺ ions, and the added salt is 0.06 mM La(NO₃)₃. The height of the two compressed planar brush layers is 9 nm, which corresponds to the parameter δ in the spherical brush system.

(SPBs) that consist of solid colloidal spheres from which long chains of a polyelectrolyte are covalently grafted. [14] Figure 4.1.1a displays the structure of these particles in a schematic fashion. The term brush indicates a grafting density of the appended chains that is dense enough to ensure strong interaction between the polyelectrolyte chains. The main feature of polyelectrolyte brushes is the strong confinement of the counterions within the brush layer first predicted by Pincus as well as Birshtein, Borisov, and Zhulina. [15, 16] In the presence of monovalent counterions, the high number of charges in such a polyelectrolyte brush will therefore lead to a strong stretching of the attached chains in order to alleviate the concomitant osmotic pressure of the counterions. The strong repulsive force between two planar brushes in this osmotic limit has already been demonstrated by direct measurements using the SFA. [3] If the ionic strength is raised in this system by adding monovalent salt, the height of the polyelectrolyte layer will decrease considerably. Rather moderate concentrations (0.1 molar) of divalent ions already lead to loss of colloidal stability and to rapid flocculation of the particles. [14] In the case of trivalent ions, minute concentrations are already sufficient to induce flocculation [17] and observable strongly attractive forces in the SFA. [18] In order to determine the force interaction between two brush layers we combine direct SFA measurements of planar brushes with measurement of the rate of slow coagulation [13] of the particles in presence of trivalent lanthanum ions.

4.3. Experimental Section

We prepared planar polyelectrolyte brushes as described earlier [3] with a contour length $L_c = 110$ nm of the grafted chains and a grafting density $\sigma = 0.006$ nm⁻² giving the number of chains per unit area. In this study, we obtain L_c by multiplying the degree of polymerization of the hydrophilic block of the grafted chains with the effective bond length of 0.25 nm. Direct measurements of the repulsive forces between two polyelectrolyte brush layers by the SFA have been done as described in previous papers. [3, 18]

The spherical polyelectrolyte brushes carry long chains of the strong polyelectrolyte sodium poly(styrenesulfonate). [14] The colloidal core of the particles consists of poly(styrene) (Figure 4.1.1a). The core particles are practically monodisperse and the hydrodynamic radius R_H determined by dynamic light scattering (DLS) is related to the brush height L through $R_H = R_C + L$, where R_C denotes the radius of the core particles. The SPB particles are fully characterized with regard to their structural parameters, namely the contour length $L_c = 48$ nm, the radius $R_C = 121$ nm of the core particles, and the grafting density $\sigma = 0.07$ nm⁻².

The coagulation rate constant k_{11} is defined through $d[P]/dt = k_{11}[P]^2$, where $[P]$ is the particle concentration at a given time. It can be obtained by simultaneous static and dynamic light scattering according to [13]

$$k_{11}[P]_0 = \frac{R_{H,2}}{R_{H,2} - R_{H,1}} \left(\frac{dR_H(t)/dt}{R_H(0)} \right) - \left(\frac{dI(q,t)/dt}{I(q,0)} \right), \quad (4.3.1)$$

where $[P]_0$ is the initial particle concentration, $R_{H,1}$ and $R_{H,2}$ are the hydrodynamic radius of single spheres and doublets, respectively, $R_H(t)$ is the hydrodynamic radius of

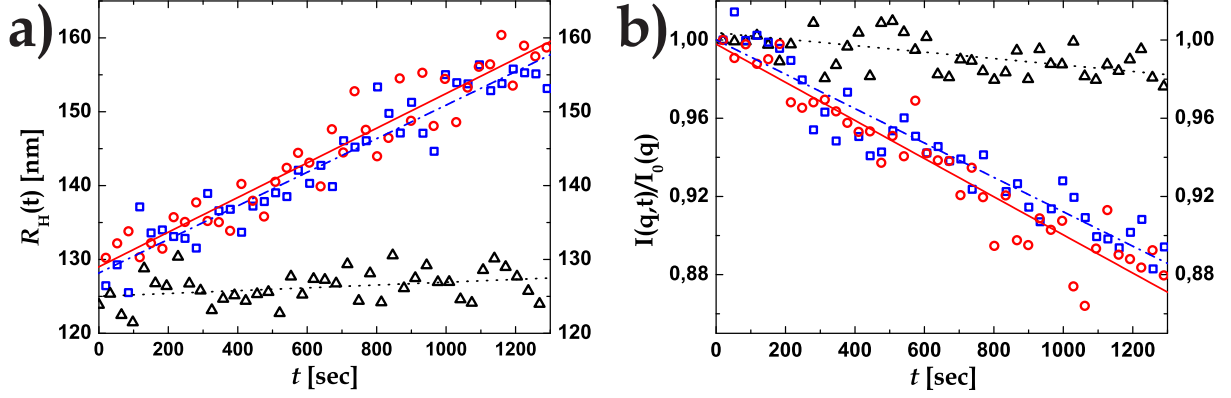


Figure 4.3.1.: The hydrodynamic radius $R_H(t)$ (a) and the normalized scattering intensity $I(q,t)/I_0(q)$ (b) as a function of time for different lanthanum concentrations c_0 with linear fits: 150 mM (circles, solid line); 0.5 mM (squares, broken line); 0.2 mM (triangles, dotted line). Here, the number concentration is $[P]_0: 1.64 \times 10^{14} \text{ m}^{-3}$ and the scattering angle θ is 90° .

the particles at a specific time t , and $I(q,t)$ is the angle-dependent scattering intensity of the suspension at time t . [13] The stability ratio W is defined as the ratio of the rate constant of the rapid coagulation and rate constant for particles with finite repulsion $W = (k_{11})_{\text{fast}}/(k_{11})_{\text{slow}}$. [13] In the slow coagulation regime, the stability ratio is a function of the interaction potential $V(r)$ and is described by the integral

$$W = 2R \int_{2R}^{\infty} \exp\left(\frac{V(r)}{k_B T}\right) r^{-2} dr, \quad (4.3.2)$$

where R gives the radius of the spheres, r the particle-particle center distance, and $k_B T$ the thermal energy of the suspension. [19]

The double layer interaction between two charged spheres can be calculated in terms of the weak-overlap-approximation. [20] For two charged spheres the interaction potential results to

$$V_{2s}(D) = \frac{24\pi R c_0 (e\Psi_0)^2}{\kappa^2 k_B T} \exp(-\kappa D) \equiv A \exp(-\kappa D), \quad (4.3.3)$$

where Ψ_0 is the effective surface potential, c_0 the electrolyte number concentration in solution, and D the particle surface-surface distance. Note that eq. (4.3.3) is only valid if $\kappa R_c \gg 1$ and $e\Psi_0/k_B T < 1$. In the scope of this work both conditions are fulfilled. The double layer interaction potential decreases exponentially with growing particle separation from its maximal value A defined through eq. (4.3.3). The Debye screening length $1/\kappa$ is related to c_0 according to $1/\kappa^2 = \epsilon_0 \epsilon k_B T / \sum_i (z_i e)^2 c_{0,i}$. Due to the solid poly(styrene) core of the SPB (Figure 4.1.1a), we must modify eq. (4.3.3) in regard to the attractive van der Waals forces given as [20]

$$V_{\text{vdW}}(D) = -\frac{HR}{12D}, \quad (4.3.4)$$

where H denotes the Hamaker constant. Therefore, the stability ratio determined by light scattering can be used to obtain the prefactor A experimentally by combining eq. (4.3.2) with eq. (4.3.3) and eq. (4.3.4).

4.4. Results and Discussion

4.4.1. Stability Ratio

Recent studies have shown that in a monovalent counterion environment, two planar polyelectrolyte brushes show purely repulsive forces. [3] However, in the presence of lanthanum ions the brushes behave very differently. Figure 4.2.1 displays the result of a typical SFA measurement in the presence of low concentrations of trivalent lanthanum. There is a strong adhesive minimum, observable on approach and separation, enabling quantification of length scales such as twice the height of the collapsed brush layers δ and $1/\kappa$. The shape of this curve is clearly that envisioned in Figure 4.1.1c, with an exponentially decaying repulsive force beyond the adhesive minimum. The functional dependence of the repulsive force on distance necessary for the subsequent analysis (see below) is thus established.

We now turn to the evaluation of the repulsive force between two spherical polyelectrolyte brushes in dilute solution. Figure 4.3.1 displays the hydrodynamic radius $R_H(t)$ and the static light scattering intensity $I(q, t)$ as the function of the time t . The rate of coagulation of the particles can be directly obtained from the slopes of R_H vs. time t . Absolute values of the rate constant are available through application of eq. (4.3.1) to both parts a and b of Figure 4.3.1. We find that the initial hydrodynamic radius $R_H(t = 0)$ stays practically constant at 128 nm for all concentrations of the lanthanum ions under consideration here (Figure 4.3.1). This result is in complete agreement with the work of Mei and co-workers [17] and simplifies the subsequent analysis of the data.

The resulting stability ratio W is shown in Figure 4.3.2. There is a sharp transition from the reaction-limited coagulation where $W > 1$ to the diffusion-limited fast coagulation regime in which $W = 1$. W is unity in case of LaCl_3 concentrations from 0.5 mM to

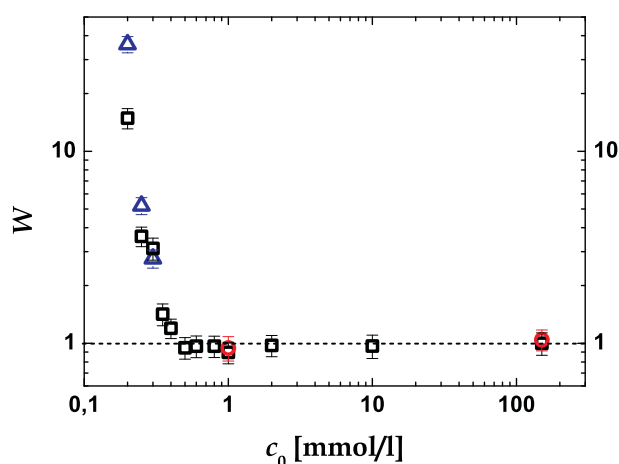


Figure 4.3.2.: Stability ratio $W = k_{11}(c_0 = 150 \text{ mM})/k_{11}(c_0)$ of the SPB as a function of the lanthanum concentration c_0 for different number concentrations $[P]_0$: $1.23 \times 10^{15} \text{ m}^{-3}$ (triangles); $1.64 \times 10^{14} \text{ m}^{-3}$ (squares); $8.20 \times 10^{13} \text{ m}^{-3}$ (circles). The scattering angle θ is 90° .

150 mM. The experimental fast coagulation rate constant is $(3.9 \pm 0.2) \times 10^{-18} \text{ m}^3/\text{s}$ and is independent of the number concentration as required by coagulation theory. We obtain $(k_{11})_{\text{fast}}$ by averaging all experimental coagulation rate constants in the diffusion-limited regime. This value is smaller than the theoretical von Smoluchowski value of $12.2 \times 10^{-18} \text{ m}^3/\text{s}$. However, the present value is in full agreement with data taken from the literature. [13, 21–23]

We now calculate the stability ratio W as a function of the LaCl_3 concentration c_0 via eq. (4.3.2) by using the interaction pair potential $V(r)$ (eq. (4.4.1), Figure 4.1.1c) that has previously been obtained by direct SFA-measurements (Figure 4.2.1). [18]

$$V(r) = \begin{cases} -\varepsilon & 2R_C \leq r \leq 2R_C + \delta; \\ Ae^{-\kappa(r-2R_C-\delta)} + V_{\text{vdW}}(r-2R_C) & 2R_C + \delta \leq r; \end{cases} \quad (4.4.1)$$

Here, r is the particle-particle center distance, R_C is the radius of the core particles, δ is twice the thickness L of the collapsed shells, and A is the prefactor of eq. (4.3.3). Note that we can determine all of these parameters independently in the SFA also (Figure 4.2.1). Upon contact of the particle shells, a strong attractive force $-\varepsilon$ results due to interparticle bridging of the polyelectrolyte chains. Further, we assume that only the solid poly(styrene) core of the SPB exhibits van der Waals forces:

$$W = (2R_C + \delta) \left[\int_{2R_C}^{2R_C+\delta} \frac{\exp\left(\frac{-\varepsilon}{k_B T}\right)}{r^2} dr + \int_{2R_C+\delta}^{\infty} \left(\frac{\exp\left[\tilde{A}e^{-\kappa(r-2R_C-\delta)}\right]}{r^2} - \frac{\exp\left[\frac{HR_C}{12k_B T(r-2R_C)}\right]}{r^2} \right) dr \right], \quad (4.4.2)$$

with $\tilde{A} = A/k_B T$. Since $\delta \ll 2R_C$, the first integral does not significantly contribute to the stability ratio. Therefore, only the second integral in eq. (4.4.2) needs to be taken into account. To correct for the hydrodynamic drag at a given surface to surface distance h , we have to modify eq. (4.4.2) and introduce the approximating function $B(h)$. [24] Also, in eq. (4.4.2) we must substitute the particle-particle center distance to $r = h + 2R_C + \delta$. Note that $2R_C + \delta = 2R_H$ with $\delta = 14 \text{ nm}$ (Figure 4.1.1). Hence,

$$W = 2R_H \int_0^{\infty} B(h) \frac{\exp\left[\tilde{A}e^{-\kappa h} - \frac{HR_C}{12k_B T(h+\delta)}\right]}{(h + 2R_H)^2} dh. \quad (4.4.3)$$

Numerical integration of eq. (4.4.3) leads to the stability ratio of the SPB at arbitrary Debye lengths κ^{-1} . For every LaCl_3 concentration we fit the prefactor \tilde{A} using eq. (4.4.3) to the values of the stability ratio determined in our light scattering experiments (Figure 4.3.2). We chose the Hamaker constant to $0.9 \times 10^{-20} \text{ J}$. [25] Plotting of the prefactor \tilde{A} as a function of c_0 reveals an increase of \tilde{A} with decreasing electrolyte concentration as expected (Figure 4.4.1). According to eq. (4.3.3), the prefactor is only proportional to the square of the surface potential of the SPB particles.

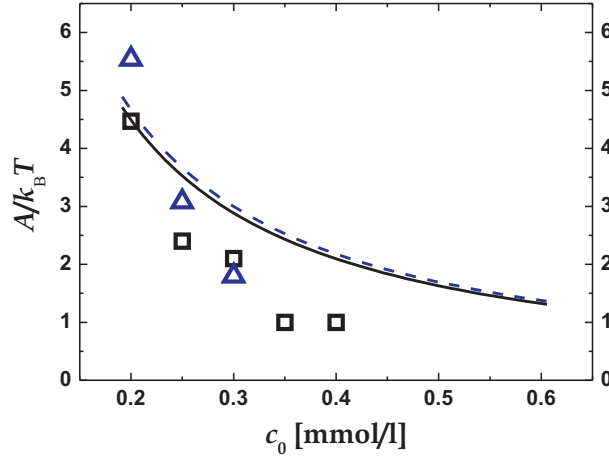


Figure 4.4.1.: Prefactor \tilde{A} as a function of salt the concentration c_0 of LaCl_3 . Experimental data are shown for two different SPB concentrations $[P]_0$: $1.23 \times 10^{15} \text{ m}^{-3}$ (triangles); $1.64 \times 10^{14} \text{ m}^{-3}$ (squares). The lines are the predictions from the mean-field theory for the same SPB concentrations $[P]_0$: $1.23 \times 10^{15} \text{ m}^{-3}$ (broken line); $1.64 \times 10^{14} \text{ m}^{-3}$ (solid line).

4.4.2. Repulsive Force and Effective Surface Charge

To compare the experimental results with theoretical predictions, we now determine the prefactor \tilde{A} from eq. (4.3.3) by calculating the surface potential Ψ_0 . The latter quantity can be related to the surface charge of the SPB, similar to the Grahame equation in the planar case. [20] Hsu et al. calculated this relation for charged spheres in the presence of asymmetric electrolytes. [26] We use the approximated analytical solution based on a perturbation method up to the order of $(\kappa R)^{-2} \approx 10^{-3}$. So far the surface charge density σ_c is unknown. Using $\sigma_c = Q^*/(4\pi R^2)$ the calculation of Ψ_0 requires the net charge Q^* of the SPB. We determine the net charge using a variational free energy calculation. [27] The main features of this mean-field approach are as follows: using a cell model, the free energy of an isolated SPB, in correspondence to a given density, consists of three contributions. The first is a Hartree-type electrostatic contribution describing the electrostatic potential of the SPB with a net charge Q^* . The second contributions are of entropic nature that account for the entropy of the salt ions inside and outside of the brush. Finally, chain contributions such as the Flory-like elastic and the excluded-volume terms need to be considered too. [28, 29] Minimizing the total free energy with respect to Q^* and also with respect to the brush thickness L , the surface charge density σ_c is readily obtained. [27, 30] We make the following simplifications. First, we neglect the entropic contribution of all adsorbed La^{3+} ions, i.e. no entropic ion contribution inside the brush. Second, we neglect any adsorption of like-charged co-ions Cl^- by the SPB. Both assumptions are justified by results from simulations and theoretical calculations of SPBs or star-like polyelectrolytes. [17, 31, 32] Having now the surface charge density σ_c , we are able to determine the surface potential Ψ_0 . [26] Using Ψ_0 in eq. (4.3.3), the prefactor \tilde{A} is calculated as a function of the salt concentration c_0 . A comparison with the experimental data is plotted in Figure 4.4.1.

As can be seen, the calculated prefactor \tilde{A} is within the experimental range, but decays slower with increasing ionic strength. However, note that no adjustable parameter has been used for this comparison. In Figure 4.4.1 the theoretical curve at high SPB density ($[P]_0 = 1.23 \times 10^{15} \text{ m}^{-3}$) is slightly higher than the low-density curve ($[P]_0 = 1.64 \times 10^{14} \text{ m}^{-3}$) due to the finite number of salt ions in solution: at given salt concentration c_0 a reduced SPB density leads to a higher number of salt ions per SPB, which decreases its effective charge and hence the prefactor \tilde{A} . The net charge of the brush is found to be located in the range of 600-800 $|e|$, corresponding to about 0.05% of the bare charge (around $1.5 \times 10^6 |e|$). The calculated brush thickness is around $L = 4.5 \text{ nm}$, comparable to the experimental value of 7 nm obtained for all concentrations of LaCl_3 . Considering the simplicity of the theoretical model, the agreement is remarkable. For the first time experimental results confirm the prediction of the free energy calculations regarding the small net charge of SPBs. [27]

4.5. Conclusion

In conclusion, we presented the first direct comparison between the force measurements of polyelectrolyte brushes by the SFA and the repulsive force between microscopic brush particles. The rate of slow coagulation of spherical polyelectrolyte brushes was used to evaluate the strength of repulsive interaction between two particles in solution. The interaction potential was modeled using the force law obtained directly from SFA measurements. This approach is capable of measuring the repulsive interaction down to strength of one $k_B T$. The data thus obtained compare favorably with theoretical values derived from the effective charge of spherical polyelectrolyte brushes.

4.6. Acknowledgements

R.F., P.P., and M.T. gratefully acknowledge support for this work from the National Science Foundation grants numbers DMR-0520415 and DMR-0710521 (Materials World Network). M.B. gratefully acknowledges support by the Deutsche Forschungsgemeinschaft. C.S. thanks the Elite Study Program Macromolecular Science in the Elite Network Bavaria for support during this work and C.S and M.B. gratefully acknowledge the Bavarian California Technology Center BaCaTec for financial support of this joint project.

4.7. References

- [1] Meyer, E. E.; Rosenberg, K. J.; Israelachvili, J. N. *Proc. Natl. Acad. Sci. U.S.A.* **2006**, *103* (43), 15739.
- [2] Israelachvili, J. N. *J. Colloid Interface Sci.* **1973**, *44* (2), 259.
- [3] Balastre, M.; Li, F.; Schorr, P.; Yang, J.; Mays, J. W.; Tirrell, M. V. *Macromolecules* **2002**, *35*, 9480.

-
- [4] Grier, D. G. *Nature* **2003**, *424*, 810.
- [5] Kegler, K.; Salomo, M.; Kremer, F. *Phys. Rev. Lett.* **2007**, *98*, 058304.
- [6] Dominguez-Espinosa, D.; Synytska, A.; Drechsler, A.; Gutsche, C.; Kegler, K.; Uhlmann, P.; Stamm, M.; Kremer, F. *Polymer* **2008**, *49*, 4802.
- [7] Claesson, P. M.; Ederth, T.; Bergeron, V.; Rutland, M. W. *Adv. Colloid Interface Sci.* **1996**, *67*, 119.
- [8] Bike, S. G. *Curr. Opin. Colloid Interface Sci.* **2000**, *5*, 144.
- [9] Walz, J. Y. *Curr. Opin. Colloid Interface Sci.* **1997**, *6* (2), 600.
- [10] Ducker, W. A.; Senden, T. J.; Pashley, R. M. *Nature* **1991**, *353*, 239.
- [11] Butt, H. J.; Cappella, B.; Kappl, M. *Surf. Sci. Rep.* **2005**, *59*, 1.
- [12] Ralston, J.; Larson, I.; Rutland, M. W.; Feiler, A. A.; Kleijn, M. *J. Macromol. Sci., Part A: Pure Appl. Chem.* **2005**, *77* (12), 2149.
- [13] Holthoff, H.; Egelhaaf, S. U.; Borkovec, M.; Schurtenberger, P.; Stricher, H. *Langmuir* **1996**, *12*, 5541.
- [14] Guo, X.; Ballauff, M. *Phys. Rev. E* **2001**, *64*, 051406.
- [15] Pincus, P. *Macromolecules* **1991**, *24*, 2912.
- [16] Borisov, O. V.; Birshtein, T. M.; Zhulina, E. B. *J. Phys. II (Fr.)* **1991**, *1* (5), 521.
- [17] Mei, Y.; Lauterbach, K.; Hoffmann, M.; Borisov, O. V.; Ballauff, M.; Jusufi, A. *Phys. Rev. Lett.* **2007**, *97*, 158301.
- [18] Li, F.; Schorr, P.; Tirrell, M. V.; Mays, J. *Polym. Prepr.* **2005**, *46*(1), 377.
- [19] Evans, D. F.; Wennerström, H. *The Colloidal Domain*; Wiley-VCH: New York, 1999.
- [20] Israelachvili, J. N. *Intermolecular and Surface Forces*; Academic Press: New York, 1998.
- [21] Behrens, S. H.; Borkovec, M. *Langmuir* **2000**, *16*, 2566.
- [22] van Zanten, J. H.; Elimelech, M. *J. Colloid Interface Sci.* **1992**, *154*, 1.
- [23] Sonntag, H.; Strenge, K. *Coagulation and Structure Formation*; VEB Deutscher Verlag der Wissenschaften: Berlin, 1987.
- [24] Behrens, S. H.; Christl, D. I.; Emmerzael, R.; Schurtenberger, P.; Borkovec, M. *Langmuir* **2000**, *16*, 2566.
- [25] Bevan, M. A.; Prieve, D. C. *Langmuir* **1999**, *15*, 7925.

- [26] Hsu, J.-P.; Kuo, Y.-C. *J. Colloid Interface Sci.* **1994**, *167*(1), 35.
- [27] Jusufi, A.; Likos, C. N.; Ballauff, M. *Colloid Polym. Sci.* **2004**, *282* (8), 910.
- [28] Alexander, S. *J. Phys. (Paris)* **1977**, *38*, 977.
- [29] de Gennes, P. G. *Macromolecules* **1980**, *13*, 1069.
- [30] Jusufi, A.; Likos, C. N.; Löwen, H. *Phys. Rev. Lett.* **2002**, *88*, 018301.
- [31] Jusufi, A.; Likos, C. N.; Löwen, H. *J. Chem. Phys.* **2002**, *116*(24), 11011.
- [32] Mei, Y.; Hoffmann, M.; Ballauff, M.; Jusufi, A. *Phys. Rev. E.* **2008**, *77*(3), 031805.

5. Investigation of the Stability Behavior of Anionic Spherical Polyelectrolyte Brushes in the Presence of La(III) Counterions

Christian Schneider¹, Arben Jusufi², Robert Farina³, Philip Pincus³,
Matthew Tirrell^{3,4,†}, Matthias Ballauff^{5,‡}

¹Physikalische Chemie I, University of Bayreuth, 95440 Bayreuth, Germany

²Institute for Computational Molecular Science, Temple University, Philadelphia, Pennsylvania
19122-6081, USA

³Departments of Chemical Engineering and Materials, Materials Research Laboratory,
University of California-Santa Barbara, Santa Barbara, California 93106-2050, USA

⁴Department of Bioengineering, Chemical Engineering and Materials Science, and
Engineering, Materials Science Division, Lawrence Berkeley National Laboratory,
University of California-Berkeley, Berkeley, California 94720-1762, USA

⁵F-12 Soft Matter and Functional Materials Helmholtz-Zentrum Berlin, Hahn-Meitner-Platz 1,
14109 Berlin, Germany, and
Department of Physics Humboldt University Berlin, Newtonstr. 15, 12489 Berlin, Germany

[†]Email: mvtirrell@berkeley.edu

[‡]Email: matthias.ballauff@helmholtz-berlin.de

Published in Physical Review E, 2010, 82, 011401.

Reproduced with permission from
Physical Review E, 2010, 82, 011401.
© 2010 The American Physical Society.

DOI: 10.1103/PhysRevE.82.011401

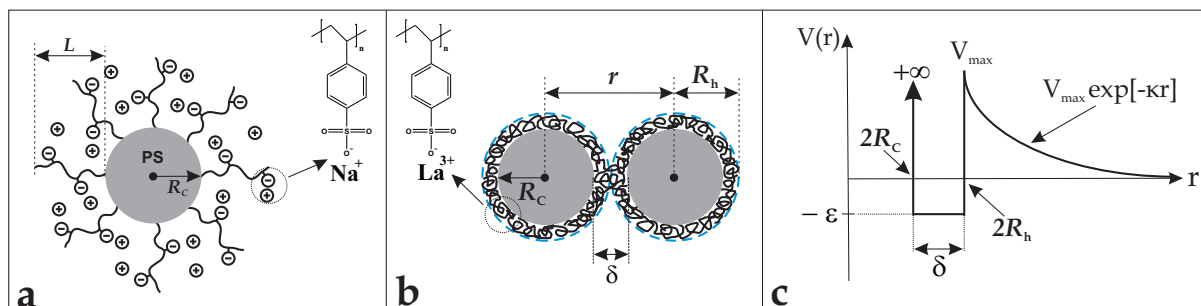


Figure 5.1.1.: (a) Schematic representation of the spherical polyelectrolyte brush investigated in this study. Anionic polyelectrolyte chains are grafted from colloidal particles (radius: $R_c = 125$ nm) made from solid poly(styrene). The particles are immersed in aqueous salt solutions with defined ionic strength. The thickness L of the brush layer is measured for different ionic strengths by dynamic light scattering. The ionic strength in the system is adjusted by changing the concentration of added salt. (b) Schematic of two aggregated SPB particles upon contact of their polyelectrolyte shells with fully collapsed brush layers. The particle-particle center distance r equals $2R_h = 2R_c + \delta$ where δ is twice the brush thickness L . In all concentrations of lanthanum ions used here the hydrodynamic radius R_h of the particles is constant. (c) Interaction potential of the SPB particles in the aqueous lanthanum solutions used in our study. [2]

5.1. Abstract

In this paper we discuss the stability behavior of spherical polyelectrolyte brushes (SPB) in the presence of trivalent lanthanum counterions. Stability behavior is measured through the rate of coagulation of the SPB as a function of the lanthanum concentration using simultaneous static and dynamic light scattering. As the counterion concentration increases, we observe coagulation of the SPB which in turn leads to a dramatic decrease in the stability of our particles. Since the rate of coagulation is dependent upon the balance between the repulsive interactions and the thermal energy of the diffusing particles (reaction-limited colloidal aggregation; RLCA), we then can relate the measured particle stability to the value of the repulsive potential in the RLCA regime. These ‘microsurface potential measurements’ (MSPM) allow us to measure repulsive energies down to the order of $k_B T$. From the repulsive energy of the particles we can then determine precise information about the net surface potential Ψ_0 of the SPB as a function of the lanthanum counterion concentration. Moreover, we demonstrate that a simple mean-field model predicts the stability of the SPB in the presence of lanthanum counterions with high accuracy.

5.2. Introduction

Colloidal dispersions consisting of solid nanoparticles dispersed in water present one of the most studied systems in colloid science. [1] In principle these systems are metastable, that is, the particles will aggregate if insufficient stabilization is present. [2] Stabilization can be achieved in two ways: Either charges are affixed to surfaces of the particles (electrostatic stabilization) or the particles can carry long polymer chains (steric stabilization). [3] Individually, both modes of stabilization are now rather well understood. In particular, electrostatic stabilization can be cast into the well-known Derjaguin-Landau-Verwey-Overbeek (DLVO) theory [4, 5] which allows a detailed prediction of colloidal stability in the presence of multivalent salt ions with valency z of a given critical concentration n_{crit} . Here the empirical Schulze-Hardy rule states that $n_{crit} \propto z^{-6}$ in direct agreement with the DLVO theory. [6]

Much less is known about electrostatic stabilization that results from appending charged polymer chains to the surface of colloidal spheres. Here, electrostatic and steric effects are combined to create the so called electrosteric stabilization. This electrosteric stabilization is the basis of many industrial polymer dispersions. [7] Hence, a profound understanding of electrosteric stabilization is of central technological importance. It is also important to note, that many applications in medicine and personal care products operate in multivalent ionic media. Spherical polyelectrolyte brushes (SPB) that consist of solid colloidal spheres onto which long chains of a polyelectrolyte are appended present excellent model systems for an in-depth study of electrosteric stabilization. [8] Figure 5.1.1a displays the structure of these particles in a schematic fashion. The term brush indicates a grafting density of the appended chains that is dense enough to ensure strong lateral interactions among the polyelectrolyte chains. [9] The main feature of polyelectrolyte brushes is the strong confinement of the counterions within the brush layer, first predicted by Pincus [10] as well as Birshstein, Borisov, and Zhulina. [11] If monovalent counterions are present, the high number of charges confined in such a polyelectrolyte brush will lead to a strong stretching of the attached chains in order to alleviate the concomitant osmotic pressure of the counterions. If the ionic strength is raised in this system by adding monovalent salt, the height of the polyelectrolyte layer will decrease considerably. [12, 13] However, the colloidal stability remains unimpeded as experimental studies have demonstrated that the SPB are fully stable even in a three molar solution of monovalent salt. [13] The results regarding the salt dependency of the brush height obtained for the spherical systems are in qualitative agreement with direct measurements using the surface forces apparatus (SFA). [14, 15]

An entirely different situation arises if di- or trivalent salt is added to aqueous solutions of spherical polyelectrolyte brushes. It has been demonstrated that rather moderate concentrations (0.1 mol/l) of divalent ions lead to the loss of colloidal stability and to the flocculation of particles. [12] In the case of trivalent ions, minute concentrations are sufficient to induce flocculation. [16] Concomitantly, the polyelectrolyte chains collapse to form a rather dense layer that does not provide any steric stabilization. [2] Hence, results obtained in the presence of monovalent counterions show a strong stability of the

SPB, while minute concentrations of trivalent ions lead to rapid flocculation. As has been discussed recently [16], the height L of the brush layer affixed to the surface of the particles can be quantitatively understood in terms of a simple model [17], if ion specific interactions with the polyelectrolyte chains as observed, e.g., for a poly(methacrylic acid) brush by Konradi and R uhe [18] can be neglected. L then results from a balance between the stretching of the chains due to the osmotic pressure of the counterions and the entropic retracting force of the coiled polymer chains. The results of this model are in excellent agreement with recent molecular dynamics (MD) simulations and experimental results. [19, 20] An important assumption of this model is a strong electrostatic interaction between multivalent ions with the polyelectrolyte chains. Multivalent ions also replace an equivalent amount of monovalent ions and thus take away significant contributions to the osmotic pressure. This explains not only the strong reduction of L but suggests also a qualitative explanation of the decreased colloidal stability of the SPB in the presence of multivalent ions. [19] In our study we use rather high concentrations of lanthanum counterions which leads to two primary effects: firstly, the shell layers of the SPB are always completely collapsed, and secondly, the shell layers of the SPB stick to each other upon contact. [2]

In a recent paper, we demonstrated that the rate of coagulation can be used to assess the repulsive force in the particle interaction potential $V(r)$ between two colloidal particles. [2] The central idea is depicted in Figure 5.1.1. The surfaces of two SPB can approach each other to a certain minimum distance $\delta = 2L$. In this configuration, the potential $V(r)$ is at a maximum value $V_{max} = V(2R_c + \delta)$ with R_c as the particle core radius. Therefore, V_{max} presents the maximum barrier that needs to be overcome by thermal motion to achieve contact between two particles in the fully collapsed state. In the presence of moderate concentrations of multivalent salt, two particles will stick to each other essentially irreversibly once their surfaces have touched [21]. Therefore, the rate of coagulation leads to direct information on the potential $V(r)$ and in particular on V_{max} . The basic theory of the rate of coagulation is well known: if $V_{max} = 0$, the limiting case of the diffusion-limited colloidal aggregation (DLCA) is reached. [6] For $V_{max} > 0$, the rate of coagulation in this reaction-limited colloidal aggregation (RLCA) regime is much slower. For $V_{max} \gg k_B T$, coagulation is slow enough that the suspension appears stable.

Up until now, careful measurements of the kinetics of coagulation have been used to test given interparticle potentials, for example the well-known DLVO-potential. [3, 22] Borokov and co-workers then demonstrated that the rate of coagulation can be obtained very accurately by a combination of static and dynamic light scattering. [23, 24] However, the procedure can be reversed. First, we measure the formation rate of particle doublets. Applying the interparticle potential of fully collapsed polyelectrolyte brushes then leads to $V(r)$ and in particular V_{max} of the SPB. These 'microsurface potential measurements' (MSPM) hence supplement the classical methods used for obtaining the repulsive pair potential. This has been done through experimental methods such as the SFA [14, 25, 26], optical tweezers (OT) [27–29], the total internal reflection microscopy (TIRM) [30–32], and the colloidal probe atomic force microscope (AFM). [33–35] In particular, MSPM allow us to assess the repulsive potential $V(r)$ between colloidal particles of

arbitrary size down to the theoretical limit, $V_{max} \approx k_B T$. In general, MSPM give precise information about the maximum of the repulsive interaction V_{max} . In many cases, the functional dependence of the potential on r is known or can be found through measurements with parallel surfaces using the SFA. With this information, MSPM can lead to a full comparison between theory and experiment. [2]

With this work we wish to extend our previous work on MSPM and to expand the discussion of the method used. Moreover, a critical comparison of the theoretical model for $V(r)$, which has been developed recently for SPB, will be given. [2] While our previous work was confined to the domain of weak repulsion, a stability ratio W close to unity, we shall discuss data of much more stable systems in which $W \approx 10^3$. Our comparison between theory and experimental work will thus provide a means to investigate electrosteric stabilization more thoroughly.

The paper is organized as follows: after the Experimental Section the theory related to the kinetics of coagulation will be reviewed. We then further investigate our theoretical model used for a comparison with experimental data. The subsequent section Results and Discussion, will first present the kinetic analysis of coagulation. This will be followed by an in-depth discussion of the comparison of this data with our theoretical model. A short conclusion will sum up the main points of this work.

5.3. Experimental Section

5.3.1. Materials and Methods

Materials. All solvents were analytical grade and used as received. Styrene (Sigma-Aldrich) was distilled under reduced pressure to remove inhibitor molecules and stored under nitrogen at 4°C until used. Sodium styrene sulfonic acid (Fluka), potassium persulfate (Merck), sodium bicarbonate (Grüssig), sodium bisulfite (Merck) and lanthanum(III)chloride heptahydrate (Sigma-Aldrich) were used without further purification. The synthesis of the photoinitiator 2-[p-(2-hydroxy-2-methylpropiophenone)]-ethyleneglycol-methacrylate (HMEM) was performed according to the method used by Guo *et al.* and purified chromatographically. [36] In all experiments we used water obtained from a Millipore ion exchange apparatus.

Instrumentation. For the dynamic light scattering (DLS) measurements and the simultaneous static and dynamic light scattering experiments we used an ALV-4000 goniometer with a 35 mW He-Ne laser operating at a wavelength of 632.8 nm, an ALV/High QE APD detector and an ALV-6010/160 External Multiple Tau Digital Korrelator unit. This setup was then able to obtain measurements at 10 s intervals using absolute particle concentrations as low as 10^{13} per m^3 at scattering angles between 20° and 150°.

Determination of the molecular weight and molecular weight distribution of the poly(styrene sulfonate) (PSS) chains was performed using aqueous gel permeation chromatography (GPC). We used linear poly(sodium styrene sulfonate) to construct a universal master curve. As eluent we used water at pH 9. For evaluation of the eluent we used an Agilent 1100 differential refractometer RID detector.

Transmission electron microscopy (TEM) images were prepared on a Zeiss CEM 902 instrument operating at an accelerating voltage of 80 kV. One drop of the aqueous suspensions (0.1% solid content) was deposited onto a copper grid coated with carbon (Plano) and air-dried at room temperature. The images were recorded digitally by a MegaView3 camera. We used the program IMAGEJ 1.37v (RSB, National Institute of Mental Health) for manually counting the mapped particles.

Synthesis of the SPB. The synthesis of the SPB follows the route mapped out by Wittmann *et al.* for anionic systems [37], with the exception of using sodium styrene sulfonic acid as the co-monomer and emulsifier in the emulsion polymerization of the core particles. Thus, the synthesis of the core is an emulsifier-free emulsion polymerization. The solid content in the emulsifier-free emulsion polymerization was chosen to be 12.5%. The amounts of sodium styrene sulfonic acid and other additives were chosen to yield core diameters of about 200 nm. [38] Before and after the photo emulsion polymerization of the PSS shell, the suspension was cleaned by a serum replacement with water. It should be noted that we avoided the use of detergent solution for the cleaning of instruments and equipment during the entire synthesis process of the SPB. Instead we used pure organic solvents and a mixture of isopropanol and potassium hydroxide. In this way, contamination of the system by surfactants was circumvented.

Characterization of the SPB. The hydrodynamic radius of the core R_c was (125 ± 2) nm, which was measured by DLS in water at very low ionic strength via cumulant analysis using the third cumulant and the Einstein-Stokes relationship. [39] The hydrodynamic radius of the SPB particles at very low ionic strength was (190 ± 2) nm, which includes the hydrodynamic shell thickness L of (65 ± 3) nm and the hydrodynamic radius of the core R_c . Note however, that this value strongly decreases in the presence of the multi-valent lanthanum counterions. For the DLS measurements the suspensions were filtered through a $1 \mu\text{m}$ PES filter. TEM gave a radius of 113.8 nm and a polydispersity index of 1.0001 for the core particles, for which we evaluated over 750 particles. The difference between the core radii values may be attributed to short polymer chains of co-monomer on the surface of the core particles, the presence of the electric double layer or very weak coagulation during the cleaning process. However, the difference does not play an essential role regarding the results shown here.

After cleaving off the chains from the core particles we determined the molecular weight distribution by GPC. [37] The contour length L_c of the chains was estimated using the molecular weight of (67500 ± 13500) g/mol of the longest chains in the shell layer. This yielded (82 ± 16) nm for L_c , where the monomer size has been estimated to be 0.25 nm. The mass ratio between the core and the shell m_c/m_s of the SPB was (12 ± 3) as determined by gravimetry. Considering m_c/m_s and the molecular weight of the longest polyelectrolyte chains of (67500 ± 13500) g/mol we calculated a grafting density σ of (0.03 ± 0.01) chains per nm^2 . Using the mass ratio m_c/m_s we also calculated the number of charged units per SPB particle to $Q(\text{NaSS}) = (1840000 \pm 644000)$.

The absolute number concentration $[P]_0$ of the SPB suspension after the photo emulsion polymerization was $(3.47 \pm 0.58) \times 10^{18}/\text{m}^3$. We calculated the particle concentration using the solid content of the suspension determined by gravimetry and the size of the

core particles determined via TEM. We also accounted for the weight of the shell layer of the SPB using the mass ratio m_c/m_s . For calculating the weight of the core particles we assumed a uniform density of 1.054 g/cm^3 , which is the polystyrene bulk density. [40]

Methods. The investigation of the coagulation kinetics of the SPB was performed using simultaneous static and dynamic light scattering as described by Holthoff and co-workers. [23] Our experiments also contained LaCl_3 in the concentration range of 0.16 to 150 mmol/l. In order to obtain a good signal for every salt concentration, we varied the absolute particle concentration between $(1.35 \pm 0.23) \times 10^{13}/\text{m}^3$ at high electrolyte concentrations and $(8.00 \pm 1.36) \times 10^{15}/\text{m}^3$ at low electrolyte concentrations. This particle concentration range was low enough to avoid multiple scattering. [23] All measurements of the stability ratio were performed at a scattering angle of 90° . For the determination of the Rayleigh-Debye (RD) form factor of the SPB, we used an absolute particle concentration of $(3.00 \pm 0.51) \times 10^{14}/\text{m}^3$ and electrolyte concentrations of 1 mmol/l and 5 mmol/l at scattering angles between 20° and 150° . In all cases, the temperature during the light scattering measurements was 25°C .

The light scattering cells were cleansed regularly with chromium sulfuric acid to eliminate organic residues. Between measurements, the light scattering cells were flushed several times with water and electrolyte solution before reuse. We compared the initial radius of the SPB particles of each individual measurement and found no major deviations. We also had high reproducibility of the fits of both the hydrodynamic and static light scattering experiments.

We prepared two different stock solutions with the absolute number concentrations of $(2.25 \pm 0.28) \times 10^{16}/\text{m}^3$ and $(3.47 \pm 0.59) \times 10^{17}/\text{m}^3$, respectively. Coagulation was then initiated by adding a latex stock solution (in the range of 15 - 40 μl) to an electrolyte solution (in the range of 1.3 - 2.6 ml) in the light scattering cell. The same latex stock solutions were used for all coagulation measurements. Data were collected at 10 s intervals to yield a data point for both the hydrodynamic radius and the scattering intensity at time t . In the dynamic light scattering measurements, we fit the autocorrelation function with a non-linear square fit using a third-order cumulant expansion with an adjustable baseline to yield one data point. The values for the hydrodynamic radius were calculated out of the first cumulant and through the use of the Stokes-Einstein relationship. For this calculation we have taken into account changes in the viscosity based on electrolyte concentration. [41] In the static light scattering measurements, we calculated the time average of the scattering intensity to give one data point every 10 s. For one coagulation measurement, we combine approximately 150 - 1000 static and dynamic data points.

For all electrolyte concentrations and scattering angles, we determined the coagulation rate constant k_{11} using eq. (5.3.1). In order to obtain the initial slope, we fit a second degree polynomial to the static and dynamic data. Extrapolating the fits to time zero yields the values of the hydrodynamic radius $R_h(0)$ and the scattering intensity $I(0)$. Due to the fact, that the lanthanum concentrations were high, the shell layer of the SPB particles was always completely collapsed. Therefore, we could determine the mean hydrodynamic radius of the collapsed SPB, $R_{h,csl}$, by averaging the values of $R_h(0)$ of all lanthanum concentrations. This yields $(137 \pm 3) \text{ nm}$ for $R_{h,csl}$. The error is the standard deviation of

the individual values. Subtracting the hydrodynamic core radius of the particles gives the mean hydrodynamic shell thickness of the SPB, L . The radius of the single particles $R_{h,1}$ is assumed to be given by the hydrodynamic radius at time zero, so that $R_{h,1} = R_h(0)$. The method of Holthoff and co-workers [23] is strictly valid only at the initial stage of the coagulation process where only doublets are formed. Therefore, we considered only data points up to the point where $R_h(t) = 1.2 R_h(0)$ for evaluation. We calculated the stability ratio using the equation $W = k_{11}[c(\text{electrolyte}) = 150 \text{ mmol/l}]/k_{11}[c(\text{electrolyte})]$ where every measurement of $k_{11}[c(\text{electrolyte})]$ was repeated at least three times. Averaging all coagulation rate constants in the fast regime yielded the experimental fast coagulation rate constant.

We determined the relative form factors as a function of the scattering angle using eq. (5.3.2) for the dynamic data to yield $I_2/2I_1$ and eq. (5.3.3) for the static measurements to give $(I_2/2I_1) - 1$, where I_1 and I_2 are the singlet and doublet light scattering intensities, respectively. In both cases, we calculated k_{11} out of each individual measurement from eq. (5.3.1). Again, we repeated the measurements at every scattering angle at least three times.

5.3.2. Simultaneous Static and Dynamic Light Scattering

The coagulation rate constant k_{11} of colloidal particles can be precisely determined by simultaneous static and dynamic light scattering. [23] Measurements of the change of the hydrodynamic radius dR_h and the scattering intensity dI during the coagulation process as a function of the time at an arbitrary scattering angle can be evaluated through [23]

$$k_{11}[P]_0 = \frac{R_{h,2}}{R_{h,2} - R_{h,1}} \left(\frac{dR_h(t)/dt}{R_h(0)} \right) - \left(\frac{dI(q, t)/dt}{I(q, 0)} \right), \quad (5.3.1)$$

where $[P]_0$ is the initial particle concentration, $R_{h,1}$ and $R_{h,2}$ are the hydrodynamic radii of single spheres and doublets, respectively, $R_h(t)$ is the hydrodynamic radius of the particles at a specific time t , and $I(q, t)$ is the angle dependent scattering intensity of the suspension at time t . The doublet hydrodynamic radius is calculated using the equation $R_{h,2} = 1.38R_{h,1}$ as introduced by the work of Borkovec and co-workers. [23] Within the Rayleigh-Debye approximation, the initial change of the hydrodynamic radius at an arbitrary scattering vector q is given by [42]

$$\frac{1}{R_h(0)} \left(\frac{dR_h(t)}{dt} \right)_{t \rightarrow 0} = \frac{I_2(q)}{2I_1(q)} \left(1 - \frac{R_{h,1}}{R_{h,2}} \right) k_{11}[P]_0 \quad (5.3.2a)$$

$$= \left(\frac{\sin(2aq)}{2aq} + 1 \right) \left(1 - \frac{R_{h,1}}{R_{h,2}} \right) k_{11}[P]_0, \quad (5.3.2b)$$

where a is the radius of the primary particles and $q = 4\pi n/\lambda \sin(\theta/2)$. Here, n is the refractive index of the medium, λ is the wavelength of the incident beam, and θ is the scattering angle. The static light scattering data allows the determination of the optical

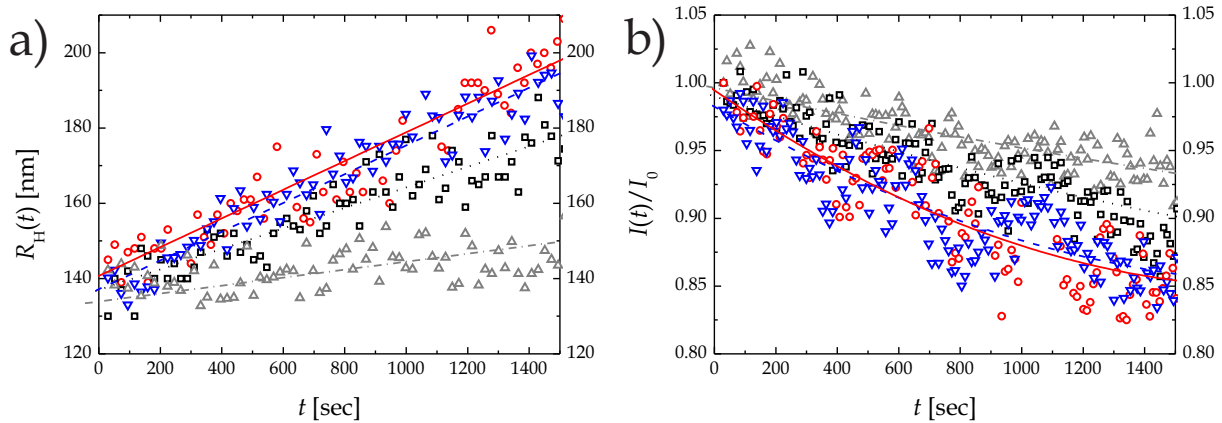


Figure 5.3.1.: (a) The hydrodynamic radius $R_h(t)$ and (b) the normalized scattering intensity $I(q, t)/I_0(q)$ as a function of time for different lanthanum concentrations c_0 with linear and 2nd order fits, respectively: 150 mmol/l (circles, solid line); 1 mmol/l (reversed triangles, broken line); 0.45 mmol/l (squares, dotted line); 0.21 mmol/l (triangles, broken dotted line). Here, the number concentration $[P]_0$ is $3.00 \times 10^{14} \text{ m}^{-3}$ and the scattering angle θ is 90° .

factor $[I_2(q)/2I_1(q)] - 1$ using [42]

$$\frac{1}{I(q, 0)} \left(\frac{dI(q, t)}{dt} \right)_{t \rightarrow 0} = \left(\frac{I_2(q)}{2I_1(q)} - 1 \right) k_{11}[P]_0 \quad (5.3.3a)$$

$$= \left(\frac{\sin(2aq)}{2aq} \right) k_{11}[P]_0. \quad (5.3.3b)$$

5.4. Theory

5.4.1. Coagulation Kinetics of SPBs

The coagulation rate constant k_{11} for the formation of doublets from singlet particles undergoing Brownian motion is defined through [43]

$$\frac{d[P]}{dt} = k_{11}[P]^2, \quad (5.4.1)$$

where $[P]$ is the singlet particle concentration at a given time t . [6] In the present work the doublet formation is assumed to be irreversible. If no repulsive forces hinder the coagulation of the particles, the coagulation process is controlled entirely by Brownian motion. For this diffusion limited, or fast coagulation process, the theory of von Smoluchowski predicts a coagulation rate constant $k_{11,Sm}$ of [44, 45]

$$k_{11,Sm} = \frac{4k_B T}{3\eta}, \quad (5.4.2)$$

where $k_B T$ is the thermal energy of the particles and η is the viscosity of the fluid. In the case of repulsive interaction between the particles, only the fraction $1/W$ of all singlet

collisions results in the formation of doublets. W is the stability ratio, which is defined as the ratio of the rate constant of rapid coagulation $k_{11,fast}$ and the rate constant for particles with nonzero repulsion $k_{11,slow}$ [6]

$$W = \frac{k_{11,fast}}{k_{11,slow}}. \quad (5.4.3)$$

Note that, for the experimental determination of W we assume $k_{11}(c_0 = 150 \text{ mmol/l}) = k_{11,fast}$. In the slow coagulation regime, the stability ratio is a function of the total interaction potential $V(r)$ and must include a correction function $B(r)$, which accounts for the hydrodynamic interactions between the two colliding particles in the process of aggregation. Using $B(r)$, W is then described by [46]

$$W \equiv \frac{\int_{2R}^{\infty} B(r) \exp\left(\frac{V(r)}{k_B T}\right) r^{-2} dr}{\int_{2R}^{\infty} B(r) \exp\left(\frac{V_A(r)}{k_B T}\right) r^{-2} dr}, \quad (5.4.4)$$

where R is the radius of the spheres, $V_A(r)$ is the interaction potential including only attractive forces, and r is the particle-particle center distance. Here, the correction function for the hydrodynamic drag $B(r)$ is given as [24]

$$B(r) = \frac{6\left(\frac{r-2R}{R}\right)^2 + 13\left(\frac{r-2R}{R}\right) + 2}{6\left(\frac{r-2R}{R}\right)^2 + 4\left(\frac{r-2R}{R}\right)}. \quad (5.4.5)$$

The double layer interaction between two charged spheres can be calculated in terms of the weak-overlap-approximation. [47] For two charged spheres in the presence of a 3:1 electrolyte solution, the interaction potential results to

$$\begin{aligned} V_{2s}(r - 2R_h) &= \frac{24\pi R_h c_0 (e\Psi_0)^2}{\kappa^2 k_B T} \exp[-\kappa(r - 2R_h)] \\ &\equiv V_{max} \exp[-\kappa(r - 2R_h)], \end{aligned} \quad (5.4.6)$$

where Ψ_0 is the effective surface potential, c_0 is the electrolyte number concentration in the solution, e is the charge of an electron, and R_h is the hydrodynamic radius of the particles. Note that eq. (5.4.6) is only valid if $\kappa R_h \gg 1$ and $e\Psi_0/k_B T < 1$. In this work both conditions are fulfilled. [48] The double layer interaction potential decreases exponentially with growing particle separation from its maximal value V_{max} defined through eq. (5.4.6). The Debye screening length $1/\kappa$ is related to c_0 according to [6]

$$1/\kappa^2 = \epsilon \epsilon_0 k_B T / \sum_i (z_i e)^2 c_{0,i}, \quad (5.4.7)$$

where ϵ_0 is the permittivity of vacuum, ϵ is the relative dielectric permittivity of water, z_i is the valency, and $c_{i,0}$ is the number concentration of the ion species i .

We also must modify eq. (5.4.6) in regard to the attractive van der Waals forces. Taking into account retardation effects, the van der Waals interaction of the solid poly(styrene) core of the SPB is given by [49]

$$V_{vdW}^{core}(r - 2R_c) = -\frac{H_c R_c}{12(r - 2R_c)} \times \left(1 - \frac{5.32(r - 2R_c)}{\lambda_{vdW}} \ln \left[1 + \frac{\lambda_{vdW}}{5.32(r - 2R_c)} \right] \right), \quad (5.4.8)$$

where H_c denotes the Hamaker constant of the particle cores, R_c is the radius of the poly(styrene) core of the particles, and λ_{vdW} is the wave length of the van der Waals interactions. Following the literature, we set λ_{vdW} to 100 nm and H_c to 0.9×10^{-20} J. [2, 49] The van der Waals interaction of two hollow shells $V_{\text{vdW}}^{\text{shell}}$ with shell thickness $\delta/2$ is given by [50]

$$V_{\text{vdW}}^{\text{shell}}(r - 2R_h) = -\frac{H_s R_h}{12} \left(\frac{1}{(r - 2R_h + \delta)} - \frac{2}{(r - 2R_h + \delta/2)} + \frac{1}{r - 2R_h} \right) - \frac{H_s}{6} \ln \frac{(r - 2R_h)(r - 2R_h + \delta)}{(r - 2R_h + \delta/2)(r - 2R_h + \delta/2)}, \quad (5.4.9)$$

where H_s is the effective Hamaker constant of the polyelectrolyte shells.

In the frame of the DLVO theory, superposition of eqs. (5.4.6) and (5.4.8) leads to the interaction potential of charged hard spheres. The interaction potential of planar anionic polyelectrolyte brushes in the presence of LaCl_3 has previously been obtained by direct SFA measurements. [2, 21] These SFA measurements show an interaction potential which decreases exponentially with distance, as expected for electrostatic interaction. [47] However, upon contact of the two polyelectrolyte brushes a strong attractive force $-\varepsilon$ results. This strong attraction is due to intershell bridging of polyelectrolyte chains via the trivalent lanthanum counterions. The shape of force-distance curves measured by the SFA can be compared very closely with Figure 5.1.1c as we see an exponentially increasing repulsive force followed by an adhesive force as the surfaces are separated. Thus, we obtain the interaction pair potential $V(r)$ of spherical polyelectrolyte brushes in the presence of LaCl_3

$$V(r) = \begin{cases} -\varepsilon & 2R_c \leq r \leq 2R_c + \delta; \\ V_{\text{max}} e^{-\kappa(r-2R_c-\delta)} & 2R_c + \delta \leq r; \\ +V_{\text{vdW}}^{\text{core}}(r - 2R_c) & \\ +V_{\text{vdW}}^{\text{shell}}(r - 2R_c - \delta) & \end{cases} \quad (5.4.10)$$

Here, r denotes the particle-particle center distance, δ is twice the thickness L of the collapsed shells and V_{max} is the prefactor of eq. (5.4.6). In the case of SFA experiments, we can determine all of the parameters in eq. (5.4.10) independently. [2] Note that in the case of only monovalent counterions, as pointed out in earlier studies with the SFA, forces between polyelectrolyte brush layers are always repulsive. [14]

Even in the totally collapsed state (at high lanthanum concentrations) the polyelectrolyte shell layer consists mostly of water. Thus, the effective van der Waals force is close to zero. However, a certain degree of surface roughness of the collapsed shell layers and interparticle chain bridging must be taken into account. We therefore assume that a weak force is acting at very short particle separations due to the van der Waals force of the shell layers. We assume that $H_s = 10^{-4} H_c$, which is consistent with the SFA measurements. [2] The van der Waals force of the shell layers described by eq. (5.4.9) is not corrected in regard to the retardation effect, due to the fact that the effective Hamaker constant of the shell layer is very small. At this point it is interesting to note, that the van der Waals

force of the shell layers causes eq. (5.4.13) to converge for $h \rightarrow 0$. Otherwise, the integral in eq. (5.4.13) would diverge for $h \rightarrow 0$ because of $B(h)$. Thus, for core-shell systems the van der Waals attraction of the shell layers overcomes the repulsive hydrodynamic drag, which is expressed through $B(h)$, at separations < 1 nm. From eq. (5.4.10) the definition of $V_A(r)$ follows naturally to

$$V_A(r) = \begin{cases} -\varepsilon & 2R_c \leq r \leq 2R_c + \delta; \\ V_{\text{vdW}}^{\text{core}}(r - 2R_c) + V_{\text{vdW}}^{\text{shell}}(r - 2R_c - \delta) & 2R_c + \delta \leq r; \end{cases} \quad (5.4.11)$$

We now calculate the stability ratio W as a function of the LaCl_3 concentration c_0 via eq. (5.4.4) by using the interaction pair potential $V(r)$ of eq. (5.4.10) and the attractive potential $V_A(r)$ according to eq. (5.4.11). This leads to

$$W = \left\{ \int_{2R_c}^{2R_c+\delta} B(r) \exp\left[\frac{-\varepsilon}{k_B T}\right] r^{-2} dr + \int_{2R_c+\delta}^{\infty} B(r) \exp\left[\tilde{V}_{\text{max}} e^{-\kappa(r-2R_c-\delta)} + V_{\text{vdW}}^{\text{core}}(r-2R_c) + V_{\text{vdW}}^{\text{shell}}(r-2R_c-\delta)\right] r^{-2} dr \right\} \times \left\{ \int_{2R_c}^{2R_c+\delta} B(r) \exp\left[\frac{-\varepsilon}{k_B T}\right] r^{-2} dr + \int_{2R_c+\delta}^{\infty} B(r) \exp\left[V_{\text{vdW}}^{\text{core}}(r-2R_c) + V_{\text{vdW}}^{\text{shell}}(r-2R_c-\delta)\right] r^{-2} dr \right\}^{-1}, \quad (5.4.12)$$

with $\tilde{V}_{\text{max}} = V_{\text{max}}/k_B T$. The first integrals in both the numerator and the denominator do not significantly contribute to the stability ratio, because $\delta \ll 2R_c$ and ε is not very negative at the initial contact of the particle surfaces. This can be reasoned from the SFA measurements. [2] Therefore, only the second integrals in eq. (5.4.12) need to be taken into account. In eq. (5.4.12), one has to substitute the particle-particle center distance by $r = h + 2R_c + \delta$ where h is the separation distance between the brush surfaces and $\delta = 2(R_h - R_c)$ (Figure 5.1.1b). Now eq. (5.4.12) reads

$$W = \frac{\int_0^{\infty} B(h) (h + 2R_h)^{-2} \exp\left[\tilde{V}_{\text{max}} e^{-\kappa h} + V_{\text{vdW}}^{\text{core}}(h + \delta) + V_{\text{vdW}}^{\text{shell}}(h)\right] dh}{\int_0^{\infty} B(h) (h + 2R_h)^{-2} \exp\left[V_{\text{vdW}}^{\text{core}}(h + \delta) + V_{\text{vdW}}^{\text{shell}}(h)\right] dh}. \quad (5.4.13)$$

In this way, the stability ratio W of the SPB can be calculated at arbitrary Debye lengths $1/\kappa$ by numerical integration of eq. (5.4.13).

5.4.2. Mean-field Model

In order to predict the stability ratio W through eq. (5.4.13) the van der Waals interactions and the prefactor $\tilde{V}_{max} = V_{max}/(k_B T)$ of the electrostatic barrier potential is required. Due to the fact, that the contribution of the van der Waals interactions are given by eqs. (5.4.8) and (5.4.9), we only have to calculate V_{max} to predict W of the SPBs. According to its definition in eq. (5.4.6), the relevant quantity is the surface potential Ψ_0 , and ultimately, the effective surface charge density $\Sigma = Q^*/(4\pi(R_c + L)^2)$ of the SPB as outlined earlier. [2] There we used an approximate solution for the relation of Ψ_0 with the surface charge density Σ . [51] However, this approximation is valid only for $\kappa(R_c + L) > 2$. For the smaller values of $\kappa(R_c + L)$, the analytical approximation of the Poisson-Boltzmann solution given by Zhou can be used. [52] It is accurate to less than 5% for $\kappa(R_c + L) > 0.03$. In the following, the details of the model calculation will be given. We start with the determination of the surface charge density Σ . For this, the net charge Q^* and the brush thickness L were calculated for each salt concentration. Both quantities can be determined through a variational free energy approach that was originally applied on polyelectrolyte stars. [53, 54] This cell model can be extended to SPB by taking into account a core of finite size. [17] In previous studies we showed, that the mean-field model successfully describes the results of computer simulations, [19] the collapse of the brush height, [16] and the effective charge of SPBs [2, 20] in the presence of multivalent counterions for SPBs of various dimensions.

The free energy of an isolated SPB with a core radius R_c , number of chains f , a degree of polymerization D_p , and a brush thickness L , in correspondence to a given density, consists of the following contributions:

A Hartree-type contribution describes the electrostatic potential of the SPB with a net charge Q^* , [17]

$$\frac{U_H}{k_B T} = \frac{Q^{*2} \lambda_B}{2e^2} u(L; R_w, R_c), \quad (5.4.14)$$

with λ_B being the Bjerrum length (0.72 nm for water at 298 K). The function $u(L; R_w, R_c)$ contains the dependency on the brush thickness L , and on the size parameters R_c and the Wigner-Seitz cell radius R_w , see Ref. [17] for more details. This function $u(L; R_w, R_c)$ depends on the charge distribution in- and outside of the brush. For monovalent counterions a parabolic decay of the charge density has been proven to be an accurate description. [54, 56–59] For the present case that contains mainly multivalent counterions the exact form of the charge distribution inside the brush is of minor importance, since the shell layer thickness is very small compared to the overall dimension of the SPB ($L/(R_c + L) \ll 0.1$). [60]

The next free energy contribution accounts for the entropic terms of the counterions and co-ions. [55] It is a reasonable approximation to consider all absorbed multivalent counterions as being osmotically inactive due to their strong correlation to the chains. [19, 56] Outside the brush there is a mixture of the monovalent counterions coming from the brush ($N_+ = |Q_b|/e$; Q_b is the bare charge of the SPB), multivalent counterions [$N_z = c_0 V_w - |Q_b - Q^*|/(ez)$] and co-ions ($N_{co} = z c_0 V_w$), where c_0 is the number density

of LaCl_3 salt, $V_w = (4\pi/3)R_w^3 = 1/\rho_{\text{SPB}}$ which corresponds to the free volume of each SPB at a given SPB density ρ_{SPB} , and l_0 is the monomer size (0.25 nm). Here Q_b is given by the number of charged units per SPB $Q(\text{NaSS})$. Note that all monovalent counterions are completely replaced by trivalent ones and the net charge is determined through the remaining trivalent ions outside the SPB. Inside the brush there are $|Q_b - Q^*|/(ez)$ multivalent ions. The co-ions do not enter the brush regime in our model. It has been shown that this is a reasonable approximation due to electrostatic repulsions between co-ions and the SPB [54]. Consequently there is only one entropic contribution from the free ions

$$\frac{S}{k_{\text{B}}T} = (N_{\text{co}} + N_+ + N_z) \left[\ln \left(\frac{N_{\text{co}} + N_+ + N_z}{V_w} l_0^3 \right) - 1 \right]. \quad (5.4.15)$$

The remaining free energy contributions result from the chains [61, 62]. A contribution related to the elastic energy of the brush chains can be written as

$$\frac{F_{\text{el}}}{k_{\text{B}}T} = \frac{3fL^2}{2D_p l_0^2}, \quad (5.4.16)$$

which stems from a Gaussian approximation of the conformational entropy of the brush chains, while the self-avoidance is accounted by a Flory-type expression

$$\frac{F_{\text{Fl}}}{k_{\text{B}}T} = \frac{3v(fD_p)^2}{8\pi [(R_c + L)^3 - R_c^3]}, \quad (5.4.17)$$

with the excluded volume parameter $v \approx l_0^3$. As usual for the case of good-solvent conditions, triplet-monomer contributions have been omitted.

The total free energy is obtained by adding up all contributions from eqs. (5.4.14)-(5.4.17). This total free energy is minimized with respect to the net charge Q^* and the brush thickness L . Having calculated the brush thickness L and the net charge Q^* of the SPB, the surface potential can be readily obtained. For this we treat the SPB as a sphere with radius $R_c + L$ and a surface charge density of $\Sigma = Q^*/[4\pi(R_c + L)^2]$ from which we determine the surface potential Ψ_0 using the asymptotic expression by Zhou. [52] In this way, one can predict the prefactor V_{max} and the stability ratio W at different salt concentrations using eqs. (5.4.6) and (5.4.13), respectively, from the experimental parameters of the SPB, namely R_c , L_c and σ .

5.5. Results and Discussion

5.5.1. Relative Form Factors

The main goal of this work was to measure exact coagulation rate constants of SPB particles using light scattering. We began by first investigating the dependence of $dI(t)/dt$ and $dR_h(t)/dt$ on the scattering vector q using simultaneous static and dynamic light scattering experiments in 1 and 5 mmol/l LaCl_3 solutions at scattering angles between 20° and 150° . Figure 5.3.1 displays the hydrodynamic radius $R_h(t)$ and the static light scattering intensity $I(t)$ as a function of the time t at a scattering angle of 90° . The

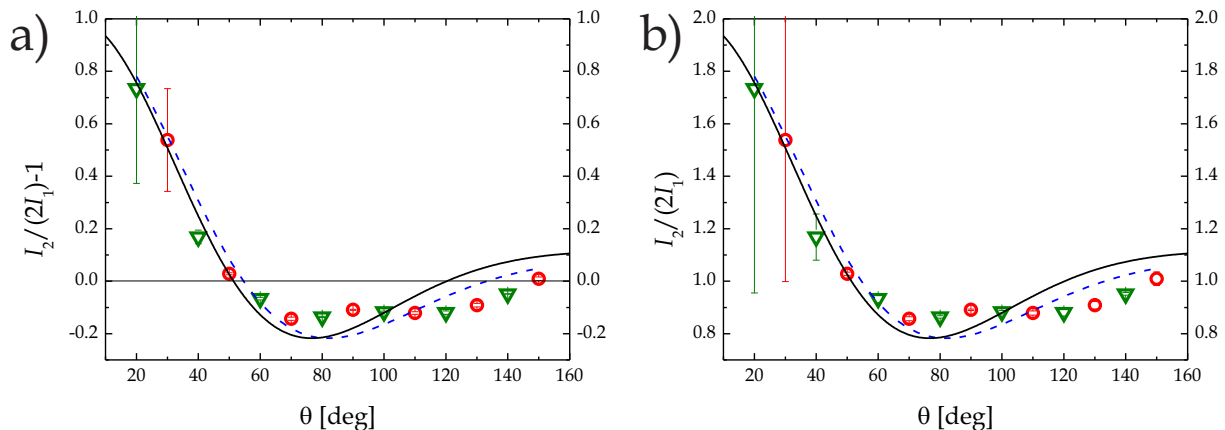


Figure 5.5.1.: Relative doublet form factor $I_2(q)/[2I_1(q)]$ measured by (a) static and (b) dynamic light scattering. The solid line is calculated via the Rayleigh-Debye approximation using a particle singlet radius of 137 nm. The broken line shows the best fit with a singlet radius of 129 nm. The data points were obtained from multiangle simultaneous static and dynamic light scattering measurements in 1 mmol/l (reversed triangles) and 5 mmol/l (circles) LaCl_3 solutions. In all cases the number concentration is $[P]_0: 3.00 \times 10^{14} \text{ m}^{-3}$.

change of $R_h(t)$ and $I(t)$ with t gives the absolute coagulation rate constant k_{11} for each concentration of LaCl_3 by applying eq. (5.3.1) to the data shown in Figures 5.3.1a and 5.3.1b. We first normalized $I(t)$ with the singlet form factor $I(t = 0)$ and $R_h(t)$ with the initial hydrodynamic radius $R_h(t = 0)$. The dependence on q of $I(t)/I(t = 0)$ and $R_h(t)/R_h(t = 0)$ are given by the optical factors $[I_2(q)/2I_1(q)] - 1$ and $[I_2(q)/2I_1(q)]$ in eqs. (5.3.3a) and (5.3.2a), respectively. [23]

We calculated these optical factors as a function of the scattering angle using eqs. (5.3.3) and (5.3.2) with $R_{h,csl}=137$ nm for the particle radius a in the Rayleigh-Debye (RD) approximation. The result is shown in Figure 5.5.1. The theoretical curves deviate slightly from the experimental data points for both the static and dynamic light scattering measurements. These deviations are more pronounced at high values of q . The best theoretical fit of the data in Figure 5.5.1 was obtained with $a = (129 \pm 3)$ nm, however discrepancies at high scattering angles still remain. The RD approximation is only valid in the limits of $|m - 1| \leq 1$ and $(4\pi a/\lambda) |m - 1| \leq 1$, where m is the ratio of the refractive index between the medium and the liquid. [63] In our case $|m - 1| = 0.2$ and $(4\pi a/\lambda) |m - 1| = 0.54$, so that both constraints are satisfied. However, since similar discrepancies were found for hard spheres as well, [23, 64] we conclude, that the RD theory simply does not provide a better description of real data.

Due to the fact that the doublet form factor of the SPB is not well enough described by the RD theory, it is necessary to measure the coagulation rates without relying on the RD doublet form factor. Therefore, we only used simultaneous static and dynamic light scattering, which is independent of any particle form factors, for determining coagulation rate constants of the SPB. We also used $R_{h,csl}=137$ nm for the radius of the collapsed SPB particles in the following sections since it is directly derived from dynamic light scattering.

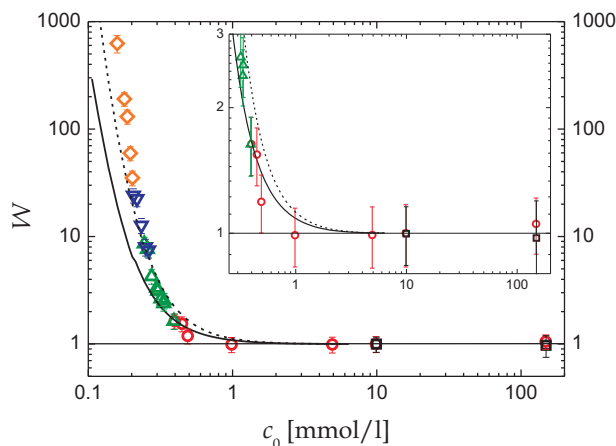


Figure 5.5.2.: Stability ratio $W = k_{11}(c_0 = 150 \text{ mmol/l})/k_{11}(c_0)$ of the SPB as a function of the lanthanum concentration c_0 for different SPB concentrations $[P]_0$: $8.00 \times 10^{15} \text{ m}^{-3}$ (diamonds); $2.00 \times 10^{15} \text{ m}^{-3}$ (reversed triangles); $6.01 \times 10^{14} \text{ m}^{-3}$ (triangles); $3.00 \times 10^{14} \text{ m}^{-3}$ (circles); $1.40 \times 10^{13} \text{ m}^{-3}$ (squares). The scattering angle θ is 90° . The lines are the predictions from the mean-field theory for a SPB concentration of $6.01 \times 10^{14} \text{ m}^{-3}$. The solid line shows the a priori predictions of W . The broken line is calculated by increasing the prediction of the effective charge of the SPB particles by 15%, as explained in Section 5.5.2. The inset shows W for intermediate and high lanthanum concentrations only.

5.5.2. Stability Ratio

For determining the stability ratio of the SPB as a function of the LaCl_3 concentration, the coagulation rate constants were measured using static and dynamic light scattering at a scattering angle of 90° . The measurement data is shown in Figure 5.3.1. It can be seen that the slopes of the hydrodynamic radius versus time curves increase with rising concentrations of lanthanum up to a concentration of 0.5 mmol/l. A further increase of salt concentration to 150 mmol/l does not result in a higher slope. This is a clear indication that these data are in the fast coagulation regime.

The resulting stability ratio is shown in Figure 5.5.2. At $c_0(\text{LaCl}_3) = 0.5 \text{ mmol/l}$ one observes a sharp transition from the reaction-limited coagulation regime where $W > 1$ to the diffusion-limited fast coagulation regime in which $W = 1$. Hence, the lanthanum concentration of $0.5 \pm 0.1 \text{ mmol/l}$ marks the critical coagulation concentration (ccc) of the SPB. The same ccc was also found for another anionic SPB, with similar bare charge Q_b , in the presence of LaCl_3 [2] despite the differences between the two SPB systems in regards to grafting density and contour length of the polyelectrolyte chains. Note that increasing $[P]_0$ with decreasing lanthanum concentration is necessary to maintain a good signal to noise ratio during light scattering experiments while the coagulation rate is reduced.

Figure 5.5.2 also shows the theoretical prediction of W from the variational free energy approach given in Section 5.4.2 (solid line). It slightly deviates from the experimental measurements, but considering the experimental error it still predicts the transition point of the ccc up to an accuracy of 0.2 mmol/l of added salt. Note that this comparison is done

without any adjustable parameters. A better overall matching of the theoretical prediction can be achieved assuming a 15% increase of the predicted net charge (Figure 5.5.2, broken line). Thus, the mean-field model underestimates the charge density and the number of counterions evading the brush layer, especially in the case of low salt concentrations.

The experimental fast coagulation rate constant $k_{11,fast}$ of the SPB in lanthanum solution is $(4.1 \pm 0.1) \times 10^{-18} \text{ m}^3/\text{s}$. This value is in very good agreement with the value found previously, [2] but smaller than the theoretical von Smoluchowski value of $12.2 \times 10^{-18} \text{ m}^3/\text{s}$. The present value also agrees well with data found in the literature for systems of comparable hydrodynamic dimensions. [23, 24, 65, 66] In agreement with our earlier study, [2] and with the work of Mei and co-workers [16, 19], we find that the initial hydrodynamic radius $R_h(0)$ stays constant for all lanthanum concentrations. This $R_h(0)$ corresponds to the radius of the SPB after the addition of salt, but before coagulation. Thus, even at the lowest salt concentration of 0.16 mmol/l a full collapse of the polyelectrolyte shell of the SPB occurs immediately.

Taking into account a hydrodynamic core radius of $(125 \pm 2) \text{ nm}$ and using $(137 \pm 3) \text{ nm}$ for $R_{h,csl}$, the hydrodynamic thickness L of the collapsed shell layer results to $(12 \pm 4) \text{ nm}$. In our previous study we found $L = 7 \text{ nm}$ for a similar SPB in the presence of LaCl_3 . [2] Considering the differences in the brush parameters of the two SPB systems and the experimental error of $R_{h,csl}$, the agreement is satisfactory. However, the brush thickness obtained from the variational free energy calculations is much smaller than the experimental value ($L = 3.8 \text{ nm}$ at $c_0 \approx 0.2 \text{ mmol/l}$). We attribute this discrepancy mainly to the various simplifications of the theoretical model employed here.

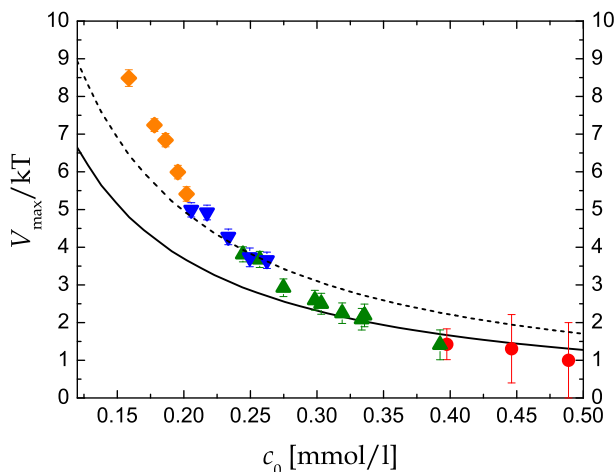


Figure 5.5.3.: Prefactor $\tilde{V}_{max} = V_{max}/k_B T$ as a function of salt concentration c_0 of LaCl_3 . Experimental data are shown for four different SPB concentrations $[P]_0$: $8.00 \times 10^{15} \text{ m}^{-3}$ (diamonds); $2.00 \times 10^{15} \text{ m}^{-3}$ (reversed triangles); $6.01 \times 10^{14} \text{ m}^{-3}$ (triangles); $3.00 \times 10^{14} \text{ m}^{-3}$ (circles). The data points were calculated from the experimental determined values of the prefactor \tilde{V}_{max} using a particle radius $R_{h,csl} = 137 \text{ nm}$, corresponding to a thickness of the collapsed brush layer of 12 nm. The lines are the predictions from the mean-field theory for a SPB concentration of $[P]_0 = 6.01 \times 10^{14} \text{ m}^{-3}$. The solid line shows the prediction of \tilde{V}_{max} . The broken line is calculated by increasing the prediction by 15%.

5.5.3. Force Balance: Repulsive Energy and Effective Surface Charge

From the stability measurements, we can then calculate the height of the maximum value of $V(r)$ (Figure 5.1.1c), which is the prefactor $\tilde{V}_{max} = V_{max}/k_B T$ in eq. (5.4.13). Using eq. (5.4.13) we fit \tilde{V}_{max} to the values of the stability ratio determined in our light scattering experiments for all LaCl_3 concentrations. Plotting \tilde{V}_{max} as a function of c_0 reveals a decrease of \tilde{V}_{max} with increasing counterion concentration (Figure 5.5.3). This is due to a charge regulation effect taking place inside the polyelectrolyte shell layer, which occurs as the polyelectrolyte brush becomes more and more neutralized by lanthanum counterions (Section 5.4.2). Figure 5.5.3 demonstrates that the repulsive energy of the system at $r = R_h$ can be accurately measured in units of $k_B T$ for high values of \tilde{V}_{max} . However, for low values of \tilde{V}_{max} the experimental error is higher due to two main reasons: the correction function for the hydrodynamic drag $B(h)$ and the van der Waals terms, H_c and H_s , are less exact at small particle separations, and the highest possible force resolution is on the order of $k_B T$. Thus, \tilde{V}_{max} is affected by a larger error in this regime.

Figure 5.5.3 also shows the comparison between theory (Section 5.4.2) and experiment. The prediction of \tilde{V}_{max} that involves no fitting parameters reveals good agreement at higher salt concentrations. However, at lower salt concentrations better agreement is achieved if the predicted value of the charge density Σ is increased by 15% (dashed line in both Figures 5.5.2 and 5.5.3). Therefore, the theory predicts \tilde{V}_{max} of the SPB within an error of no more than 4 units of $k_B T$ at lanthanum concentrations of 0.16 to 0.5 mmol/l.

From the experimental data of \tilde{V}_{max} , the number of effective charges N_{eff} per SPB particle can also be calculated. According to eq. (5.4.6), V_{max} is proportional to the square of the surface potential of the SPB particles. From the surface potential, the surface charge density of the particles is attainable using the approximate analytic expression for 3:1

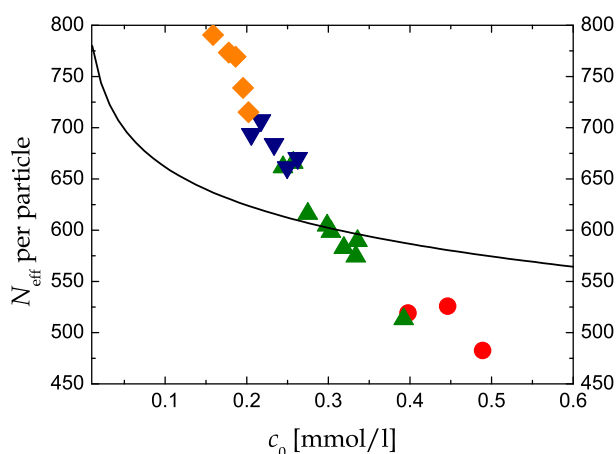


Figure 5.5.4.: Number of effective charges per SPB particle for four different SPB concentrations $[P]_0$: $8.00 \times 10^{15} \text{ m}^{-3}$ (diamonds); $2.00 \times 10^{15} \text{ m}^{-3}$ (reversed triangles); $6.01 \times 10^{14} \text{ m}^{-3}$ (triangles); $3.00 \times 10^{14} \text{ m}^{-3}$ (circles). The data points were calculated from the experimental determined values of the prefactor V_{max} using a thickness of the collapsed brush layer of 12 nm. The solid line is the prediction from the mean-field theory for a SPB concentration of $[P]_0 = 6.01 \times 10^{14} \text{ m}^{-3}$.

salts according to Zhou. [52] We then calculated the number of effective charges per SPB as a function of c_0 using $R_{h,csl}=137$ nm for the particle size. The results are shown in Figure 5.5.4.

Through comparing Figures 5.5.3 and 5.5.4 we can see that at 450-500 effective charges the electrostatic repulsion between the SPB particles approaches the value of $1 k_B T$. Here the coagulation becomes diffusion-limited. In the slow coagulation regime, N_{eff} rises to 800 charges per particle at $c_0=0.16$ mmol/l, corresponding to 8.5 units of $k_B T$ and a stability ratio of about 700. Thus, the present experimental approach enables us to measure the decrease of the maximum of the repulsive interparticle energy with an accuracy on the order of $k_B T$. The number of effective charges per SPB particle can be measured within $\pm 20\%$.

This data is in the range of the theoretical prediction, as demonstrated in Figure 5.5.4 (lines). At first sight, the comparison of the experimental and theoretical values for the effective charge and its dependency on added multivalent salt is not satisfactory. However, given the fact that the bare charge of the SPB is on the order of two million charges per SPB ($Q_b \approx 1.9 \times 10^6$), its reduction to 500-800e at lanthanum concentrations of less than 0.5 mmol/l confirmed by experiments and theory is remarkable.

5.6. Conclusion

We presented a detailed account of an investigation related to repulsive forces between colloidal spherical polyelectrolyte brushes in aqueous solutions of trivalent ions. Using accurate measurements of the rate of coagulation, the strength of the repulsive potential could be measured down to values of the order of $k_B T$ ('microsurface potential measurements'). The experimental data could be modeled in terms of a simple mean-field theory that accounts for the drastic reduction of the effective charge of the brushes by trivalent ions. The comparison of theory and experimental data demonstrates that the weakening of electrostatic repulsion can be understood on a quantitative level. Moreover, the MSPM has been shown as a reliable method for assessing weak repulsion between colloidal particles.

5.7. Acknowledgements

R.F., P.P., and M.T. gratefully acknowledge support for this work from the National Science Foundation Grants No. DMR-0520415 and No. DMR-0710521 (Materials World Network). M.B. gratefully acknowledges support by the Deutsche Forschungsgemeinschaft. C.S. thanks the Elite Study Program Macromolecular Science in the Elite Network Bavaria and the Bavarian Graduate Support Program for financial support during this work. C.S and M.B. gratefully acknowledge the Bavarian California Technology Center BaCaTec for financial support of this joined project. The work at Berkeley was supported by the Laboratory Directed Research and Development Program of Lawrence Berkeley National Laboratory under the Department of Energy Contract No. DE-AC02-05CH11231.

5.8. References

- [1] Swanton, S. W. *Adv. Colloid Interface Sci.* **1995**, *54*, 129.
- [2] Schneider, C.; Jusufi, A.; Farina, R.; Li, F.; Pincus, P.; Tirrell, M.; Ballauff, M. *Langmuir* **2008**, *24*, 10612.
- [3] Russel, W. B.; Saville, D. A.; Schowalter, W. R. *Colloidal Dispersions*; Cambridge University Press: Cambridge, 2001.
- [4] Derjaguin, B. V.; Landau, L. *Acta Physicochim. USSR* **1941**, *14*, 633.
- [5] Verwey, E. J. W.; Overbeek, J. T. G. *Theory of the Stability of Lyophobic Colloids*; Elsevier: Amsterdam, 1948.
- [6] Evans, D. F.; Wennerström, H. *The Colloidal Domain*; Wiley-VCH: New York, 1999.
- [7] Tadros, T. *Adv. Colloid Interface Sci.* **1993**, *46*, 1.
- [8] Ballauff, M. *Prog. Polym. Sci.* **2007**, *32*, 1135.
- [9] Ballauff, M. *Curr. Opin. Colloid Interface Sci.* **2006**, *11*, 316.
- [10] Pincus, P. *Macromolecules* **1991**, *24*, 2912.
- [11] Borisov, O. V.; Birshtein, T. M.; Zhulina, E. B. *J. Phys. II (Fr.)* **1991**, *1*, 521.
- [12] Guo, X.; Ballauff, M. *Phys. Rev. E* **2001**, *64*, 051406.
- [13] Guo, X.; Ballauff, M. *Langmuir* **2000**, *16*, 8719.
- [14] Balastre, M.; Li, F.; Schorr, P.; Yang, J.; Mays, J. W.; Tirrell, M. V. *Macromolecules* **2002**, *35*, 9480.
- [15] Dunlop, I. E.; Briscoe, W. H.; Titmuss, S.; Jacobs, R. M. J.; Osborne, V. L.; Edmondson, S.; Huck, W. T. S.; Klein, J. *J. Phys. Chem. B* **2009**, *113*, 3947.
- [16] Mei, Y.; Lauterbach, K.; Hoffmann, M.; Borisov, O. V.; Ballauff, M.; Jusufi, A. *Phys. Rev. Lett.* **2006**, *97*, 158301.
- [17] Jusufi, A.; Likos, C. N.; Ballauff, M. *Colloid Polym. Sci.* **2004**, *282*, 910.
- [18] Konradi, R.; Rühle, J. *Macromolecules* **2005**, *38*, 4345.
- [19] Mei, Y.; Hoffmann, M.; Ballauff, M.; Jusufi, A. *Phys. Rev. E* **2008**, *77*, 031805.
- [20] Hoffmann, M.; Jusufi, A.; Schneider, C.; Ballauff, M. *J. Colloid Interface Sci.* **2009**, *338*, 566.
- [21] Li, F.; Schorr, P.; Tirrell, M. V.; Mays, J. *Polym. Prepr.* **2005**, *46*(1), 377.

- [22] Hanus, L.; Hartzler, R.; Wagner, N. *Langmuir* **2001**, *17*, 3136.
- [23] Holthoff, H.; Egelhaaf, S. U.; Borkovec, M.; Schurtenberger, P.; Stricher, H. *Langmuir* **1996**, *12*, 5541.
- [24] Behrens, S. H.; Christl, D. I.; Emmerzael, R.; Schurtenberger, P.; Borkovec, M.; *Langmuir* **2000**, *16*, 2566.
- [25] Israelachvili, J. N. *J. Colloid Interface Sci.* **1973**, *44*, 259.
- [26] Meyer, E. E.; Rosenberg, K. J.; Israelachvili, J. N. *Proc. Natl. Acad. Sci. U.S.A.* **2006**, *103*, 15739.
- [27] Grier, D. G. *Nature* **2003**, *424*, 810.
- [28] Kegler, K.; Salomo, M.; Kremer, F. *Phys. Rev. Lett.* **2007**, *98*, 058304.
- [29] Dominguez-Espinosa, G.; Synytska, A.; Drechsler, A.; Gutsche, C.; Kegler, K.; Uhlmann, P.; Stamm, M.; Kremer, F. *Polymer* **2008**, *49*, 4802.
- [30] Claesson, P. M.; Ederth, T.; Bergeron, V.; Rutland, M. W. *Adv. Colloid Interface Sci.* **1996**, *67*, 119.
- [31] Bike, S. G. *Curr. Opin. Colloid Interface Sci.* **2000**, *5*, 144.
- [32] Walz, J. Y. *Curr. Opin. Colloid Interface Sci.* **1997**, *6*, 600.
- [33] Butt, H. J.; Cappella, B.; Kappl, M. *Surf. Sci. Rep.* **2005**, *59*, 1.
- [34] Ralston, J.; Larson, I.; Rutland, M. W.; Feiler, A. A.; Kleijn, M. *J. Macromol. Sci., Pure Appl. Chem.* **2005**, *77*, 2149.
- [35] Ducker, W. A.; Senden, T. J.; Pashley, R. M. *Nature* **1991**, *353*, 239.
- [36] Guo, X.; Weiss, A.; Ballauff, M. *Macromolecules* **1999**, *32*, 6043.
- [37] Schrunner, M.; Haupt, B.; Wittemann, A. *Chem. Eng. J.* **2008**, *144*, 138.
- [38] Kim, J. H.; Chainey, M.; El-Aasser, M. S.; Vanderhoff, J. W. *J. Macromol. Sci., Pure Appl. Chem.* **1992**, *30*, 171.
- [39] Brown, W. *Light Scattering*; Clarendon Press: Oxford, 1996.
- [40] Elias, H.-G. *Macromolecules*; Wiley-VCH: Weinheim, 2006.
- [41] Spedding, F. H.; Pikal, M. J.; *J. Phys. Chem.* **1966**, *70*, 2430.
- [42] Holthoff, H.; Borkovec, M.; Schurtenberger, P. *Phys. Rev. E* **1997**, *56*, 6945.
- [43] Hunter, R. J. *Foundations of Colloid Science*, 2nd ed.; Oxford University Press: New York, 2004.

-
- [44] von Smoluchowski, M. *Phys. Z.* **1916**, *17*, 557.
- [45] von Smoluchowski, M.; *Z. Phys. Chem.* **1917**, *92*, 129.
- [46] Honig, E. P.; Roeberson, G. J.; Wiersema, P. H. *J. Colloid Interface Sci.* **1971**, *36*, 97.
- [47] Israelachvili, J. N. *Intermolecular and Surface Forces*; Academic Press: New York, 1998.
- [48] Converting the value of V_{max} at $c_0=0.16$ mM into the corresponding surface potential Ψ_0 gives $\kappa R_h = 13.7 \gg 1$ and $e\Psi_0/k_B T = 0.29 < 1$.
- [49] Gregory, J. *J. Colloid Interface Sci.* **1981**, *83*, 138.
- [50] Tadmor, R. *J. Phys.: Condens. Matter* **2001**, *13*, L195.
- [51] Hsu, J.-P.; Kuo, Y.-C. *J. Colloid Interface Sci.* **1994**, *167*, 35.
- [52] Zhou, S. *J. Colloid Interface Sci.* **1998**, *208*, 347.
- [53] Jusufi, A.; Likos, C. N.; Löwen, H. *Phys. Rev. Lett.* **2002**, *88*, 018301.
- [54] Jusufi, A.; Likos, C. N.; Löwen, H.; *J. Chem. Phys.* **2002**, *116*, 11011.
- [55] Ni, R.; Cao, D.; Wang, W.; Jusufi, A. *Macromolecules* **2008**, *41*, 5477.
- [56] Jusufi, A. *J. Chem. Phys.* **2006**, *124*, 044908.
- [57] Groenewegen, W.; Egelhaaf, S. U.; Lapp, A.; van der Maarel, J. R. C. *Macromolecules* **2000**, *33*, 3283.
- [58] Roger, M.; Guenoun, P.; Muller, A.; Belloni, L.; Delsanti, M. *Eur. Phys. J. E* **2002**, *9*, 313.
- [59] Dingenouts, N.; Patel, M.; Rosenfeldt, S.; Pontoni, D.; Narayanan, T.; Ballauff, M. *Macromolecules* **2004**, *37*, 8152.
- [60] The difference between a uniform and non-uniform brush density at $r = R_c$ and the edge of the brush at $r = R_h$ is below 10%, if the density profile decays with r^{-2} , and $< 5\%$ in the case of a decay with r^{-1} .
- [61] Alexander, S. *J. Phys.* **1977**, *38*, 977.
- [62] de Gennes, P. G. *Macromolecules* **1980**, *13*, 1069.
- [63] Zaccone, A.; Wu, H.; Lattuada, M.; Morbidelli, M. *J. Phys. Chem. B* **2008**, *112*, 1976.
- [64] Holthoff, H.; Schmitt, A.; Fernández-Barbero, A.; Borkovec, M.; Cabrerizo-Vílchez, M. Á.; Schurtenberger, P.; Hidalgo-Álvarez, R. *J. Colloid Interface Sci.* **1997**, *192*, 463.

- [65] Sonntag, H.; Strenge, K. *Coagulation and Structure Formation*; VEB Deutscher Verlag der Wissenschaften: Berlin, 1987.
- [66] van Zanten, J. H.; Elimelech, M. *J. Colloid Interface Sci.* **1992**, *154*, 1.

6. Summary / Zusammenfassung

Summary

The focus of this thesis was aimed at the investigation of colloidal particle stability. In a first step we established a method to assess the repulsive interaction energy of dispersed colloids based on the measurement of the rate of slow coagulation with light scattering. Due to an energy resolution in the order of magnitude of the thermal energy, the method was termed 'microsurface potential measurements' (MSPM).

We then used the MSPM to measure the potential at the outer Helmholtz plane (oHp) Ψ_d , which determines the electric double layer of surface charged colloidal particles. The MSPM were performed on anionic particles in the presence of di- and trivalent counterions as a function of the bulk electrolyte concentration. We found that Ψ_d does only weakly depend on the Mg^{2+} but strongly on the La^{3+} concentration. In both cases the absolute value of Ψ_d decreases with increasing electrolyte concentration. The absolute values of Ψ_d are always lower for the trivalent counterions as compared to the divalent results. To supplement the results of the MSPM, we measured the ζ potential of the particles under similar conditions. Here we detected charge reversal in the experiments with the di- and trivalent counterions. In the salt concentration range of the MSPM ζ and Ψ_d were closely related for both ion species but could not be described by Poisson-Boltzmann based models. In the case of the trivalent counterions, we could experimentally verify the strong influence of counterion adsorption in the destabilization of the surface charged colloids. Furthermore, we showed that ζ is not suited for calculating the particle stability in the experiments involving trivalent counterions and found strong experimental indications for counterion correlations.

We also used MSPM to investigate an anionic SPB in the presence of trivalent counterions. For this purpose we measured the interaction force of two planar polyelectrolyte brush layers across an aqueous medium containing trivalent counterions with the surface forces apparatus. We found that steric repulsion does not occur. The repulsion only arises from residual charges inside the brush layers. From the resulting force curves we were able to deduce an interaction profile of SPB particles in aqueous solution containing multivalent counterions. Thus, we were able to measure the effective repulsive energy of SPB particles using MSPM with an accuracy of $k_B T$. Due to the increase of confined lanthanum counterions in the brush layer the electrostatic repulsion decreased with rising lanthanum concentration. Furthermore, the experimental results were well predicted by a mean-field model. For the first time, we described the means to measure and predict the repulsive energies of SPB particles in aqueous solution in the presence of multivalent counterions.

In a next step we refined the theoretical basis of the MSPM and expanded the electrolyte concentration range of the stability experiments. We also measured the form factors of the SPB doublets and found pronounced deviations between the data points and the predictions of the Rayleigh-Debye approximation. We showed that the MSPM are now accurate enough to measure the effective charges per SPB particle with a sub millimolar concentration resolution. Furthermore, we used the mean-field model to predict the particle stability and the effective charge per SPB particle. In both cases we found the deviations between the experimental data and the model to be within an error margin of 20%. Therefore we predicted the particle stability of SPBs in aqueous solution for the first time .

In conclusion, this thesis provides a deeper insight into the mechanisms of particle stability and coagulation of electrostatically and electrosterically stabilized dispersions. It offers a new method to investigate the repulsive interactions between colloidal particles which is applicable to a wide variety of colloidal systems. Moreover, we made the first steps toward a more complete understanding of the stability of SPB particles, which is important for potential industrial applications of these kind of systems.

Zusammenfassung

Der Schwerpunkt der vorgelegten Arbeit lag auf der Untersuchung der Stabilität von kolloidalen Partikeln. Als erster Schritt wurde eine Methode zur Messung der repulsiven Wechselwirkungsenergien zwischen dispergierten Kolloiden erarbeitet. Die Technik basiert auf der Messung der Geschwindigkeitskonstanten der Teilchenkoagulation mittels Lichtstreuung. Auf Grund einer Genauigkeit der Energiemessungen in der Größenordnung der thermischen Energie wurde die Methode als 'microsurface potential measurements' (MSPM) bezeichnet.

Unter Verwendung der MSPM wurde von oberflächengeladenen Kolloiden das diffuse Potential Ψ_d gemessen, welches die Eigenschaften der elektrischen Doppelschicht festlegt. Die MSPM wurden an einem anionischen Modellsystem in Gegenwart von di- und trivalenten Gegenionen als Funktion der Salzkonzentration durchgeführt. Hierbei zeigte sich im Fall der divalenten Mg^{2+} Gegenionen eine schwach, im Falle der trivalenten La^{3+} Gegenionen eine deutlich ausgeprägte Abhängigkeit des diffusen Potentials bezüglich der Salzkonzentration. In beiden Fällen nimmt der absolute Wert von Ψ_d mit Zunahme der Salzkonzentration ab. Es zeigte sich, dass die Potentialbeträge in den Messungen mit La^{3+} Gegenionen immer höher als im Fall der Mg^{2+} Ionen waren. Ergänzend zu den Ergebnissen der MSPM wurden Messungen des ζ Potentials der Partikel unter ähnlichen Bedingungen durchgeführt. In diesen Experimenten wurde Ladungsumkehr der anionischen Partikel in Gegenwart der Mg^{2+} und La^{3+} Ionen beobachtet. In dem Konzentrationsbereich der MSPM waren die Ergebnisse von Ψ_d und ζ in beiden Messreihen stark korreliert. Die ζ Potentiale konnten aber nicht durch ein Poisson-Boltzmann Modell beschrieben werden. Im Fall der dreiwertigen Gegenionen konnten wir den starken Einfluss der Gegenionenadsorption auf die Destabilisierung der oberflächengeladenen Kolloide nachweisen. Des Weiteren

wurde in den Experimenten mit den dreiwertigen Gegenionen gezeigt, dass sich ζ nicht für die Berechnung der Partikelstabilität eignet. Die experimentellen Befunde konnten darüber hinaus durch den Effekt der Gegenionenkorrelation qualitativ erklärt werden.

Unter Verwendung der MSPM wurde das Verhalten einer anionischen SPB in Gegenwart von mehrwertigen Gegenionen untersucht. Hierzu wurden die Wechselwirkungen zwischen zwei planaren Schichten mit aufgetragenen Polyelektrolytbürsten mittels des 'surface forces apparatus' untersucht. In wässrigem Medium mit mehrwertigen Gegenionen wurde zwischen den separierten planaren Oberflächen nur eine repulsive elektrostatische Wechselwirkung beobachtet. Aufbauend auf diesem Ergebnis konnten wir ein Wechselwirkungspotential von Polyelektrolytbürsten unter der Einwirkung von mehrwertigen Gegenionen ableiten. Hierdurch wurde die Messung der repulsiven Wechselwirkung von SPB Partikeln durch MSPM mit einer Genauigkeit in der Größenordnung der thermischen Energie möglich. Auf Grund eines erhöhten Anteils an adsorbierten Gegenionen in den kollabierten Polyelektrolytschichten nahm die elektrostatische Repulsion mit Zunahme der Lanthankonzentration ab. Ein Vergleich der experimentellen Befunde mit den Vorhersagen eines 'mean-field' Modells zeigte eine gute Übereinstimmung. Somit konnten neue Methoden zur Bestimmung und Vorhersage der repulsiven Wechselwirkung zwischen dispergierten SPB Partikeln unter Einwirkung multivalenter Gegenionen erarbeitet werden.

In der nachfolgenden Arbeit wurden die theoretischen Grundlagen der MSPM verbessert und der Konzentrationsbereich der Stabilitätsmessungen erweitert. Darüber hinaus wurden die Formfaktoren der SPB Dubletts experimentell gemessen und Abweichungen zu den Vorhersagen des Rayleigh-Debye Modells gefunden. Wir konnten zeigen, dass die MSPM die Bestimmung der Anzahl an effektiven Ladungen pro SPB Partikel bei sehr kleinen Salzkonzentration ermöglichen. Das Modell ermöglichte ebenso die Vorhersage der gemessenen SPB Stabilität. In beiden Fällen betrug die Abweichungen der theoretischen Vorhersagen zu den Messergebnissen weniger als 20%. Zum ersten Mal wurde somit die Stabilität von dispergierten SPBs durch ein theoretisches Modell erfolgreich vorhergesagt.

Im Rahmen dieser Arbeit ist es gelungen, dass Verständnis bezüglich der Stabilität von elektrostatisch und elektrosterisch stabilisierten kolloidalen Systemen zu verbessern. Es wurde eine neue experimentelle Methode vorgestellt, welche die Messung der repulsiven interpartikulären Wechselwirkung ermöglicht und bei einer Vielzahl von Systemen anwendbar ist. Insbesondere konnten die ersten Schritte hin zu einer besseren theoretischen Beschreibung der Stabilität von SPBs unternommen werden. Dies ist vor allem in Bezug auf industrielle Anwendungen der SPBs von Bedeutung.

A. List of Publications

A.1. Publication of this Thesis

- Schneider, C.; Jusufi, A.; Farina, R.; Li, F.; Pincus, P.; Tirrell, M.; Ballauff, M.: Microsurface Potential Measurements: Repulsive Forces between Polyelectrolyte Brushes in the Presence of Multivalent Counterions, *Langmuir* **2008**, *24*, 10612.
- Schneider, C.; Jusufi, A.; Farina, R.; Pincus, P.; Tirrell, M.; Ballauff, M.: Investigation of the Stability Behavior of Anionic Spherical Polyelectrolyte Brushes in the Presence of La(III) Counterions, *Phys. Rev. E* **2010**, *82*, 011401.
- Schneider, C.; Hanisch, M.; Wedel, B.; Jusufi, A.; Ballauff, M.: Interaction of Colloidal Particles: the DLVO Potential and Charge Inversion, *submitted*.

A.2. Publication as a co-Author

- Bolisetty, S.; Schneider, C.; Polzer, F.; Ballauff, M.; Li, W.; Zhang, A.; Schlüter, A. D.: Formation of Stable Mesoglobules by a Thermosensitive Dendronized Polymer, *Macromolecules* **2009**, *42*, 7122.
- Hoffmann, M.; Jusufi, A.; Schneider, C.; Ballauff, M.: Surface Potential of Spherical Polyelectrolyte Brushes in the Presence of Trivalent Counterions, *J. Colloid Interface Sci.* **2009**, *33*, 566.

B. Presentations at International Conferences and Meetings

- Macromolecular Systems for NanoScience - Chemistry, Physics and Engineering Aspects; Kloster Irsee, Germany; September 6 - 9, 2007; *poster presentation*: Coagulation Kinetics of Spherical Polyelectrolyte Brushes in Presence of Trivalent Counterions.
- Macromolecular Symposium; Freiburg, Germany; February 28 - March 1, 2008; *poster presentation*: Coagulation Kinetics of Spherical Polyelectrolyte Brushes in Presence of Trivalent Counterions.
- BASF International Summer Course; Ludwigshafen, Germany; July 21 - August 1, 2008; *poster presentation*: Collapse Transition in Polyelectrolyte Brushes in Presence of multivalent counterions
- Bayreuther Polymer Symposium; Bayreuth, Germany; September 13 - 15, 2009; *poster presentation*: Polyelectrolyte Brushes in Presence of Multivalent Counterions: From Collapse Transition to Coagulation.
- Conference of the European Colloid and Interface Society; Prague, Czech Republic; September 5 - 10, 2010; *oral presentation*: Colloidal Stability of Spherical PE Brushes in Multivalent Counterion Environment - Experiment and Theory.

C. Abbreviations

AFM	atomic force microscopy
CCC	critical coagulation concentration
CR	charge reversal
DLCA	diffusion limited colloidal aggregation
DLS	dynamic light scattering
DLVO	Derjaguin-Landau-Verwey-Overbeek
GPC	gel permeation chromatography
HMEM	2-[p-(2-hydroxy-2-methylpropiophenone)]-ethyleneglycol-methacrylate
iHp	inner Helmholtz plane
MD	molecular dynamics
MSPM	microsurface potential measurements
oHp	outer Helmholtz plane
OT	optical tweezers
PB	Poisson-Boltzman
PCS	photon correlation spectroscopy
PE	polyelectrolyte
PES	poly(ethersulfone)
PS	polystyrene
PSS	poly(styrenesulfonate)
PtBS	poly(4-tert-butylstyrene)
RD	Rayleigh-Debye
RLCA	reaction limited colloidal aggregation
SCL	strongly correlated liquid
SFA	surface forces apparatus
SLS	static light scattering

SPB	spherical polyelectrolyte brush
SS	styrenesulfonate
SSDLS	simultaneous static and dynamic light scattering
TEM	transmission electron microscopy
TIRM	total internal reflection microscopy
WC	Wigner crystal

D. Danksagung

Ich möchte mich an dieser Stelle bei allen bedanken, die mir für und während meiner Promotion und meines Studiums zur Seite standen.

Zuallererst möchte ich mich bei Herrn Prof. Dr. Matthias Ballauff für die interessante und anspruchsvolle Themenstellung, die vielen Anregungen und Hilfestellungen, seine stetige Diskussionsbereitschaft und fortwährendes Interesse an meiner Arbeit bedanken. Dies gilt umso mehr für meine großzügig eingeräumten Freiheiten in der Bearbeitung der Themenstellung und das hiermit verbundene Vertrauen.

Für finanzielle Unterstützung möchte ich mich bei BaCaTec im Rahmen des Projekts 'Mehrwertige Gegenionen in Polyelektrolyt-Bürsten', bei der National Science Foundation und der Deutschen Forschungsgesellschaft im Rahmen des Projekts 'BA 758/32-1' und bei dem Elite Netzwerk Bayern im Rahmen des Bayerischen Graduierten Programms bedanken.

Bei Prof. Philip Pincus und Prof. Matthew Tirrell möchte ich mich für die gute Zusammenarbeit im Rahmen des NSF/DFG Projekts und für meine herzliche Aufnahme in Kalifornien bedanken.

Besonderer Dank gebührt hier Rob Farina für die Betreuung während meines Aufenthaltes an der UCSB und unsere freundschaftliche Zusammenarbeit.

Bei Arben Jusufi möchte ich mich für die intensive und herzliche Zusammenarbeit bei allen Veröffentlichungen dieser Arbeit bedanken.

Meinen ehemaligen Praktikanten Mathias Hanisch, Bastian Wedel und Christian Probst bedanke ich mich herzlich für ihre große Motivation und ihren unermüdlichen Eifer bei der Bearbeitung ihrer Themen. Alles Gute für eure Promotionen in Nürnberg-Erlangen, Bielefeld und Bayreuth!

Besonderen Dank für das gute Zusammenwirken auch an meine mit-Promovenden im Arbeitskreis von Herrn Prof. Thomas Hellweg am ehemaligen Lehrstuhl der physikalischen Chemie I der Universität Bayreuth. Guten Umzug und viel Erfolg in Bielefeld!

Herzlichen Dank auch an alle Kollegen des Lehrstuhls für Physikalische Chemie II der Universität Bayreuth.

Karlheinz Lauterbach, Elisabeth Dünfelder und Christa Bächer möchte ich für die gute Zusammenarbeit und Unterstützung bei Arbeiten jeglicher Art bedanken.

Bei allen Mitgliedern des Lehrstuhls für Physikalische Chemie I der Universität Bayreuth möchte ich mich für die ständige Hilfs- und Diskussionsbereitschaft und für das außerordentlich gute Arbeitsklima bedanken. Dies gilt auch für meine neuen Kollegen am Institut für weiche Materie und funktionale Materialien am Helmholtz-Zentrum Berlin für Materialien und Energie. Danke für die freundliche Aufnahme in eurem Hause.

Frank Polzer danke ich nochmals für die hochwillkommenen und zahlreichen aufmuntern-

den Diskussionen.

Herzliche Grüße und großen Dank an meine Studienkollegen und Freunde in Bayreuth und anderswo.

Besonders herzlich möchte ich mich bei meinen Eltern und meiner Familie bedanken, die mich über alles Maß hinaus und in bewundernswerter Weise unterstützten und mir immer mit Rat und Tat beistanden. Ohne euer Vertrauen und eure Hilfe wäre mein bisheriger Weg in dieser Form nicht möglich gewesen. Meinen besonderen Dank gilt meiner Mutter, der ich alles zu verdanken habe.

Sarah, ich danke dir für deine wundervolle Begleitung während der letzten vier Jahre und die zahlreichen erholsamen Wochenenden in Würzburg. Es ist schön, den Weg nicht alleine gehen zu müssen.

E. Schlusserklärung

Hiermit erkläre ich, dass ich die vorliegende Arbeit selbständig verfasst und keine anderen als die angegebenen Quellen und Hilfsmittel benutzt habe.

Ferner erkläre ich, dass ich nicht anderweitig mit oder ohne Erfolg versucht habe eine Dissertation einzureichen oder mich einer Doktorprüfung zu unterziehen.

Bayreuth, den 17. November 2010,

Christian Schneider